ProQuest LLC.
789 East Eisenhower Parkway
P.O. Box 1346
Ann Arbor, MI 48106 – 1346

EFFECT OF HEAT TREATMENT ON THE MICROSTRUCTURE OF A 2CrMoNiWV ROTOR STEEL

Cheng Li

A thesis submitted in partial fulfilment of the requirements of Sheffield Hallam University for the degree of Doctor of Philosophy

February 1996

Collaborating Organisation: GEC ALSTHOM

PREFACE

This thesis is submitted in partial fulfilment of the requirements of Sheffield Hallam University for the degree of Doctor of Philosophy. It contains an account of research carried out between February 1993 and February 1996 in the Materials Research Institute, Sheffield Hallam University, under the supervision of Dr. J. Cawley, Dr. A. Strang and Dr. R. Stratton. Except where acknowledge and reference is appropriately made, this work is, to the best my knowledge, original and has been carried out independently. No part of this thesis has been, or is currently being, submitted for any degree or diploma at this, or any other, university.

Cheng Li

February 1996

ACKNOWLEDGEMENTS

I am indebted to Dr. J. Cawley for his encouragement and support during the course of this research, and for the provision of laboratory facilities in the Materials Research Institute and School of Engineering at Sheffield Hallam University.

I would like to thank GEC Alsthom for providing experimental material, and especially Dr. A. Strang, head of laboratories, for the helpful discussions and interest he has shown in this work. I must also thank Prof. F. B. Pickering for his invaluable advice.

Thanks are also extended to British Steel Technical, for their generous help in using an MMC Quenching Dilatometer at Swinden Laboratory. I am also grateful to the staff at the National Physical Laboratory, particularly Dr. H. Davies and Dr. J. Gisby, for the provision of MTDATA, a program for the calculation of chemical equilibria in multicomponent systems, and their instruction on its use.

I must also thank all staff and my friends in the Materials Research Institute, especially Dr. I. Wadsworth for his early help with transmission electron microscopy, Dr. R. Stratton for his constructive discussions, and Prof. J. Titchmarch for his help in the interpretation of electron diffraction patterns and EDX analysis. Technical support from Mr. G. Gregory, Mr. P. Slingsby, Mr. S. Creasey, Mr. A. Sheldon and Mr. K. Blake are acknowledged with pleasure.

Finally, I wish to thank my family for their unfailing support and encouragement.

ABSTRACT

A wide range of experiments have been carried out on a 2CrMoNiWV low alloy steel to investigate the effect of various heat treatment conditions on microstructural change, alloy carbide transformation mechanism and mechanical properties.

Two complete continuous cooling transformation (CCT) diagrams were constructed for this steel on the basis of experimental dilatometry thermal analysis, metallographic examination and current phase transformation theory. The significance of these two diagrams is in that they can be directly utilised in industrial practice as a reference during heat treatment for this material. Meanwhile it was confirmed that this 2CrMoNiWV steel can be transformed to a fully bainitic microstructure over a wide range of cooling rates and this feature proved this steel suitable for large diameter steam turbine rotor application.

An innovative carbide extraction technique for the XRD identification of carbide phase has been developed. The detailed description of this new technique and its advantages are discussed in this thesis. The extensive work using TEM/EDX has set up essential "finger prints" for the quick examination of large amounts of individual carbide existing at various heat treated conditions. Simultaneous measurements and determinations were made on particle composition, morphological change, the type, amount and distribution of these carbide phases. Thus the sequence of carbide transformation for this 2CrMoNiWV steel during tempering has been established.

The characteristic microstructures of various heat treated specimens were carefully examined and discussed. Theoretical thermodynamic equilibria predictions were calculated using MTDATA. A very good agreement was found between experimental results and theoretical predictions on those critical transformation temperatures and a good correlation of carbide evolution sequences was obtained. Based on experimental results and theoretical predictions, the role of tungsten in promoting creep resistance to the material is elucidated.

The usefulness of equilibrium thermodynamic calculations using MTDATA in predicting the microstructural changes and carbide evolution has been demonstrated in this work, particularly the separate effect of composition on the stable carbide dispersion where a thermodynamic approach offers great benefits.

A possibly optimised heat treatment route is suggested for the large diameter rotor forgings which involves austenitising at 980°C for 10 hours following by oil quenching and then tempering at 675°C for 20 hours following by air cooling.

Some general conclusions are drawn from this study, especially with regard to the effect of heat treatment on the microstructure of this 2CrMoNiWV steel and suggestions for further work are made.

CONTENTS

NOMENCLATURE AND ABBREVIATIONS

a_0	Lattice parameter
at.%	Concentration in atomic percent
A	Constant
A.C.	Air cooling
A_{C1}	Austenite reaction start temperature
A_{C3}	Fully austenitised temperature
b	Burgers vector
B	Constant
bcc	Body-centred cubic
B_s	Bainite start temperature
B_f	Bainite finish tempeature
$\bar{c}$	Average concentration in the alloy
C	Constant
C_A	Weight fraction of element A
CCT	Continuos Cooling Transformation
CRS	Creep Rupture Strength
d	Interatomic spacing along a specific crystallographic orientation
D	Diffusion coefficient
D_0	Pre-exponential factor for the diffusion coefficient
e	electronic charge
eV	Electron volt
E	Strain energy
EDX	Energy-dispersive X-ray analysis
f'	Critical cooling rate for proeutectoid ferrite formation
fcc	Face-centred cubic
F_s	Ferrite start temperature
F_f	Ferrite finish temperature

G	Shears modulus
h	Plank's constant
HP	High pressure
hrs	Hours
Hv	Vicker's hardness
I	Integrated intensity per unit length of diffraction line
I_A	Real intensity of signal from an element A
$I_A^{'}$	Observed intensity of signal from an element A
ICP	Inductively coupled plasma
ILS	Invariant line strain
IP	Intermediate pressure
IPS	Invariant plane strain
k	Boltzmann constant
k_{AB}	Experimental constant
K_y	Experimental constant
L	Camera length
LP	Low pressure
LVDT	Linear variable differential transducer
m	Electronic mass
M_s	Martensite start temperature
MLI	Mean Linear Intercept
MTDATA	Metallurgical and Thermodynamic Data
n	Number of atoms
N	$\sqrt{h^2+k^2+l^2}$ where h, k and l are plane indices
NPL	Nation Physical Laboratory
O.Q.	Oil quenching
r	Radius of a spherical particle
R	Distance between transmitted and diffracted electron beams
ss	Supersaturated
STEM	Scanning Transmission Electron Microscopy

t	Time
t_c	Time to reach a specific concentration
T	Temperature
TEM	Transmission Electron Microscopy
TTT	Time-Temperature-Transformation
us	Unsaturated
V	Volts
V_b	Volume fraction of bainite
V_α	Volume fraction of ferrite
$\bar{x}$	Mean concentration in bulk alloy

α	Ferrite
α'	Martensite
α_{lb}	Lower bainite
$\alpha_{lb,ss}$	Supersaturated lower bainite
$\alpha_{lb,us}$	Unsaturated lower bainite
α_{ub}	Upper bainite
$\alpha_{ub,ss}$	Supersaturated upper bainite
$\alpha_{ub,us}$	Unsaturated upper bainite
α_w	Widmanstätten ferrite
γ	Austenite
γ_{en}	Enriched austenite
ε	Epsilon carbide
ε_f	Epsilon carbide in ferrite
θ	Bragg angle
θ	Cementite
θ_f	Cementite in ferrite
$\theta_{f/f}$	Cementite between ferrite plates
λ	Wavelength of the electrons
ρ	Specimen density

σ	Stress
σ_d	Dislocation strengthening
$\sigma_{g.b.}$	Grain boundary strengthening
σ_i	Inherent friction stress
σ_p	Precipitate strengthening
σ_{sg}	Strengthening due to subgrains
σ_{ss}	Solid solution strengthening
σ_t	Crystallographic texture strengthening
σ_y	Lower yield stress
σ_{ref}	Reference stress
τ	Shear stress

ADVANCED STUDIES

As part of the course of study I attended the following conferences and workshops combined with a number of informal research seminars presented at Sheffield Hallam University by academic staff from the Materials Research Institute and the School of Engineering.

- "Performance of Bolting Materials in High Temperature Plant Application" organised by the High Temperature Materials Committee of the Materials Engineering Division of The Institute of Materials, 16-17 June, 1994, York, UK

- "Materials for Advanced Power Engineering 1994", 5th conference organised by C.R.M., a European collaborative programme initiated and supported by the European Commission, 3-6 October, 1994, Liege, Belgian

- "Quality Steel -- Advances in Process Technologies to Meet Customer Requirements" organised by Sheffield Metallurgical and Engineering Association, 3-4 April, 1995, Sheffield, UK

- "MTDATA Users' Training Programme" organised by Division of Materials Metrology, National Physical Laboratory, 7-8 September, 1995, Teddington, UK

- "Seventh MTDATA Users' Group Meeting" organised by MTDATA Users' Group and National Physical Laboratory, 23 November, 1995, Teddington, UK

Chapter 1

INTRODUCTION

The most common materials used in high temperature components in power plant have been the low alloy steels of the type 1Cr½Mo, 2¼CrMo, ½Cr½Mo½V and 1CrMoV. These steels have been used extensively world-wide because of their good creep resistance and relative low cost (Townsend, 1993). In order to improve the thermal efficiency of steam turbines in power plants, there is a trend towards increasing the unit size and operating temperature of the steam turbine. As turbine rotors become larger in size and increase in operating temperature and pressure, materials with high creep rupture strength and good toughness are urgently required (Berger, Scarlin, Mayer, Thornton and Beech, 1994).

There were indications that the best combination of creep properties, particularly the toughness of these conventional 1CrMoV rotor materials could not be further improved only by optimisation of heat treatment conditions (Strang, 1972; Roberts and Strang, 1987). A new 2CrMoNiWV rotor steel was claimed to give good physical properties and distinctly higher core toughness in 1000 mm oil quenching rotor forgings (Wiemann, 1991). The improved toughness over conventional 1CrMoV steel will give good "cold rapid start" performance for turbine rotor applications. A considerable amount of research work has been carried out on this material, but the interrelations between heat treatment, microstructure, precipitation characteristics, creep and rupture properties of the alloy have not been systematically studied or understood. Many research workers (Barford and Willoughby, 1971; Murphy and Branch, 1969) suggested in their work on CrMoV steels that by understanding the carbide precipitation sequences related to the heat treatment and compositional

changes, the creep properties can be improved whilst retaining good ductility and toughness.

There is a lack of information regarding the microstructural evolution and compositional changes on the newly developed 2CrMoNiWV rotor material. This area of work deserves further attention and the profound influence of heat treatment on the creep properties of the material should be systematically explored. Tempered samples covering a wide range of tempering temperatures and tempering times are needed for such an investigation.

The intention of this investigation is to study the effect of heat treatment on microstructure and carbide transformation of a commercial 2CrMoNiWV creep resisting steel with a view to optimising the creep properties by variation of the heat treatment conditions, which mainly involve the austenitising temperature, the primary transformation product and subsequent tempering treatment. The predominant objectives of this research are to investigate various heat treatment conditions by which fine dispersions of alloy carbide can be obtained in this steel; characterise the precipitate dispersions and morphologies; and then relate these microstructures to their high temperature creep properties.

The effect of microstructure has been of major concern in the development of steam turbine rotor steels. In previous investigations the role of microstructure has generally been assessed by taking specimens from different regions of large heat treated components, evaluating the microstructural features, and correlating these with the creep behaviour(Bates and Ridal, 1963; Buchi, Page and Sidey, 1965; Murphy and Branch, 1969, Norton and Strang, 1968). Because the heat treated rotors are transformed from austenite by continuous cooling, such specimens contain a range of primary microstructure which may vary from directly transformed proeutectoid ferrite, to different types of bainite. After tempering, the state of the final carbide dispersion in these

steels is likely to be strongly influenced by the primary microstructure following transformation from austenite.

The high temperature stability of particle dispersions is of major importance in determining the effectiveness of dispersion strengthened alloys in high temperature service. The role of alloy carbides in promoting creep resistance and their precipitation mechanism in this steel has been elucidated, and has revealed that the primary heat treatment condition is very critical for any given actual composition.

It is realised that various heat treatment conditions produce changes in metallurgical structure and carbide dispersion characteristics. Based on experimental results and analysis of the data generated from this work, an optimised heat treatment route has been proposed. From this point of view, the best combination of creep, rupture and toughness properties of the new rotor steel in service might be established, thus ensuring possibly improved performance.

The experimental work was complemented by a review of the available literature on the strengthening mechanisms of creep resistant low alloy steels, the effect of heat treatment on microstructure and also on the role of carbides in low alloy steels. During the course of the work a wide range of advanced experimental techniques have been strengthened and developed. These included dilatometry, X-ray diffraction (XRD), scanning electron microscopy (SEM), transmission electron microscopy (TEM) and energy dispersive X-ray microanalysis (EDX), *etc.* It will be demonstrated how modern electron microscopes equipped with microanalytical facilities together with other analytical systems now permit the acquisition of data on chemical composition and crystallographic structure in a more quantitative fashion than hitherto possible.

The results of thermal analysis for this 2CrMoNiWV steel are presented in the form of continuous transformation diagrams with the comparison of theoretical thermodynamic calculation results.

An innovative carbide extraction technique has been developed for the X-ray diffractometer studies which has been proven to be simple and effective. This sample preparation method could be widely applied to similar research work and the remnant creep life prediction of precipitation strengthened alloy steels in high temperature service.

This new material is different from conventional 1CrMoV steels in that it can, with the addition of W, form very stable carbides at the commercial austenitising temperature range and may decrease the proportion of carbon available for other alloy carbides precipitation during tempering and creep testing. The W addition seems useful for the improvement of creep rupture strength of ferritic steels , the reasons of the physical processes responsible for such improvements had not been realised (Colbeck and Rait, 1950). In this investigation, the role of W addition has been examined, and unique effects of W in the steel have been analysed. The precipitation behaviour that is specific to this 2CrMoNiWV rotor steel has further been discussed by the variation of W content using the metallurgical thermodynamic databank (MTDATA).

Chapter 2

LITERATURE REVIEW

2.1 Strengthening Mechanisms of Low Alloy Steels

The principal influence on development of steam turbine rotor materials is provided by the compositional balance to form the required fine and stable dispersion of alloy carbides (Strang, 1972). However, the heat treatments that are performed to transform from austenite to bainitic structure, and to modify the bainitic microstructure to produce the desired properties in the final product is of great importance. When the high temperature face-centred cubic (fcc) phase, austenite, in steel decomposes to the less dense body-centred cubic (bcc) phase, a number of different microstructures and morphologies can form which depend on the cooling rate, the presence of alloying elements, and the conditions and availability of lower energy nucleation sites for heterogeneous nucleation.

2.1.1 The Hall-Petch Equation

It was empirically established by Hall (1951) and Petch (1953) that the lower yield stress, σ_y, in a discontinuously yielding material was related to the grain diameter, d, by

$$\sigma_y = \sigma_o + K_y d^{-1/2} \quad \text{.....(2.1)}$$

Where σ_o and K_y were taken as experimental constants.

The theoretical model for the above equation assumed that a dislocation source, operating within a grain, produced a pile-up of dislocations at the grain boundary. The dislocation pile-up caused the development of a stress within the adjacent grain which, at a critical value, nucleated slip by the formation of a new dislocation source within that grain. Thus slip propagated from grain to grain and since the grain size determined the number of dislocations in the pile-up, and consequently the stress generated, it can be seen that the coarser the grain size the higher the stress generated, *i.e.* the lower the applied stress required for yielding (Gladman and Pickering, 1983).

The term σ_o was identified as the friction stress opposing the movement of individual dislocations. Since the development of the basic Hall-Petch equation, the friction stress term, σ_o, has been expanded to take into account various strengthening mechanisms that contribute to the friction stress. A general equation of the form

$$\sigma_y = (\sigma_i + \sigma_{ss} + \sigma_p + \sigma_d + \sigma_{sg} + \sigma_t) + K_y d^{-1/2} \quad \text{.....(2.2)}$$

is often quoted where σ_i is the inherent friction stress, σ_{ss} is the solid solution strengthening, σ_p is the precipitate strengthening, σ_d is the dislocation strengthening, σ_{sg} is the strengthening due to subgrains and σ_t a crystallographic texture strengthening parameter.

Equation (2.2) suggests that all the strengthening mechanisms are additive to each other. The linear summation is a simplifying assumption and is very commonly used. However, as suggested by Gladman and Pickering (1983), it may be erroneous. It has been shown, for example, that for coherent precipitates, the grain size and precipitation hardening components may be additive, but for non-coherent particles the yield stress may be independent of

grain size (Hornbogen and Staniek, 1974). Onel and Nutting (1979) have shown that when the carbide particles were precipitated only at the grain boundaries they had no effect on the strength and a simple Hall-Petch equation was adequate for explaining the yield strength. However, when the precipitates were also present within the grains a precipitation hardening term must be added to the grain size dependence of yield strength. In this latter case they observed that the value of K_y increased, indicating non-linear interactions between the two strengthening contributions.

A root mean square summation

$$\sigma = \sqrt{(\sigma_A^2 + \sigma_B^2)} \quad \text{.....(2.3)}$$

where σ_A and σ_B are the flow stresses associated with two distinct modes of strengthening, can also be used for the prediction of the yield strength.

A number of investigators (Baker, 1983; Irvine and Baker, 1984) have shown preference for the root mean square summation and found good agreement with experimental results. Kocks (1979) concluded from statistical calculations that the root mean square summation applies over a large range of obstacle strengths and densities, whereas the linear summation is better for many weak and few strong obstacles, but only over a limited range of these variables.

2.1.2 Grain Boundary Strengthening

In the case of polygonal ferrite-pearlite structures much quantitative work has been done on the effect of grain size on yield strength and the values of the constants in equation (2.1) can be quoted with some confidence (Gladman and

Pickering, 1983). However, in the case of bainite, martensite and their tempered structures, much less success has been achieved in quantitatively describing the grain boundary contribution to the total strength. The reason for this is that in these structures, the definition of grain size is not particularly straightforward since there are usually several types of boundaries present. The prior austenite boundaries are still present but account only for a small fraction of total grain boundary surface. However, Grange (1966) and Porter and Dabkowski (1970) showed that when the prior austenite grain size of both as quenched and tempered low alloy steels, was varied over a wide range, significant changes resulted in the strength. The strength variations followed Hall-Petch relationships in which the austenite grain size was the controlling structural parameter.

More recently the strength of lath martensite and bainite has been related to the size of the packets of parallel laths that subdivide the original austenite grains into roughly equiaxed units. Many workers showed a linear dependence of martensite packet size on prior austenite grain size (Roberts, 1970; Marder and Krauss, 1970). When using the lath size as the grain size the crystallography of the laths, with respect to the operative slip systems, and their relationship to the tensile axis, then becomes important. There is also doubt as to whether the lath length, width or thickness should be used as a measure of grain size. However, Gladman and Pickering (1983) suggested that because of the multiplicity of slip systems in the body-centred cubic structure and the 24 possible variants of the Kurdjumov-Sachs orientation relationship, the effect was effectively random so that a simple measure of the mean linear intercept was sufficient.

It seems that a complete model for grain boundary strengthening in martensite should include the strengthening contributions of both packet and

lath boundaries. In fact Whiteman (1977) developed the following empirical equation for grain boundary strengthening, $\sigma_{g.b.}$, in martensite

$$\sigma_{g.b.}\ (MPa) = 28d^{-1/2} + \sigma_b \quad \text{.....(2.4)}$$

where d is the mean linear intercept packet size in millimetres and σ_b the lath boundary strengthening term given by the difference between the observed yield strength and the sum of all other strengthening contributions.

2.1.3 Solid Solution Strengthening

It is well known that the introduction of solute atoms into iron causes an increase in strength (Irvine and Pickering, 1960; Pickering and Gladman, 1963). For binary Fe-X alloys, the strengthening produced was a function of the concentration of the alloying element; with several alloying elements present, they showed that effects of the individual elements were simply additive.

Irvine and his colleagues (1961) found that interstitially dissolved elements such as carbon and nitrogen were the most effective in producing strengthening. Substitutionally dissolved elements were less effective and could be distinguished between the ferrite forming elements and austenite forming ones, the latter resulting in only marginal increases in strength. Carrying on from this work, Irvine and his co-workers (1969) developed the following empirical equation for the strength of austenitic stainless steels.

$$\begin{aligned} 0.2\%\ \text{Proof Stress}\ (N/mm^2) = {} & 4.1 + 32(N\%) + 23(C\%) + 0.29(W\%) \\ & + 2.6(Nb\%) + 1.7(Ti\%) + 0.82(Al\%) \\ & + 0.16(\delta_\alpha\%) + 0.46d^{-1/2} \quad \text{.....(2.5)} \end{aligned}$$

where the concentrations of the alloying elements are in *wt.*%, δ_α% is the percentage of delta ferrite in the structure and *d* the austenite grain size in mm.

Similar behaviour was observed by Pickering and Gladman (1963) for plain carbon steels with a ferrite-pearlite microstructure. They showed that all the alloying elements examined, with the exception of chromium, increased the yield strength and extended the Hall-Petch equation to include solid solution strengthening

$$\sigma_{L.Y.P.} = \sigma_i + \Sigma K' (X\% \text{ alloy}) + K_y d^{-\frac{1}{2}} \quad \text{.....(2.6)}$$

where $\sigma_{L.Y.P.}$ is the lower yield stress, σ_i is the friction stress, both in ton/in^2, K' is a proportionality constant for the effect of each solute and X% the alloy concentration in *wt.*%.

The effect of substitutional alloying elements on the strength of iron-carbon martensite is always minor in comparison with the effects of carbon and nitrogen and it is difficult to separate solution hardening from indirect effects on grain size and M_s temperature (Christian, 1971). Irvine and his colleagues (1960) found that a hardness increase of 100-160 VPN can be obtained by the addition of up to 4% of alloying elements in iron-carbon alloys. They concluded, however, that the strengthening produced was partly due to the reduction in the amount of autotempering and partly due to solid solution hardening.

Several theories have been brought forward to explain solid solution hardening (Fleischer, 1967). All models show that the intensity of solid solution strengthening is dependent upon: (a) the difference in size between the solute and solvent atoms. (b) the difference in shear modulus between solute and

solvent. A suitable expression for the modulus interaction is more complex and several have been proposed (Pickering, 1978).

The general outcome of the solid solution strengthening theories was that the substitutional solutes cause symmetrical distortion of the solvent lattice and this leads to relatively moderate strengthening effects (Seeger, 1957). On the other hand, interstitial solutes, such as carbon and nitrogen in α-iron, introduce asymmetrical lattice distortions and thus exert much greater strengthening effects than substitutional solutes. This is further augmented by the very strong interaction that occurs between interstitial solute atoms and dislocations, coupled with the fact that the solute atoms tend to segregate to dislocations (Seeger, 1957).

2.1.4 Work Hardening

A number of theories have been developed to explain the work hardening of metals (Cottrell, 1953; Nabarro *et al.*, 1964). These theories consider the mutual observation of dislocations gliding on parallel or intersecting slip systems. There are a number of ways in which dislocation interaction can occur: (1) through an interaction of the stress field of the dislocations (Cottrell, 1953); (2) through interactions which produce sessile locks (Mott, 1960) and (3) through the interpenetration of one slip system by another, which results in the formation of dislocation jogs (Nabarro *et al.*, 1964). Detailed descriptions of the work hardening theories are given in the reviews by Nabarro and his colleagues (1964) and McLean (1962).

Livingston *et al.* (1963) suggested that all work hardening theories predict that the flow stress is proportional to $\rho^{1/2}$ where ρ is the dislocation density. Nabarro and his colleagues (1964) considered the flow stress, σ,

corresponding to different models of the work hardened state and found that all models led to formulae of the type

$$\sigma = \frac{Gb}{w} \rho^{1/2} \quad \text{.....(2.7)}$$

where ρ is the dislocation density, G is the shear modulus, b is the Burgers vector and w a number of the order of 3-5.

The above equation has been generally accepted and the familiar equation

$$\sigma_d = \alpha G b \rho^{1/2} \quad \text{.....(2.8)}$$

where α is a proportionality constant and ρ is the dislocation density, has been used by many investigators to calculate the dislocation strengthening contribution, σ_d, to the yield strength (Cox, 1967; Lapointe and Baker, 1982).

There is, however, considerable disagreement as to the appropriate value of the proportionality constant, α. Therefore there could be an appreciable error in the estimate of the dislocation strengthening contribution to the yield stress (Baker, 1983).

2.1.5 Precipitation strengthening

There is fairly general agreement that the strengthening effects of second-phase particles differ depending on whether the particle itself does or does not deform during the yielding of an alloy (Kelly and Nicholson, 1971; Kelly, 1973). The particles may act as impenetrable barriers to dislocation

motion and force the glide dislocations to bow-out and by-pass them following the Orowan mechanism. Alternatively, the second-phase particles may be cut or sheared by the dislocations. In either case the theoretical treatments of second-phase particle strengthening are based on the following model.

A dislocation moving through an array of obstacles bows out between the particles as shown in Figure 2.1. When the angle ϕ between the two arms of the dislocation reaches a certain critical value, the dislocation breaks free from the obstacles. At this critical point the obstacle strength, F, is related to the dislocation line tension, T, by

$$F = 2T \cos(\phi/2) \quad \text{.....(2.9)}$$

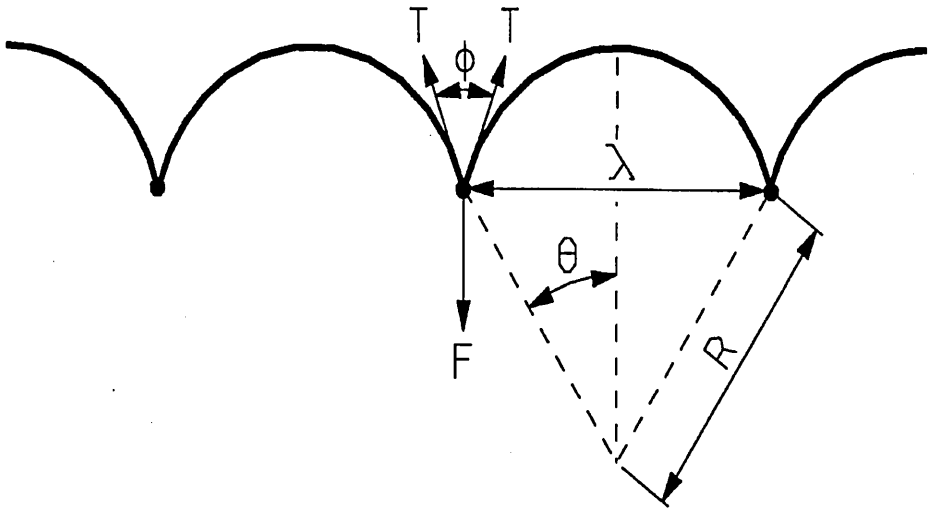

Figure 2.1 Dislocation held up at obstacles and bowing angle ϕ is defined as shown (after Kelly, 1973)

When the breaking angle ϕ = 0, the particle behaves as an impenetrable obstacle, while for values of ϕ > 0, the particle can be sheared by the glide dislocation, where the required shearing force is equal to *F* (Kelly, 1973). The shear stress, τ, needed to cause the dislocation to break away from the obstacle is given by

$$\tau = F / b\lambda = \frac{2T\cos(\phi/2)}{b\lambda} \quad \text{.....(2.10)}$$

where λ is the effective spacing between the particles and *b* is the Burgers vector.

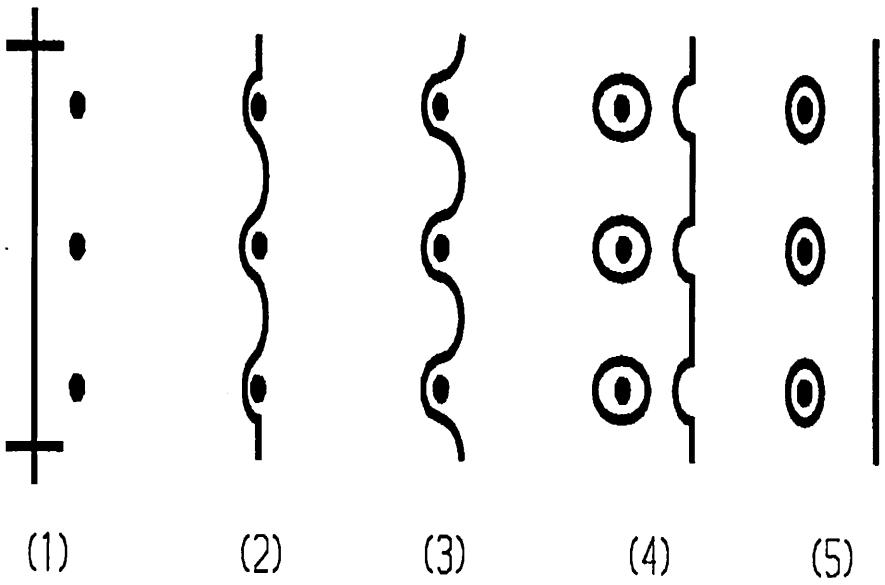

Figure 2.2 Schematic of stages in passage of a dislocation between particles by the Orowan process (after Orowan, 1948)

In the case of deformable obstacles, such as zones or coherent precipitates that can be cut by the dislocations, the strengthening effect of the particles is due to the additional work required to make the dislocation cut the particles. This process, which usually occurs in alloys age-hardened up to maximum hardness, produces strengthening from various sources such as coherency strains, chemical hardening, order hardening, stacking faults and modulus hardening.

For alloys containing strong non-deformable particles, the dislocation by-passes the obstacle (Figure 2.2) rather than passing through it. Orowan (1948) first showed that when particle by-passing occurs the applied stress is equal to

$$\tau = 2T/b\lambda \quad \text{.....(2.11)}$$

The Orowan equation is adequate for approximate calculations of the strengthening contribution to the yield stress due to the presence of undeformable particles. When attempting to identify the actual strengthening mechanism as an Orowan process, however, certain modifications to equation (2.11) are required (Martin, 1980).

There are two mechanisms of creep: dislocation creep and diffusion creep. The rate of both is usually limited by diffusion. Diffusion becomes appreciable at about 0.3 T_M -- that is why materials start to creep above this temperature.

Diffusion of atoms can help to "unlock" dislocations from obstructions in their path, and the movement of these unlocked dislocations under the applied stress controls the rate of dislocation creep. Consider the case of a dislocation which cannot glide because a precipitates blocks its path, see Figure 2.3. The glide force (τb per unit length) is balanced by the reaction f_0 from the precipitates. But unless the dislocation intersects the precipitate at its mid-

plane there is a vertical component of force. It is the component τb tan θ, which tries to push the dislocation out of its slip plane.

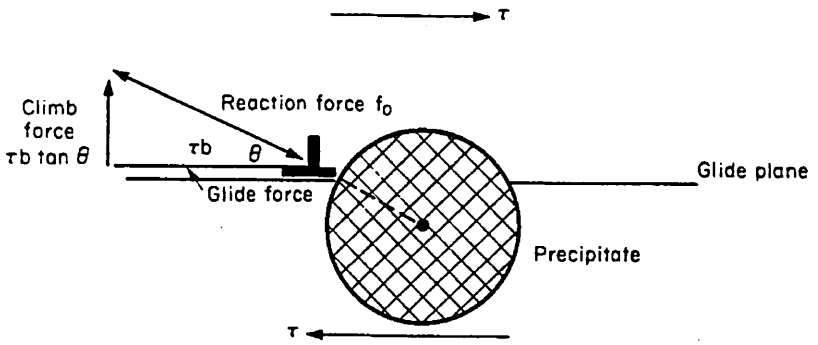

Figure 2.3 The climb force on a dislocation (after Ashby and Jones, 1980)

The dislocation cannot glide upwards by the shearing of atom planes -- the atomic geometry is wrong for the dislocation to work in this way -- but the dislocation can move upwards if atoms at the bottom of the half-plane are able to diffuse away. The process is called "climb", and since it requires diffusion, it can occur only when the temperature is above 0.3 T_M. At lower temperatures (0.3-0.5 T_M) core diffusion tends to be the dominant mechanism, and at higher temperatures it is bulk diffusion that dominates (Ashby and Jones, 1980).

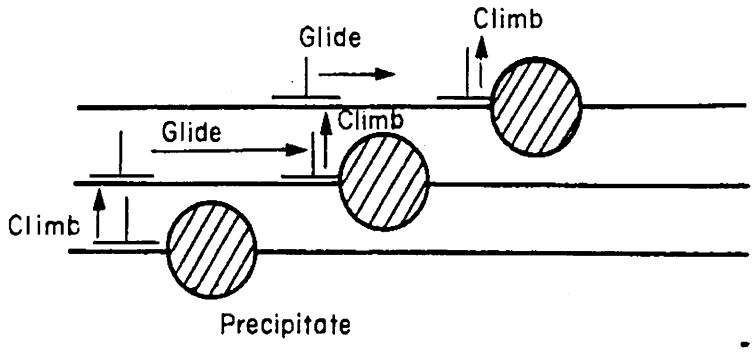

Figure 2.4 How the climb-glide sequence leads to creep (after Ashby and Jones, 1980)

The climb process unlocks the dislocations from the precipitates which pin them and further slip can then take place (Figure 2.4). Similar behavior takes place for pinning by solute, and by other dislocations. Ultimately, of course, the unlocked dislocations glide up to adjacent obstacles, and the whole cycle of events takes place again. This explains the progressive, continuous nature of creep.

2.2 Microstructure of Creep Resistant Low Alloy Steels

Past studies on the effect of microstructure on the creep strength of CrMoV steels have mainly considered the effect of primary transformation products (martensite, bainite or directly transformed ferrite) which have generated in sections of material continuously cooled from the austenitising temperature and consequently tempered to precipitate and coarsen alloy carbides (Norton and Strang, 1969; Bates and Ridal, 1963; Murphy and Branch, 1969). Continuous cooling treatments have been used in these experimental studies largely because steam turbine rotors are generally oil quenched in industrial practice. Thus the transformation products in the cross-sections of a large rotor could be correlated to the structure obtained by different cooling rates.

2.2.1 The Effect of Prior Microstructure

In the low alloy creep resisting steels, prior structure *i.e.* ferrite, bainite or martensite, can have a distinct effect on the creep properties (Pickering, 1990). Norton and Strang (1969) found that an initial upper bainite structure showed the highest creep resistance compared with a lower bainite or ferrite structure

(Figure 2.5). The reason why upper bainite was a better initial structure than lower bainite or martensite was that after tempering, it showed generally superior tempering resistance which was due to the most satisfactory dispersion of fine vanadium carbide. Other work on 2¼%Cr-1%Mo and 1%Cr-¼%Mo steels (Toft and Marsden, 1961) had shown although the initial structure may control the creep rupture strength, when the steels of different initial structure were tempered to simulate structural degradation during a creep test their rupture strengths all converge. Also, prior spheroidisation of the structure produced a short time rupture strength dependent on the degree of spheroidisation but a long time rupture strength which was independent of the degree of spheroidisation. The higher the short time strength, the more rapidly did the stress versus rupture life curve decrease until at long rupture times the rupture strength was constant.

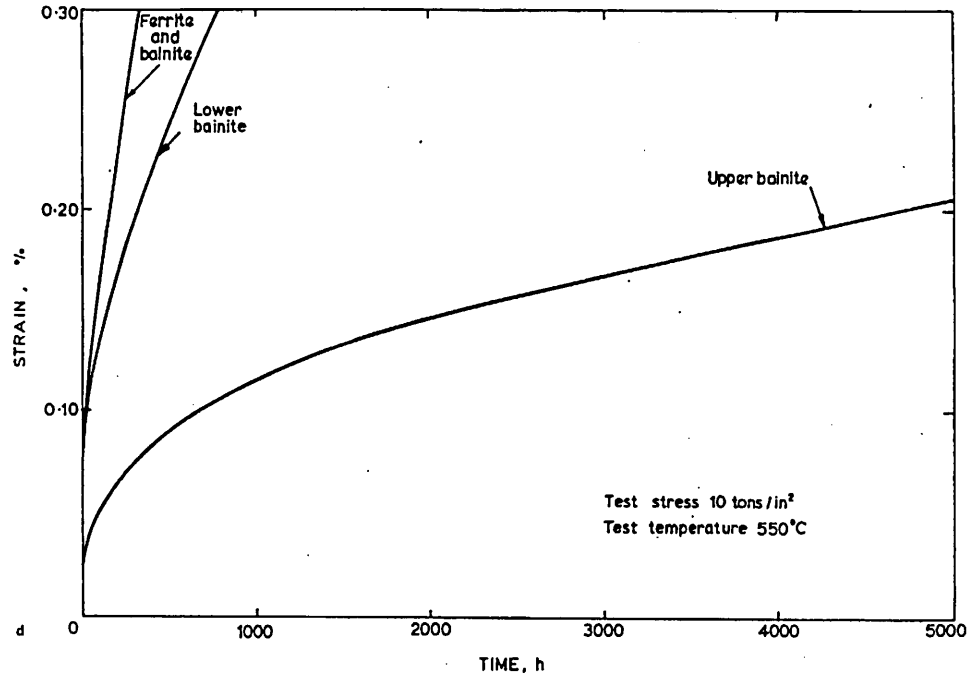

Figure 2.5 Relationship between creep strength and transformation product (after Norton and Strang, 1969)

Bainitic CrMoV steels were extensively used for their good high temperature mechanical properties in a variety of applications, such as rotors, bolts, and steam pipework (Bates and Ridal, 1963; Murphy and Branch, 1969; Barford and Willoughby, 1971). These steels were usually used in the normalised and tempered condition at service temperatures of the order of 450-565°C. The mixed microstructures produced by normalising, they were often referred to as granular bainite, although an appreciable amount of upper bainite can be identified by electron optical examination. The proportion of upper bainite in the microstructure varied with both composition and heat treatment, but test data have been published showing improved high temperature strength for bainitic content up to 70%. This was generally considered to be due to a fine dispersion of V carbide which confers high strength and stable dislocation substructure which resists recovery, thereby promoting a reduction in the overall creep rate. However, while creep rates were low, the rupture ductility was also reduced, and it has been claimed that the ferrite/bainite boundaries were sites for early initiation of creep cavitation and, therefore, can be responsible for the low creep ductility (Strang, 1972).

In solid solution alloys, cold working reduces the primary creep rate by introducing a high initial dislocation density (Sellars, 1974) but recovery during creep decreases the dislocation density which can then lead to creep rates equivalent to those of an initially recrystallised matrix. Extreme cold work causes recrystallisation during creep and so rapidly allows the creep rate to increase. However, second phase particles, such as carbides in steels can stabilise the dislocation structure and maintain a reduced creep rate. Such an increased dislocation density can be introduced to steels by shear type transformations which produce bainitic or martensitic structures and these dislocations can lead to more widespread carbide nucleation, but the stability of the dislocation structure depends critically on the spacings of the precipitated carbides. During creep the increased stored energy can cause recrystallisation to occur at much smaller particle spacings, and such an effect has been

observed in a very long time creep specimen in Cr-Mo-V steel despite the profuse precipitation (Williams and Wilshire, 1981). It is generally accepted that the reduction in creep strength associated with this degradation is responsible for the initiation of tertiary creep in low alloy steels and McLean (1967) has calculated the critical spacing above which the creep rate increases rapidly.

Variable effects of prior precipitation treatments on the creep rate have also been observed (Irvine, Murray and Pickering, 1961). Precipitation at low temperatures can lead to a marked decrease in the creep rate whilst precipitation at higher temperatures results in a marked increase in the creep rate. This may be explained as a small particle size, for a given volume fraction, giving a small inter-particle spacing and during the creep test the particles will grow and increase the particle spacing to the optimum, thus maintaining a low creep rate. On the other hand, a large particle size with a spacing greater than the optimum will lead to still further increase in the particle size and spacing during creep test with concomitant higher creep rate. The importance of particle size, particle spacing and particularly the particle coarsening rate are clearly of great significance.

2.2.2 Microstructural Changes During Creep

Reference has been made to recovery and recrystallisation occurring during creep which can lead to increased creep rates (Williams and Wilshire, 1981). This is often referred to as microstructural degradation, but as can be seen from the effects of precipitate particle size and spacing, not all microstructural changes occurring during creep should be classed as degradation. Some may be positively beneficial during creep, such as dynamic strain ageing by interactive solute effects, growth of particles of less than the optimum size for the minimum creep rate, and also precipitation of new alloy carbide phases.

The coarsening of carbides is of great importance and it is possible to produce large reductions in the rate of carbide coarsening by having metal/carbon ratios very much lower than the stoichiometric ratio (Pickering, 1990). Thus it decreases the dissolved metal atom content in the matrix so that the metal flux during Ostwald ripening is decreased and the rate of carbide coarsening is also decreased. This could have a marked effect in preserving a low creep rate over a longer period of time, but unfortunately results in a smaller volume fraction of carbides so that the minimum creep rate, whilst being stable over prolonged periods, is not so low as would be achieved with a stoichiometric metal/carbon ratio.

Another feature of carbide precipitation during creep is that in steels which have been tempered above the creep or service temperature, as is usually the case to enhance microstructural stability, further precipitation can occur at the creep or service temperature due to the temperature dependence of solubility (Williams and Wilshire, 1981). These carbides precipitated during creep are often very small and improve the creep resistance. Moreover they may be of a different type from those formed during the initial tempering treatment.

Finally, during creep, transformations in the precipitated carbides may occur from one carbide type to another. This may alter the coarsening rate of the carbides with considerable effect on the creep rate. But the effects of creep on the rates of different carbide transformations are very variable, some being accelerated and others being retarded by the creep deformation. The $M_7C_3 \Rightarrow M_{23}C_6$ transformation seems generally to be retarded whilst the $M_2C \Rightarrow M_6C$ transformation is accelerated (Sellers, 1974). Mechanisms have been proposed to explain these effects (Bilby and Pickering, 1959), but the important feature is that the creep rate could suffer considerable changes during the creep test.

2.2.3 The Distribution of Alloying Elements in Steels

In steels in which the austenite transforms to ferrite and carbides on slow cooling, the role of alloying elements can be split into three categories. Firstly, there are elements which are normally found mostly in the ferrite phase such as Ni, P and Si, their solubility in cementite or in alloy carbides being quite low. Secondly, there are elements which can both form stable carbides and can be found in solid solution within the ferrite. Typical elements which exhibit this type of behaviour are Mn, Mo, Cr, V, W, Ti and Nb. The amount of each element needed in different carbide depends on the carbon content of the steel and heat treatment conditions. However, alloying elements are usually present in excess of carbide consumable amount, with the remainder going into solid solution in ferrite (Honeycombe, 1981).

2.2.4 The Effect of Alloy Elements and Cooling Rate on the γ/α Transformation

Increases in undercooling and rate of cooling from the austenite region limit the ability of alloying elements in Fe, and the Fe atoms themselves, to diffuse during the transformation to form the equilibrium structure, hence leading to an increased tendency for the formation of metastable structures (Krauss, 1980).

The alloying elements are divided into two types, those in substitutional and those in interstitial sites. Substitutional elements (e.g. Cr, Mo etc.) occupy lattice sites within the Fe lattice and require vacant sites in order to diffuse, whereas interstitial elements (e.g. C, N) can diffuse much more quickly, occupying and moving between interstices within the Fe lattice (Honeycombe, 1981). Diffusion of the interstitial elements can only be suppressed at high

undercoolings or fast cooling rates. In the case of the diffusion mode of the substitutional elements being dominant, it was found that growth occurs with partition of the element between α and γ under local equilibrium conditions. The ferrite grows at a slow rate determined by diffusivity of the alloying elements within the austenite (Bhadeshia, 1992). It is in fact more common for a reaction to be controlled by the diffusion of carbon (interstitial), in which case growth occurs with no partitioning of the alloying element. The observed growth rates, since they are controlled by the diffusivity of carbon, are relatively high (Bhadeshia and Edmonds, 1979). It is also possible to have a diffusionless transformation such as the martensite reaction. Whether the reaction process and rate is controlled by either diffusion of interstitials or substitutionals, or is diffusionless, is determined by a combination of thermodynamic and kinetic constraints (Thomson, 1992). Hence, both the cooling rate and alloying element content are critical to the development of a particular microstructure.

2.2.5 The Effect of Heat Treatment

For power plant applications, the rotor steels are usually oil quenched after austenitisation. The times specified for all the treatments depend on the component size, ostensibly to allow the steels to reach a uniform temperature. The temperature to which the steels are heated for austenitisation is usually at least 50°C above the A_{C3} temperature, and hence depends on the steel composition. Lower temperatures lead to correspondingly smaller austenite grain size, a factor that can be beneficial to mechanical properties, but can be adverse to the creep properties (Honeycombe, 1981).

It is impossible to achieve uniform cooling throughout the thick section components typically found in power generation industry, the heat treatments cover a wide range of cooling rates. For a typical range of chemical compositions encountered within the 2.25Cr-1Mo designation, the normalised

microstructures consist of mixtures of ferrite and bainite. The effect on the mechanical properties of such large variations in microstructure is very pronounced during the early stages of service, but after long periods at elevated temperatures, the differences in creep strength can become insignificant (Murphy and Branch, 1971).

The use of steels for castings in the normalised condition, rather than a quenched and tempered martensitic condition, seems to be based on the fact that the ferrite and bainite microstructure is more creep resistant than the martensitic microstructure (Senior, 1988). A continuous cooling heat treatment is also more convenient for large components. Steels in power plant can be required in very large sections; uniformly martensitic microstructures are then impossible to produce using commercial heat treatments. In fact, one of the most important characteristics of these CrMoV low alloy steels are their high bainitic hardenability, which allows ferrite growth to be avoided during cooling, making it suitable for heavy section applications, such as rotors. A more detailed discussion is given below because it is within this bainitic structure that changes in carbide are carefully examined.

2.3 Bainitic Structure in Low Alloy Steels

The vast majority of creep resisting steels are used in power plant typically within the temperature range 400-565°C (Strang, 1995). In rotors, the main stress normally originates from rotational centrifugal force due to the dead weight of the rotor and large assembly of blades. The most important property requirement is creep resistance, since increased creep strength can prolong service life. There are many advantages to be achieved by using extra strength to reduce the rotor size.

2.3.1 Bainite Morphology and Carbide Precipitation

Bainite is a mixture of ferrite and carbides which is formed by the decomposition of austenite at a temperature above the martensite start temperature, M_s, but below the temperature at which pearlite can form. The bainite transformation, being intermediate between the diffusionless martensite and diffusional pearlite reactions has presented difficulties in interpretation in the past (Aarronson, 1986), although these are now beginning to be resolved (Christian and Edmonds, 1984; Bhadeshia, 1988; Bhadeshia and Christian, 1990).

There are three controversies regarding the formation of bainite. One concerns the mechanism by which lattice atoms leave the fcc lattice and form the new bcc lattice. The second one concerns the question of local equilibrium and the role of carbon diffusion. The third one concerns the question whether each little region transforms in two steps or not (Hillert, 1995).

The formation of bainitic ferrite leads to an increase in the carbon concentration of retained austenite. There are two different morphologies associated with bainite formation. Upper bainite forms at the higher temperature within the range, the cementite precipitating from films of carbon-enriched austenite which separate the sheaves of bainitic ferrite. The platelets within a sheaf are all in the same orientation in space and the orientation between α_b and γ is the same as for α/γ (Bhadeshia, 1988). In lower bainite, however, cementite also forms within the platelets of ferrite. In contrast to the cementite obtained after tempering supersaturated martensite, the carbides formed within any given lower bainitic plate usually occur in a single crystallographic orientation (Bhadeshia, 1988). There are therefore two kinds of cementite particles, those growing from carbon-enriched austenite and those precipitating from supersaturated ferrite. The precipitation of cementite

generally occurs as a secondary reaction after the growth of bainitic ferrite. The precipitation sequences are summarised as follows (Thomson, 1992):

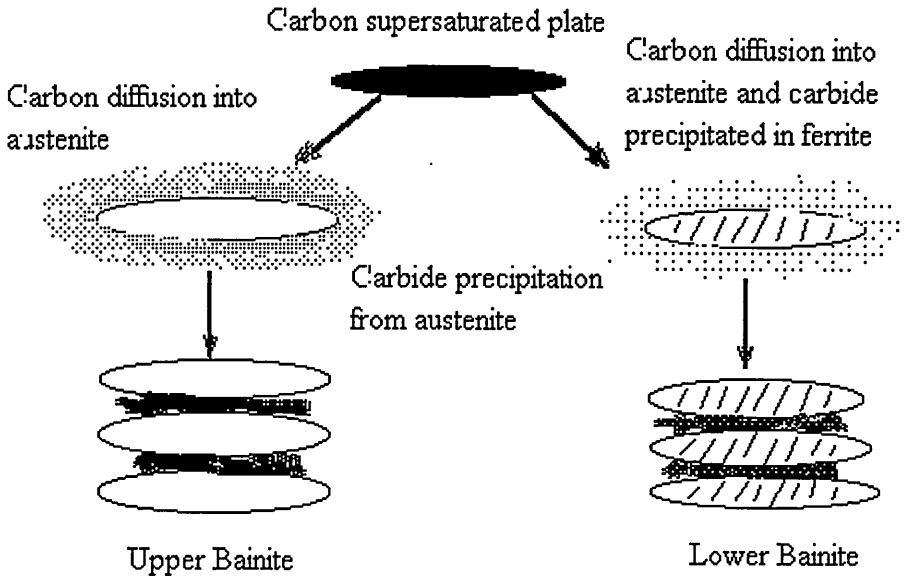

Figure 2.6 The mophologies of upper and lower bainite (Thomson, 1992)

1. Upper bainite

$$\gamma \rightarrow \gamma + \alpha_{ub,ss} \rightarrow \alpha_{ub,us} + \gamma_{en} \rightarrow \alpha_{ub,us} + \alpha + \theta$$

2. Lower bainite

(a). High dislocation density

$$\gamma \rightarrow \gamma + \alpha_{lb,ss} \rightarrow \theta_f + \alpha_{lb,us} + \gamma_{en} \rightarrow \alpha_{lb,us} + \alpha + \theta_{f/f} + \theta_f$$

(b). Low dislocation density

$$\gamma \rightarrow \gamma + \alpha_{lb,ss} \rightarrow \varepsilon_f + \alpha_{lb,us} + \gamma_{en} \rightarrow \alpha_{lb,us} + \varepsilon_f + \alpha + \theta_{f/f} \rightarrow \alpha_{lb,us} + \theta_f + \theta_{f/f} + \alpha$$

The two different morphologies of bainite are illustrated in Figure 2.6

2.3.2 The Shape Change Associated with the Transformation

It has been found (Bhadeshia and Waugh, 1982; Stark *et al.*, 1987) that iron and substitutional atoms do not diffuse during the bainite reaction. Various observations imply that the formation of bainite involves the co-ordinated movement of the substitutional solute and iron atoms across a glissile transformation interface. These include the fact that the shape change gives rise to an elestically accommodated stored energy in the sheaves in the region of 400 J/mol. The high temperature associated with the transformation result in the yield strength of both phases being comparatively low, and so plastic deformation can occur. The high dislocation density induced by attempts to relieve some of this strain is then responsible for hindering the advance of the transformation front, and thus limiting the size of the bainite sheaves (Bhadeshia and Edmonds, 1979). The ferrite plates always have a crystallographic orientation relationship with γ which is similar to that found between γ and α. This type of co-ordinated movement cannot generally be sustained across randomly oriented grains, and so bainite growth is impeded by austenite grain boundaries. This is in contrast to diffusional transformations in which the product phase may readily grow across grains of the parent phase which are in different orientations.

2.3.3 The Role of Carbon in the Bainite Transformation

There are several explanations concerning the precise role of carbon during the bainite transformation (Christian and Edmonds, 1984; Bhadeshia, 1988). Bainite should form below a certain temperature, at which α and γ of the same composition have the same free energy, which can be shown to make it thermodynamically possible for the transformation to be diffusionless. It is also possible to have a paraequilibrium transformation in which the substitutional lattice is configurationally frozen, but the carbon redistributes to equalise the chemical potential in all phases. An intermediate degree of partitioning is also possible.

If growth involves diffusionless transformation then any excess carbon in bainitic ferrite can partition into the retained austenite after the transformation because of the high diffusivity of interstitial carbon. So it is not possible to determine directly the carbon concentration of the ferrite during its growth. The bainite reaction is found to stop before the carbon concentration of the retained austenite reaches that of the equilibrium or paraequilibrium phase boundary, *i.e.* when diffusionless transformation of carbon-enriched austenite becomes thermodynamically impossible. The extent of the reaction is a function of temperature, increasing as the temperature is reduced (Christian and Edmonds, 1984).

Bhadeshia (1987) summarised the bainite reaction as a displacive transformation in which there is no diffusion of substitutional element or iron across the transformation interface. The excess carbon trapped in bainitic ferrite is removed by a combination of diffusion into the residual austenite, and by the precipitation of carbides between the ferrite. The retained austenite eventually decomposes by a diffusional transformation into a mixture of more carbides and ferrite. The plate morphology of bainite is explained by the minimisation of strain energy due to the invariant plane strain (IPS) shape

change associated with the displacive mechanism of the transformation. The kinetics of bainite are also shown to be consistent with the proposed diffusionless, displacive transformation mechanism (Bhadeshia, 1990).

2.4 Role of Carbides in Low Alloy Steels

The mechanical properties of ferritic steels are controlled in part by the inherent strength of the matrix and in part by the way in which deformation of the matrix is affected by its interaction with carbide particles (Honeycombe, 1985). On exposure to high temperature there will be change in composition, structure, and morphology of the carbides and these changes may have consequential effects upon the deformation behaviour of the steel.

2.4.1 Carbide Phase in Alloy Steels

In steels, the pure binary carbides do not generally occur as there is always some solubility of the alloying elements in the various carbide phases; in some cases these solubilities may be very extensive. It is usual to refer to the carbides by general formulae, *e.g.* $M_{23}C_6$, M_6C, where M indicates a matrix of metal atoms. It should also be aware of the fact that N can and will substitute for C or be in combination with C to form carbides. Often the carbides are stable over an appreciable composition range, *i.e.* they are not stoichiometric, and the general formulae should be regarded as representing certain structure types rather than specific chemical species.

(a) M_3C This is an Fe rich carbide having the orthorhombic structure of cementite; consequently it is often referred to as Fe_3C. However, this carbide can take into solution very considerable amounts of some other elements. Cr is

highly soluble in M_3C; up to one fifth of the Fe atoms may be replaced Cr (Woodhead and Quarrell, 1965).

(b) M_7C_3 This is a Cr rich carbide with the hexagonal structure of Cr_7C_3; it has a very high solubility for Fe which can, in fact, become the major element. This carbide also takes small amount of Mo in CrMoV steels (Dyson and Andrews, 1969).

(c) $M_{23}C_6$ In steels free from Mo and W, this is again a Cr rich carbide having the complex fcc structure of $Cr_{23}C_6$. In such steels Fe can replace Cr up to a metal-atom ratio of about 0.4. In steels containing Mo or W, the $M_{23}C_6$ structure can occur in the total absence of Cr. A true ternary carbide $Fe_{21}Mo_2C_6$ or $Fe_{21}W_2C_6$ can form (Woodhead and Quarrell, 1965).

(d) M_6C This carbide is essentially a ternary carbide of Fe and Mo or Fe and W although it shows appreciable solubility for other elements. The structure is complex cubic and in simple ternary systems has compositions ranging from Fe_4Mo_2C to Fe_3Mo_3C or corresponding formulae with W replacing Mo. Both carbides are of great importance in the high speed steels, but the Fe-Mo carbide is the one of prime interest in creep resistant materials. This carbide is an example of an interesting series of double carbides formed by the transition metals. These have been discussed in detail by Kuo (1953) who has called them η-carbides. Kuo has shown that there are two general forms of η-carbides, η_1 having the formula A_3B_3C and η_2 with formula A_2B_4C. It will be noticed that the M_6C of primary interest in steels has a composition range covering both η_1 and η_2 types.

(e) MC This formula is usually used to denote a carbide with the NaCl-cubic structure. Actually MX is the better description where X stands for C or N. In creep resisting steels the most common example is the V carbide, often

termed V_4C_3. The V carbide is basically VC but the composition limit extends to V_4C_3 by the formation of a defect lattice (Senior, 1988).

(f) M_2C This carbide is usually a Mo rich compound with the hexagonal structure of Mo_2C. This phase shows considerable solubility for Cr and V. The M_2C type of phase is an example of the general hexagonal compounds of type M_2X which have been studied by Andrews and Hughes (1958). In these compounds X may be either C or N and in many cases both types of interstitial atom are present. Extensive mutual solubility of the various isomorphous compounds occurs and it appears that in complex steels the phase is best regarded as $(Cr,Mo,V)_2(C,N)$.

(G) MoC and WC These carbides are distinguished from the general MC type discussed previously by having hexagonal structures. They are found in Fe-Mo-C alloys and Fe-W-C alloys respectively but do not normally occur in alloy steels because of the stabilisation of other phases by solution effects, e.g. $M_{23}C_6$ is stabilised by Cr and M_2C by V (Woodhead and Quarrell, 1965).

2.4.2 Sequence of Alloy Carbide Precipitation

Cementite is not the equilibrium carbide in many alloy steels, but it is nevertheless kinetically favoured because its formation can occur by a mechanism which does not necessitate the long range diffusion of substitutional solutes. The actual equilibrium carbide depends on the precise steel composition, and the change from cementite to the equilibrium carbide may occur via a number of other transition carbides. Baker and Nutting's study (1959) on the Fe-2.12Cr-0.94Mo-0.15C wt.% alloy showed that in the case of bainite, Mo_2C is the first alloy carbide to form and that it precipitated independently of the cementite, in the form of needles. Later work has shown that the Mo_2C in fact contains substantial amounts of other elements and is

better represented as M_2C (Woodhead and Quarrel, 1965; Murphy and Branch, 1971). Similarly, the Cr_7C_3 that Baker and Nutting referred to is here called M_7C_3 to indicate that other metal atoms are likely to be incorporated into the carbide structure. Mo_2C then begins to dissolve, giving way to $M_{23}C_6$, and both $M_{23}C_6$ and M_7C_3 are eventually replaced by the equilibrium carbide M_6C. Enhanced Cr concentrations are known to accelerate the formation of $M_{23}C_6$ and this can be of crucial importance in determining the sensitivity of the microstructure to severe hydrogen attack (Ritchie *et al.*, 1984; Spencer *et al.*, 1989).

Baker and Nutting (1959) indicated that with the exception of M_2C, new transition carbides precipitated at the positions of pre-existing carbides. The sequence of changes can be summarised as follows:

$$\begin{array}{ccccccc} Fe_3C & \Rightarrow & Fe_3C + M_2C & \Rightarrow & M_{23}C_6 & \Rightarrow & M_6C \\ & & \Downarrow & & & & \\ & & M_7C_3 & \Rightarrow & & \Rightarrow & M_6C \end{array}$$

Baker and Nutting also reported the presence of ε-carbide in the Fe-Cr-Mo-C bainite, but the evidence presented was rather indirect and has not been confirmed by subsequent work. A later study by Pilling and Ridley (1982) on a similar set of Fe-Cr-Mo-C alloys containing lower carbon concentrations (0.018-0.09 wt.%) revealed a somewhat different precipitation sequence

$$\begin{array}{ccccccc} Fe_3C & \Rightarrow & M_2C & \Rightarrow & M_{23}C_6 & \Rightarrow & M_6C \\ & & + & & & & \\ & & M_7C_3 & \Rightarrow & & \Rightarrow & M_7C_3 \end{array}$$

The explanation for the differences between these two studies is not clear. An analysis based on the thermodynamic stability of carbides as a

function of alloy chemistry and temperature could in principle explain the results, because there is some evidence to suggest that small chemical composition differences can significantly alter the tempering behaviour.

Baker and Nutting also studied the precipitation sequence in initially martensitic or ferritic microstructures. With martensite, the sequence was found to be essentially similar to that in bainite. The ferrite, on the other hand, contained M_2C precipitates, which presumably formed during its growth. Subsequent ageing led to the dissolution of M_2C, which was replaced by M_6C particles. This difference between bainite and ferrite has not been explained in detail, but must related to the mechanism of transformation. The ferrite forms by a reconstructive transformation mechanism, and atomic mobility inherent in the process could also permit the simultaneous precipitation of alloy carbides. The growth of bainite and martensite is displacive, precluding the formation of alloy carbides during transformation.

2.4.3 Change in the Composition of Alloy Carbides

Most of the experimental data on alloy carbide composition changes during the tempering of bainite come from experiments on steels used in the power generation industry. Changes in the chemical composition after precipitation are usually complicated by phase transformations involving the precipitation of other more stable particles, and these effects need much further investigation before any clear rationalisation can be attempted. Pilling and Ridley's (1982) careful investigations on the Fe-Cr-Mo-C alloys, revealed that the compositions of the Cr based M_7C_3 and $M_{23}C_6$ carbides remain essentially constant during prolonged annealing at 700°C. The M_2C and M_6C carbides on the other hand, became richer in Mo. The enrichment of M_2C was found to occur even during the period when its volume fraction was decreasing, the dissolving particles providing a source of Mo for the coarser M_2C particles and

for the more stable M_6C precipitates. The Mo concentrations in these carbides were found to increase as the average C concentration of the steel decreased (with a fixed Mo concentration), presumably because the amount of Mo approaches the stoichiometrically required quantity.

It is not surprising that changes in alloy carbide chemistries, as induced by tempering, are found to be less striking than those observed for cementite. The growth of the alloy carbides involves considerable long range substitutional atom diffusion and there is therefore a greater opportunity for the carbide to be closer to equilibrium when it first forms. Thomson and Bhadeshia (1992) concluded in their work that there is no enrichment occurring on tempering 12Cr1MoV steel is in contrast to the low alloy steels. Du (1986) found that the Cr content in $M_{23}C_6$ precipitating in a 0.5Cr0.5Mo0.25V steel increased with time. Whether or not alloy carbides precipitate at their equilibrium composition is therefore dependent on the concentration of alloying elements available in the base composition of a steel.

Many researchers (Wilson, 1990; Townsend, 1993) have recently conducted some work to determine the fundamental factors controlling the rate at which carbide compositions change, so that the extrapolation of experimental data can be used as a method of remanent creep life prediction. Thomson (1992) indicated that once the cementite transforms to alloy carbides, any changes in their composition are not large enough to be used as a quantitative estimation of remanent life. The enrichment kinetics of alloy carbide precipitation in high alloyed steels (*e.g.*12Cr1MoV) are much faster than in a low alloy steel, the attempts to predict remanent creep life were unsuccessful. Low alloy steels, however, contain cementite for a considerable fraction of their useful service life. Examination of the progressive development of the carbide composition under service condition thus becomes useful for the prediction of remanent creep life.

2.5 An Overview of MTDATA

A knowledge of phase equilibria is fundamental to the understanding of problems in metallurgy, materials science and chemistry faced by scientific research and industry. By definition these problems tend to be complex in nature, involving the interaction of many elements and phases. An experimental exploration of the potential range of compositions and conditions is likely to be very expensive and time consuming. This is where a thermodynamic approach offers great benefits in this study.

The MTDATA databank (Davies *et al*, 1991) comprises a number of modules for data management and calculation (Gisby *et al*, 1993). The principal calculation module is MULTIPHASE which, as the name suggests, solves problems involving many phases and components. Inevitably multicomponent calculations relevant to industrial problems entail the need for data for all the subsystems involved and the ability to use a variety of models to describe the behaviour of alloy phases, slags, salts, minerals and aqueous solutions as a function of temperature, pressure and composition.

2.5.1 Principles of MULTIPHASE Module

The essential principle of MTDATA is that mathematical models incorporated in the software enable equilibria in multicomponent systems to be calculated on the basis of critically assessed data for the thermodynamic properties of similar systems. Thus, using the facilities within MTDATA, it is possible to explore compositions and conditions of temperature and pressure for which no direct experimental data exist. Moreover, by linking process

models to MTDATA through its application interface, non-equilibrium phenomena can also be investigated (Gisby *et al*, 1993).

MULTIPHASE calculates equilibria using a unique and very robust Gibbs energy minimisation procedure developed by Hodson (1988), in which the integral Gibbs energy always moves to a lower value at each iteration and which requires no initial guesses. A particular feature of MTDATA lies in the procedures incorporated to search for immiscibility within phases if these are suspected or the data indicate the possibility. In addition to the default Stage-1 algorithm, the Stage-2 process, similar to other established chemical equilibrium programs may be invoked to give extra accuracy in small species amounts when each thermodynamic component has well established and independent activity in the system. Instead of the results being available to a constant tolerance in species amounts, Stage-2 determines the species to a tolerance on a logarithmic scale. If some information about the equilibrium state is available, it may be useful to evaluate equilibria by applying this information as a constraint.

MULTIPHASE is able to calculate and plot equilibria in systems with up to 20 components under a variety of constraints which include temperature, pressure or volume, composition (mole or weight) and potentials of products. The results of stepped calculations can be plotted selectively (for example the composition of an individual phase or the distribution of a particular component) as a function of the originally stepped variable or dependent variables.

2.5.2 Applications of MTDATA

Materials problems faced by industry involving interactions between different materials, including alloys, ceramics, glasses, cements and minerals, as well as melts, aqueous solutions and gases. The number of process

variables is often large, making feasibility studies and experimental optimisation expensive. MTDATA computes chemical equilibrium as a function of composition and conditions, with results presented as tables or diagrams (Dinsdale *et al*, 1988). For the purpose of assessment, validation and management of data for these subsystems MTDATA incorporates other modules, which can also be used for problem solving and their functions are given a brief account as follows:

THERMOTAB is used for tabulating and plotting data for individual substances and chemical equations and for amending and storing data. The equations can be auto-balanced.

COPLOT calculates and plots predominance area diagrams (also called phase stability or Pourbaix diagrams) for multicomponent systems not involving non-ideal solutions.

ACCESS allows the selective retrieval of data for systems of up to 20 components for chosen phase. The resultant datafiles can be used by MULTIPHASE, TERNARY and COPLOT.

BINARY calculates and plots binary temperature-composition diagrams and lists invariant points. The diagrams may be annotated.

G_PLOT is used for tabulating and plotting thermodynamic functions for binary systems.

TERNARY provides an interactive, automatic procedure for calculating and plotting phase boundaries and tielines in ternary systems in mole or weight fraction. Experimental data and labels may be added.

FITANDPLOT is a flexible procedure for fitting data to chosen functions. Facilities include automatic error checking of input data for typing errors, control of fitting accuracy and range splitting, as well as import and export of data from and to THERMOTAB.

2.5.3 Recent Developments in MTDATA

The APPLICATION module provides an interface that allows "application", *i.e.* user supplied software and associated data, to be linked with MTDATA. A set of tools is provided to facilitates the writing of applications and the plotting of the results. The external software may be written for a particular purpose or it may be an existing process modelling system (Davies, 1995).

The power of MTDATA to make predictions that go beyond the range of experience of the user introduces a problem. The question of how the user checks that the results are correct before using them for some critical process has been considered by Barry and Rand (1992). In an system of 20 or even more components it is possible, even likely, that the data for some potential products will be missing or in error. Moreover, because the number of options available to the user of MTDATA is large it is always possible for the user to undertake inappropriate calculations. For this reason MTDATA incorporates a system of audit trails that allows calculations to be traced back with respect to both user control and data sources. The system has the advantage that the user input can be replayed to repeat calculations with or without modification to the commands or the data (Gisby, 1993).

The successful application of MTDATA in predicting carbide phase precipitation sequences and equilibrium carbide compositions of a 12Cr1MoV power plant steel was reported (Thomson and Bhadeshia, 1992). It will be very interesting to know whether MTDATA can be applied to low alloy steel studies. Because there are 9 elements involved in this 2CrMoNiWV rotor steel, any one

of them having a slight compositional change, will affect the carbide transformation mechanism. With the aid of MTDATA, the effect of various alloying elements at different temperature could be predicted, particularly the role of W and its variations in content in this complex steel can be predicted without extra expenses.

Chapter 3

EXPERIMENTAL TECHNIQUE

3.1 Introduction

This chapter includes a description of the experimental programme and the relevant techniques employed, as summarised in Figure 3.1

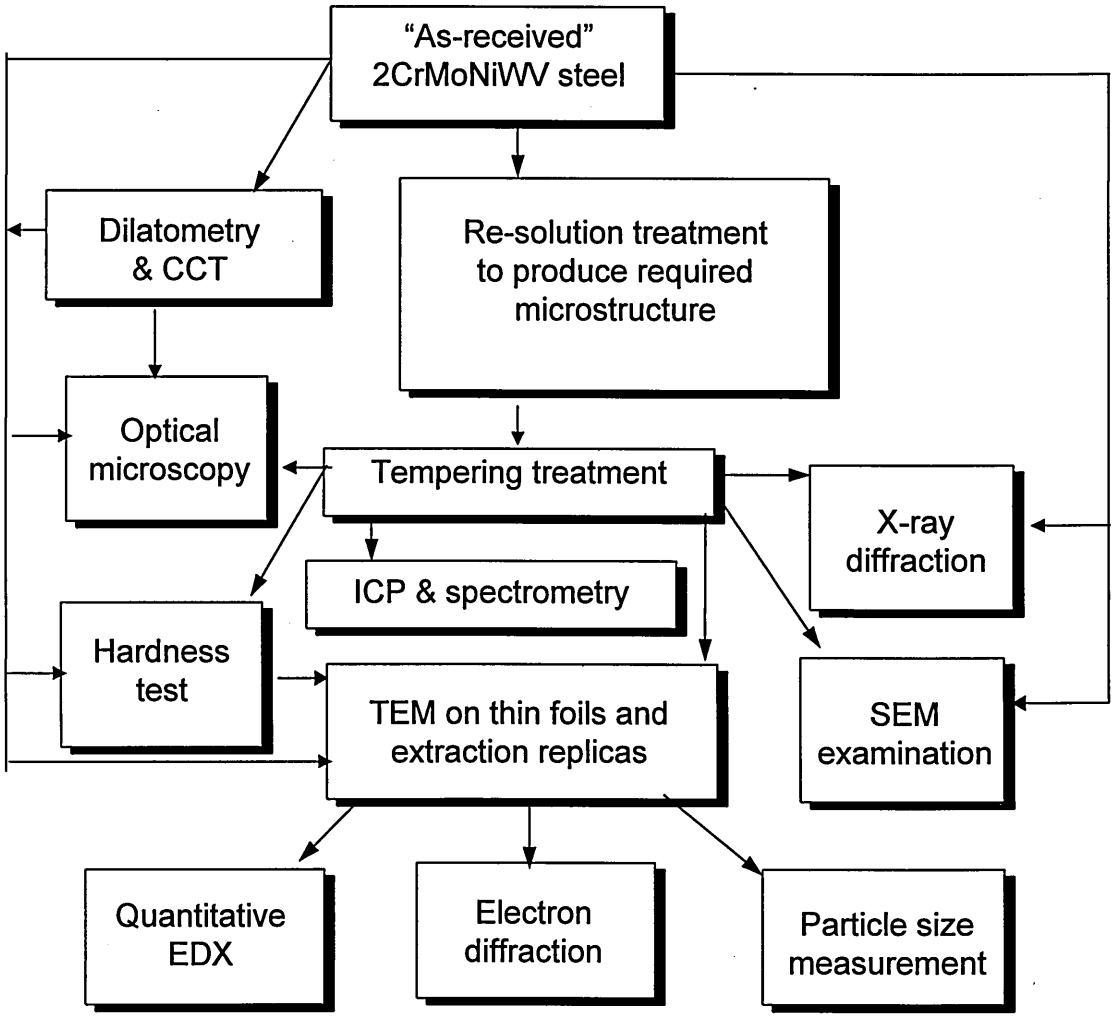

Figure 3.1 Flow chart illustrating the outline of experimental programme

Experimental material for this investigation was taken from a 1000 mm diameter production rotor rim produced by the VCD Steel making route in the fully heat treated condition and supplied by GEC ALSTHOM. The details of the material composition and commercial heat treatment practice are given in Table 3.1.

Table 3.1 Composition (mass%) and commercial heat treatment of 2CrMoNiWV turbine rotor forgings

Composition (mass%)	C	Si	Mn	Cr	Mo	Ni	W	V
	0.23	0.24	0.68	2.03	0.83	0.74	0.68	0.30
Heat Treatment	Austenitised: 16 hrs at 940-950°C, Oil Quenched Tempered: 30 hrs at 660-670°C, Furnace Cooled							

In this study material was examined in the "as-received" condition and after a series of experimental heat treatments.

3.2 Heat Treatment

All of the experimental heat treatments were carried out in Carbolite furnaces and a programme controlled muffle furnace. Heat treatments were conducted on 10 mm^3 blocks to study changes in microstructure, hardness and grain size. It was found that specimens which were protected only by Birkatec underwent severe scaling and decarburising during high austenitising temperature and/or longer time exposure, *i.e.* the Birkatec protection was inadequate for the experimental work in the high temperature austenitising range. Therefore prior to any heat treatments, the samples were sealed in

silica tubes under a partial pressure of argon to minimise any oxidation or decarburisaton.

Furnace temperature accuracy was controlled by built in thermocouples with an extra calibrated K-type NiCr-NiAl thermocouple attached to the specimens. The specimen temperatures were checked by a temperature recorder with a Philips PM9874A type TC linearlizer during the heat treatments and the errors of target temperature in the furnaces were confirmed to be within ±2°C.

3.3 Hardness Measurement

Heat treated specimens were ground to a surface finish of 1200 grit prior to measurement of hardness. The Vickers hardness determination was made using a pyramidal diamond indentation with 30 kg load to suit the hardness of the material. The diagonals of the indentation were measured using a micrometer ocular and movable gating which gave a numerical value. This value was translated into the hardness (Hv30) using conversion tables. Nine readings were taken for each sample. The averaged ocular reading was then used to give the HV30 hardness number and the standard deviation. BS427 (1990) was applied in Vickers hardness test machine calibration and measurement procedure.

Measurements were made on material in the "as-received" and all heat treated conditions. This gave information on the effects of austenitising parameters and tempering conditions on hardness.

3.4 Optical Microscopy

Optical microscopy was carried out on a Vannox optical microscope, capable of magnification of up to 750x. Observations on polished to 1μ diamond finish and etched specimens were made in the "as received" and all heat treated conditions.

The prior austenite grain size were measured on a Vickers 55 microscope. The measurement of grain size were made according to BS4490 Section 3 (1989) and the mean linear intercept method (Pickering, 1976).

Specimens were normally etched in 2% nital (2% nitric acid in methanol) to reveal the microstructure. Delineation of prior austenite grain boundaries for grain size measurements was carried out using an electrolytic etch. The etchant comprised of 5% chromium trioxide and 10% phosphoric acid diluted in water. Electrolytic etching current and voltage may vary for different heat treated samples, and a duration of 15-30 minutes was therefore used accordingly. It was found later in repeated experiments that using oxalic acid mixed with peroxide solution as etchant was more efficient in revealing prior austenite grain boundaries.

3.5 Scanning Electron Microscopy

Scanning electron microscopy (SEM) was carrying out using a JEOL 840 and Philips XL 40 instruments. These two instruments are fitted with Link System Energy Dispersive X-ray (EDX) analysis equipment.

The major advantages of SEM are its great depth of field, the ease of specimen preparation and increased spatial resolution. Throughout this work

conventional metallography specimen preparation techniques were employed, but the mounting material was conductive bakelite.

3.6 Transmission Electron Microscopy

Transmission electron microscopy (TEM) was performed using a Philips CM20 instrument equipped with both a scanning transmission (STEM) facility and energy dispersive X-ray (EDX) microanalysis system. In the Philips CM20 microscope, element spot analysis was achieved by focusing the electron beam to a fine spot, within the volume of interested area, and observing the X-ray counts generated via an energy dispersive X-ray detector connected to a PV9900 computer system. The structural changes that occurred during heat treatment were studied by direct carbon extraction replica technique and thin foils.

3.6.1 Thin Foil Preparation

Thin foil preparation involved the initial production of 3 mm diameter discs cut from the heat treated samples using a silicon carbide disc wheel. The discs were lightly ground on 1200 grit silicon carbide paper by hand to remove burring and give the final thickness of 80~120 μm. An electropolishing technique was used to make perforated foils suitable for observation by TEM. A Tenupol-3 twin jet polishing unit was used. The solution used in this apparatus was a standard metal polishing solution of 5% perchloric acid in methanol (AR) maintained at a temperature of -50°C to -40°C. Electropolishing was achieved using conditions of 30-40 V, 100-200 mA at a pump flow rate setting of 3. Foils were washed in several batches of methanol and also stored under methanol (AR) prior to examination by TEM.

3.6.2 Carbon Extraction Replica Preparation

The carbon extraction replica technique was very useful for the identification or counting of carbide phases in the metallic system. The main advantages of replicas over foils were that they eliminated any effects due to the steel matrix and thus enabled the chemical composition of the carbides to be measured more accurately, and problems associated with working with a magnetic specimen in the TEM were avoided.

Single stage carbon extraction replicas were prepared using the method described by Smith and Nutting (1957) from surfaces prepared as for optical microscopy. For initial etching of the sample (before carbon coating), a 2% nital solution was used to give a light etch (carbides just being resolved by optical microscopy). A piece of acetate was dipped in acetone and then put on the specimen after etching as stripping cleaning. The mounting bakelite was well masked before carbon coating. The specimen was placed in a carbon evaporator (see schematic Figure 3.2) with a vacuum of 1.333×10^{-3} N/m^2. It is important to ensure that the surface of the mounted specimen is clean and free from grease to give a good adhesion of the deposited carbon film (colour blue-brown). Carbon is deposited from a height of 100 mm directly above the specimen surface to obtain as even a coverage as possible.

The etchant used for releasing the carbon film from the surface of the specimen was a 6% nital solution. The specimen was scored with a sharp blade into squares approximately 3 mm across to allow reasonable access for the etchant to bare metal surface, and to ensure that the carbon replica pieces would be of suitable size. As soon as the carbon layer had peeled off the metal surface, the specimen was washed in methanol, and the fragments of carbon layer were floated using the surface tension provided by a 20% methanol and

80% distilled water mixture. Each replica was then collected onto a 3 mm diameter, 200 square mesh copper grid and was ready for analysis in the TEM.

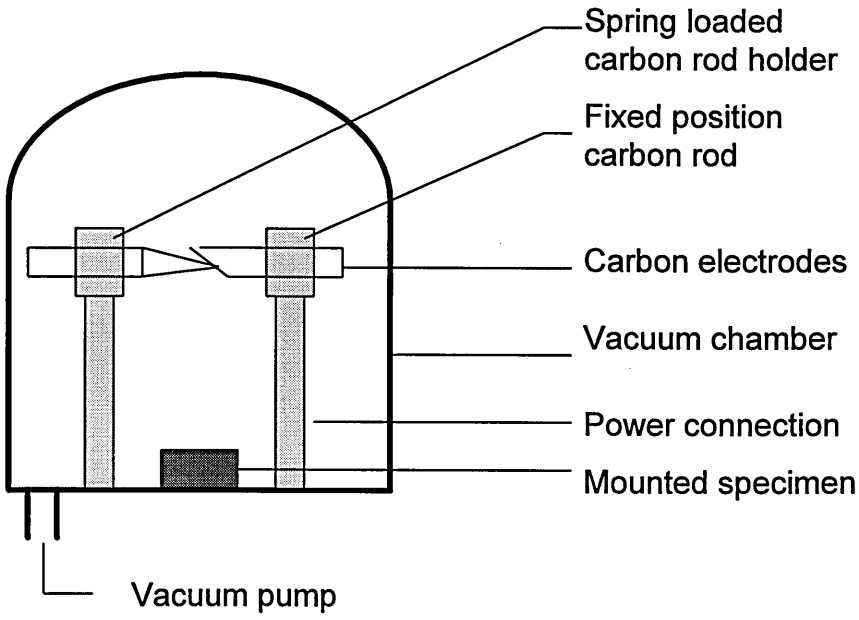

Figure 3.2 Schematic diagram of the carbon evaporator apparatus

3.6.3 Calculation of the TEM Camera Constant

The settings of the various magnetic lenses within the column of a TEM affect the magnification of diffraction patterns. Usually the microscope was operated at 200 kv accelerating voltage (λ = 0.0251Å) and with the lenses at fixed settings so that the magnification of the diffraction pattern was a constant. This magnification factor was expressed in terms of an equivalent camera length which is illustrated schematically in Figure 3.3.

Due to Bragg's Law gives: $\lambda = 2d_{\{hkl\}} \sin\theta$ .....(3.1)

From geometry: $\tan 2\theta = \frac{R}{L}$ .....(3.2)

Typically 2θ is only one or two degrees and therefore $\tan 2\theta \approx 2\sin\theta \approx 2\theta$(rad), from equations (3.1) and (3.2):

$Rd_{\{hkl\}} = L\lambda$ = camera constant .....(3.3)

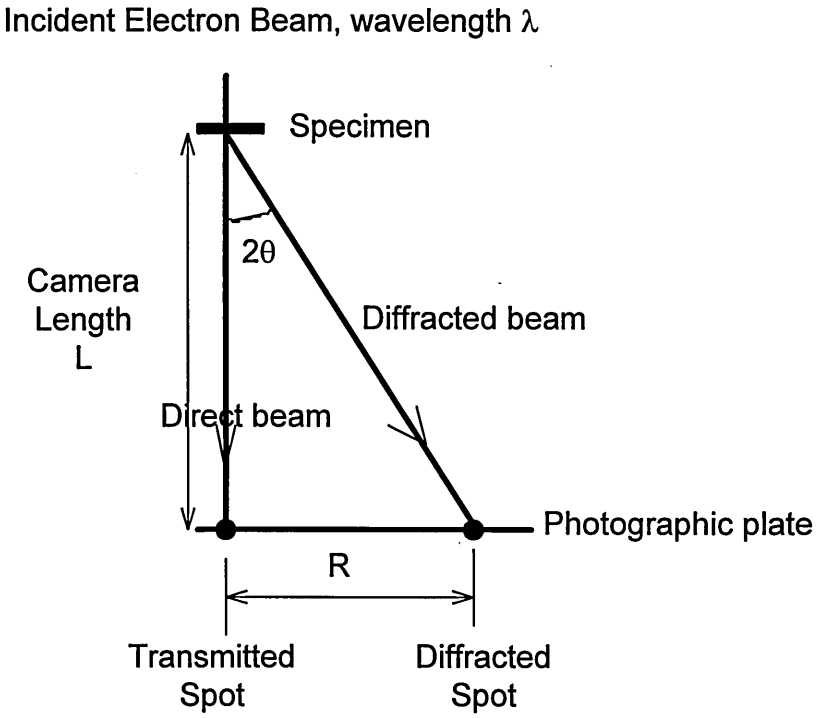

Figure 3.3 Schematic illustration of the magnification of a diffraction pattern

It was very important to determine a very accurate camera constant for the identification of the various carbide phases by electron diffraction patterns. This was achieved by examination of the ring diffraction pattern (Figure 3.4) from an evaporated polycrystalline Cu film on Al support grid.

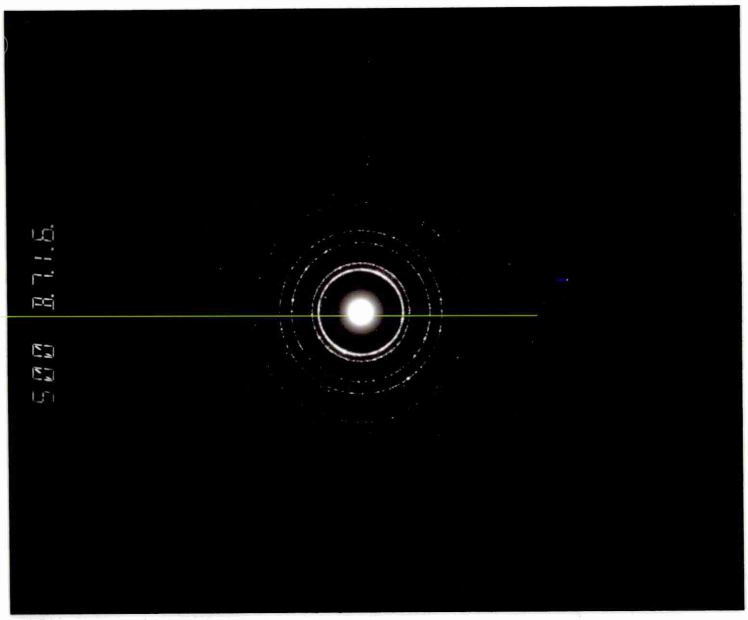

Figure 3.4 A diffraction pattern from an evaporated Cu film used for the determination of the camera constant in the TEM

Table 3.2 Calculation of the camera constant from the ring diffraction pattern produced by a film of Cu sputtered onto a Al support grid

Ring Number	Associated (hkl)	Associated $h^2+k^2+l^2$	$d_{\{hkl\}}$ 10^{-10} m	Measured R 10^{-3} m	Rd 10^{-13} m
1	111	3	2.087	5.625	11.74
2	200	4	1.808	6.525	11.79
3	220	8	1.278	9.225	11.79
4	311	11	1.090	10.775	11.75
5	222	12	1.044	11.275	11.77

The calibrating material, Cu, is fcc with lattice parameter, a_0 = 3.6150 Å (Andrews, Dyson and Keown, 1967). From this information, together with a knowledge of the allowed reflections, interplanar spacings $d_{\{hkl\}}$ could be calculated and results are illustrated in the Table 3.2. The average of all the Rd values from the individual rings was used for the best accuracy, from which the camera constant together with a standard deviation $\lambda L = 11.768 \pm 0.023$ at the eucentric specimen height was obtained and could be used for other subsequent electron diffraction patterns analyses.

3.6.4 TEM Camera Constant Correction Factor

It was found that the camera constant varied significantly with objective lens current, which had to be adjusted to focus on the sample to obtain a good image. The physical height of the sample varied as it was titled in the double tilt holder, which required adjustment of focus. Consequently a calibration of the camera constant was conducted against objective lens current. The Cu {113} d-spacings were measured at different objective lens current value by physically altering the height of the sample in the sample holder and the results summarised in Table 3.3.

Because the TEM CM20 calibrated objective lens current was 5432 mA, the ratio between measured mean {113} d-spacings against the d-spacing at the eucentric height (from which the camera constant λL was calculated) was obtained. Figure 3.5 shows that at different objective lens currents, corresponding camera constant correction factors were required caused by different specimen heights. Bearing this in mind after tilting the specimen to get a low order zone axis for a diffraction pattern, the specimen should be refocused and the objective lens current at focus should be recorded accordingly. When the diffraction pattern is analysed, the nominal camera

constant λL (accurate at the eucentric height only) should be multiplied by the correction factor relating to the objective lens current.

Table 3.3 Measured Cu {113} d-spacing at different objective lens current value

Objective lens current (mA)	Measured Cu {113} d-spacing (Å)				
	First	Second	Third	Fourth	Average
4988	1.03	1.01	1.03	0.99	1.015±0.019
5097	1.04	1.04	1.03	1.03	1.035±0.006
5174	1.06	1.06	1.05	1.04	1.053±0.010
5272	1.07	1.06	1.05	1.05	1.058±0.010
5360	1.09	1.07	1.08	1.07	1.078±0.010
5432	1.09	1.09	1.09	1.08	1.088±0.005
5532	1.11	1.09	1.10	1.09	1.098±0.010
5632	1.12	1.13	1.11	1.12	1.120±0.010
5738	1.14	1.13	1.14	1.12	1.133±0.010
5835	1.15	1.14	1.13	1.13	1.138±0.010
5936	1.16	1.16	1.16	1.14	1.155±0.010
6027	1.17	1.18	1.16	1.17	1.170±0.010

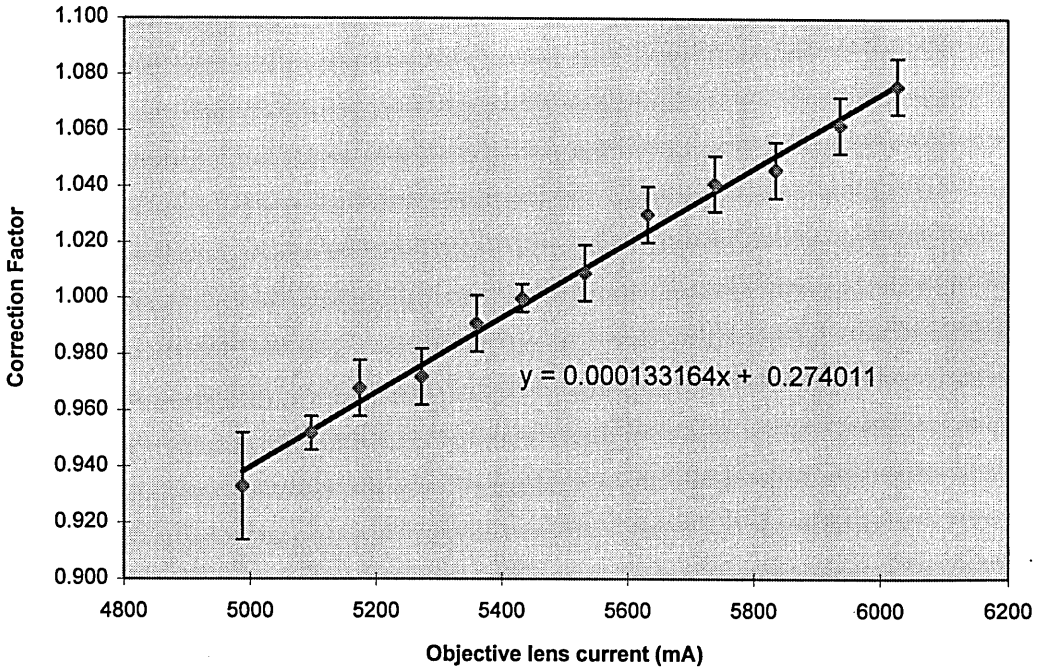

Figure 3.5 TEM camera constant correction factors for different objective lens current

3.7 Analytical Electron Microscopy

3.7.1 Procedure for EDX Analysis

The carbon extraction replicas were analysed on a Philips CM20 transmission electron microscope using EDX technique, with 200 kv accelerating voltage, with the specimen titled at a 30° angle to the EDX detector. The CM20 was fitted with a EDAX analytical system, and the spectra were collected and processed using the EDAX 9900 microanalysis program (which includes corrections for atomic number, absorption and fluorescence effects).

Spurious signals from the system were reduced by using a beryllium specimen holder (Z = 4, so the EDX signal from the holder was negligible), although some spurious X-rays arising from the copper grids on which the replicas were mounted could not be eliminated entirely.

At least 100 carbides were analysed from each tempering treatment, selected as randomly as reasonably possible from the replica. This number of analyses was found to give data of reasonable statistical significance except at low temperatures or very short tempering times for cementite. In each case the EDX spectrum was collected over a 50 seconds live time. Micrographs were also taken for each heat treatment condition from which a spectrum was obtained so that a comparison of particle sizes could be made.

Diffraction patterns were obtained occasionally in order to check that each type of alloy carbides was classified correctly, and to identify any other alloy carbides which may appear after higher temperature and/or longer tempering times.

3.7.2 Inaccuracies in EDX Measurement due to Matrix Effects

The essence of the EDX technique lies in the ability to convert relative X-ray signal intensities for two elements within a specimen (say, I_A/I_B) to the relative concentration of the elements present (C_A/C_B), in accordance with equation (3.4) below (Cliff and Lorimer, 1975), where k_{AB} is a constant for constant accelerating voltage and specimen thickness.

$$\frac{C_A}{C_B} = k_{AB}\frac{I_A}{I_B} \qquad \text{.....(3.4)}$$

Factors affecting the proportionality between the two are therefore of considerable concern, and care must be taken to quantify and if necessary

correct for such factors before the compositional data produced by the technique could be used. Consideration is given to two such problems: unequal level of absorption of different X-ray emissions (from different elements) by the specimen; and fluorescence within the specimen.

3.7.2.1 Absorption

The EDAX system used in analysing the EDX spectra includes a routine to make a correction for matrix absorption from specimen thickness and density. A brief consideration of the physical situation is given below.

The relationship between the observed intensity of signal from an element A present in the specimen, I'_A, and the real intensity of emission which would be observed in the absence of any absorption, I_A, follows the exponential law as equation (3.5).

$$I'_A = I_A \phi_A(\rho x) exp\{-(\mu/\rho)^A_{spec} \rho x\} \quad \text{.....(3.5)}$$

where x is the distance the signal travels through the material, ρ is the density of the material, ϕ_A is a measurement of the attenuation of incident electron energy during its passage through the material, and $(\mu/\rho)^A_{spec}$ is the mass absorption coefficient for X-ray emission attributable to element A for the whole specimen, obtained as a sum over all elements in the specimen of $c_i(\mu/\rho)^A_i$, where c_i and $(\mu/\rho)^A_i$ are the weight fraction and mass absorption coefficient associated with the element i.

In a practical situation for a specimen of finite thickness, d, Goldstein *et al.* (1976) thus propose equation (3.6) for the relationship between I'_A and I_A.

$$\frac{I'_A}{I_A} = \frac{1}{d}\int_0^d \phi_A(\rho x)\exp\{-(\mu/\rho)^A_{spec}\csc(\varphi)\rho x\}dx \quad \text{.....(3.6)}$$

where φ is the take-off angle, and for practical purposes, is assumed to fit the relationship

$$csc(\varphi) = \frac{1}{sin\alpha cos\theta + cos\alpha sin\beta} \quad \text{.....(3.7)}$$

where α is the tilt angle, θ is the angle between the detector and tilt axes, and β is the elevation of the detector, which is zero for Philips instruments such as the one used in the current work.

If it is assumed that the electrons lose negligible energy during passage through the specimen (that is to say, the rate of production of X-ray photons is constant through the thickness *d*), then $\phi(\rho x) = 1$ (Cliff and Lorimer, 1975). Thus equation (3.6) can then be reduced to equation (3.8). This assumption is generally considered a reasonable approximation in thin films, although for slightly thicker specimens it may break down.

$$\frac{I'_A}{I_A} = \frac{1-exp\{-(\mu/\rho)^A_{spec}csc(\varphi)rd\}}{(\mu/\rho)^A_{spec}csc(\varphi)\rho} \quad \text{.....(3.8)}$$

A correction factor for intensity ratios can then be obtained by combining the above equation with an identical equation for an element B. This approach allows the ratio I_A / I_B to be quantified as equation (3.9), which makes it apparent that the effect of absorption depends on the difference between the mass absorption coefficients for the two elements, as well as on specimen density and thickness.

$$\frac{I_A}{I_B} = \frac{I_A'}{I_B'} \times \frac{(\mu/\rho)^A_{spec}(1-exp\{-(\mu/\rho)^A_{spec}csc(\varphi)\rho d\})}{(\mu/\rho)^B_{spec}(1-exp\{-(\mu/\rho)^B_{spec}csc(\varphi)\rho d\})} \quad \text{.....(3.9)}$$

An approximation has been proposed by Cliff and Lorimer (1975) that all X-rays are produced at the centre of the foil. The use of this approximation simplifies the evaluation of equation (3.6), producing equation (3.10) below

$$\frac{I_A'}{I_A} = exp - \{(\mu/\rho)^A_{spec}csc(\varphi)\rho(d/2)\} \quad \text{.....(3.10)}$$

Table 3.3 A summary of data for the various alloy carbides encountered in this work (Andrew *et al*, 1967)

Carbide	Structure	Lattice Parameter (Å)	Formula Units (Cell)	Density (g/cm^3)
M_3C	Orthorhombic	a = 4.5241 b = 5.0883 c = 6.7416	4	7.704
M_7C_3	Hexagonal	a = 13.982 c = 4.506	8	6.965
$M_{23}C_6$	Cubic F	a = 10.638	4	6.996
M_6C	Cubic F	a = 11.082	16	6.325
M_2C	Hexagonal	a = 3.002 c = 4.724	1	9.188

The use of this further approximation produces the correction factor for observed against true concentrations as in equation (3.11)

$$\frac{I_A}{I_B} = \frac{I'_A}{I'_B} \times exp\{-[(\mu/\rho)^B_{spec} - (\mu/\rho)^A_{spec}]csc(\varphi)\rho(d/2)\} \quad \text{.....(3.11)}$$

The practical problem in quantifying absorption thus becomes one of obtaining reasonable estimates for ρ and d. Data for the various alloy carbides encountered in this work are summarised in Table 3.3, but actual density of each carbide depends on its actual solution of alloying elements.

3.7.2.2 Fluorescence

Fluorescence effects in EDX microanalysis can arise either from the continuum or from a characteristic line. It is generally held that continuum fluorescence is likely to present a serious problem only in bulk samples, and can reasonably be ignored for thin foils, where continuum fluorescence will be sufficiently small to be trivial compared with other sources of error.

In the case of characteristic fluorescence some problems have been reported even for thin foils, notably for CrK_α radiation for low Cr concentrations in Fe (Lorimer *et al.*, 1977). The levels of fluorescence found were smaller than for bulk specimens, but still appreciable at Cr concentrations of below about 10%, with the measured Cr composition being overestimated by a factor of 30% for a Cr concentration of 1%. This result was obtained from a thin foil which Lorimer *et al.* estimated to have a thickness of around 200 nm and hence may be of relevance to this work. More recent work suggests that secondary fluoescence is significantly less than this in many specimen geometry (Anderson, 1995).

In view of the fact that the observed systematic error is relatively small compared with other uncertainties in these EDX measurements, then the effect

is exaggerated at small values of cementite composition, so accuracy will improve with enrichment during tempering.

3.7.3 Inaccuracies in EDX Measurement due to Instrumental Effects

Spurious X-rays which do not arise from a single event in the specimen by the central electron beam, might be attributed to several instrumental factors (Goldstein and Williams, 1978).

(I) Bremsstrählung radiation from the condenser apertures and electrons uncollimated by the condenser may generate X-rays from both the specimen and its surroundings.

(II) Electrons scattered in the chamber can generate a signal from specimen or surroundings.

(III) X-rays can be generated in the specimen or surroundings by electrons scattered from the specimen.

(IV) X-rays generated within the specimen can cause fluorescence of the surroundings.

(V) In the case of extraction replicas, X-rays may be produced by the copper grid used to support the specimen.

Effects (II)-(IV) can be reduced to a insignificant level by appropriate experimental practice (constant electron beam, shielding of the specimen with low atomic number materials - hence the beryllium holder, *etc.*). The fifth effect is only a problem if copper is also present in the material (in which case a different grid could be used), in this study the spurious Cu signal can be safely

ignored. However, it is important to maintain vigilance to ensure that these effects do not constitute a serious problem in the collected data.

3.7.4 Inaccuracies in EDX Measurement due to Specimen Based Sources

Spurious results in EDX analysis may arise from problems in the specimen. In particular, variation in specimen thickness is liable to give variable results, because any difficulty in determining an accurate thickness will introduce an error into any estimate of the magnitude of thickness dependent effects (fluorescence and absorption). In this study, various particle sizes have large effect in this connection. It is good practice when performing EDX analysis of thicker particles to minimise X-ray self-absorption by positioning the electron probe on a thin edge of the particle at the point on the circumference of the particle image closest to the EDX detector. Because the image rotates as the magnification is changed, it is convenient always to work at a fixed magnification for which the effective direction of the detector has been previously been determined, so that the optimum analysis point can be quickly selected. In addition, it has been suggested that enrichment of one species relative to another in a surface film (such as an oxide layer), will produce further variations of EDX spectra with specimen thickness (Morris, Davies and Traverton, 1977).

Spurious results arising from species at the specimen preparation stage are also possible (e.g. residues from etching and polishing solutions), emphasising the need for care in replica preparation: high-purity carbon rods were used as the evaporation source; the specimen were scrupulously cleaned before inserting into the evaporator (which is also essential for good carbon film adhesion); and the replicas were thoroughly washed in pure ethanol before the lifting stage (in the ethanol/distilled water solution) to remove etching residues.

3.7.5 Stochastic Scatter in EDX Measurements

Even when systematic errors in the EDX results, such as could arise from absorption, fluorescence, spurious X-rays *etc.*, have been accounted for, an individual EDX composition will be subject to an error attributable to stochastic scattering in the X-ray signal intensity (both background and characteristic). The EDX spectrum analysis program makes an estimate of this error on the basis of the observed noise in the collected spectrum, enabling the problem to be quantified approximately, and the scatter can be reduced by extending the time period over which the spectrum is collected, to increase the signal/noise ratio.

In practice, the composition which is measured from an EDX spectrum, c_{obs} will related to the actual composition, c_{real}, by equation (3.12)

$$c_{obs} = c_{real} \pm x \quad \text{.....(3.12)}$$

where x is a factor representative of the stochastic scatter in the observed signal intensity at the characteristic frequency under analysis. The stochastic nature of the error imposed on individual measurements by this factor means that confidence limits in the measured mean composition for a given heat treated condition (hence over 100 particles were measured at each tempering condition in the current work).

It is evident that, where the characteristic peak intensity is small (for a small concentration of the element concerned), and the noise in the background signal is of a similar order of magnitude, it is possible that the stochastic scatter in carbide composition is larger than the magnitude of carbide composition, which will produce an occasional negative result for the concentration of the element when the spectrum is analysed. Such a result

indicates that the X-ray intensity at the characteristic frequency in that particular spectrum is less than that would be expected from background radiation alone, as a result of the stochastic noise in the background signal.

A negative value for carbide composition is clearly of no physical significance and results obtained from specimens where this problem arises must be treated with considerable suspicion; the true composition is so small to be of a similar order of magnitude to the resolution of the technique. Nevertheless, because such results arise from a random process inherent in the EDX technique, it is necessary that they be included when mean compositions are calculated from a large number of observed carbide composition values. In the current work, where substitutional alloying content is relatively small at low temperature and/or short tempering times, conditions were set as carefully as possible to reduce the stochastic scatter to a minimum.

3.8 Bulk Extraction of Carbides and X-ray Diffraction

It is possible to isolate the carbide precipitates in steels by electrochemical dissolution. Thus quantitative analysis, including accurate lattice parameter measurements and volume fraction data for the various carbides formed in the steel during tempering could be examined by X-ray diffraction. This technique was discussed in detail by Andrew and Hughes (1958), Stuart and Ridley (1966), Leitnaker *et al.* (1975), and more recently by Stevens and Lonsdale (1987).

However in experiments it was found that for samples containing the M_3C carbide few of these carbides were extracted. An innovative carbide extraction technique has been developed in this regard and will be separately described in details in Chapter 6.

A Philips 1830 generator with CuK_α long fine focus (LFF) radiation tube was used to scan between 30° and 60°. Goniometer was coupled with 2θ at a step of 1 second duration with sample spinner (1 revolution/sec) and with 35 kV/45 mA working condition at 1600 watts power. The diffraction peak positions were located using a computer with APD 3.5B control and analysis software.

The specimens were also anodically dissolved in a cell with a platinum cathode and a solution of 5% HCl in distilled water as electrolyte at a voltage of 1.5 V. The filtered solution were used for inductively coupled plasma (ICP) and spectrometric techniques to determine alloying element content remained in the matrix.

3.9 Grain Size and Particle Size Determination

Grain size variation with austenitising temperature and exposure time were measured by using the method of mean linear intercept (MLI). The MLI is measured by counting the number of grain boundaries which intercept a linear traverse of length L.

The MLI is given by

$$MLI = \frac{L}{N} = \frac{1}{N_L} \quad \text{.....(3.13)}$$

where N is the number of grain boundaries and N_L is the number of grain boundaries or grains per unit length of traverse.

It must be appreciated that the MLI, d is less than the average diameter of the grains D_M. The relationship between d, D and D_M depend on the grain shape assumed, but by assuming reasonable shapes for real grains and obtaining a mean diameter of rotation

$$D \approx 1.75MLI \quad \text{.....(3.14)}$$

Also, assuming D_M to be the circumscribed sphere of rotation

$$D_M \approx 1.86MLI \quad \text{.....(3.15)}$$

For each specimen over 750 intercepts were made with a 95% confidence limit of ±5% (Pickering, 1976)

3.10 Dilatometric Work

Thermal transformation studies were carried out at British Steel Technical Swindon Laboratories using an MMC Quenching Dilatometer.

The test specimens (10 mm long x 5 mm diameter) were small to allow for rapid heating and cooling cycles and to prevent temperature gradients within the sample. The furnace was induction heated and the temperature measured using a platinum-platinum/10% rhodium thermocouple which was spot welded onto the specimen. Length measurements were monitored by push rods connected to a frictionless and very sensitive linearly variable differential transducer (LVDT).

Dilatometer samples were heated in vacuum at a constant rate of 500°C/min to 950°C and 1000°C , held for twenty minutes before being

continuously cooled over a range of nine different cooling rates. The range spanned from approximately 600°C/min to 0.2°C/min. One specimen of the steel was initially heated linearly at a rate of 2°C/min to determine the A_{C1} and A_{C3} temperatures.

The phase transformations were recorded by plotting directly the length and temperature measurements on an XY recorder. The recorded cooling curves were replotted in the co-ordinate system of temperature versus log time.

The "as-cooled" samples were prepared for metallographic examination and hardness testing to assist in the interpretation of the results. In this way, the dilatometric curves could be checked and the transformation products identified. In addition, this technique can be used to estimate the strengthening effects obtainable through cooling at various rates.

Chapter 4

CONSTRUCTION OF CCT DIAGRAMS FOR THE 2CrMoNiWV STEEL

4.1 Introduction

Among the metallurgical features of conventional large CrMoV steam turbine rotor forgings, probably the most important are bainitic hardenability, and formation of alloy carbides (Norton and Strang, 1969). Whether the 2CrMoNiWV steel is suitable for large diameter rotor applications very much depends on its bainitic hardenabilty, which means that whether the 2CrMoNiWV can transform to a fully bainitic microstructure over a wide range of cooling rates. This feature requires the steel to have a well balanced alloy content to ensure that the stabilities of various alloy carbides are close to each other. Thus, provided the heat treatment was appropriate, the transformation of one carbide species to the other should be sluggish, which gives a high elevated temperature stability to the steel.

The range of structures attained in the ferritic steels on initial heat treatment can be extremely complex and depends critically on the composition, the time and temperature achieved during austenitising and on the cooling rate (Townsend, 1993). The continuous cooling transformation (CCT) diagram provides useful information on hardenability, defining quite accurately the cooling rates at which various transformation products will form, which can then be related to the cooling rate from the rim to the core of a large diameter rotor oil quenched after austenitisation. Thus the possible microstructure of a large diameter rotor from rim to core can be predicted.

4.2 Interpretation of Dilatometer Data

An MCC dilatometer was used to determine the A_{C1} and A_{C3} temperatures by heating a specimen linearly at a rate of 2°C/min and the test record is shown in Figure 4.1. The dilatometer was also used to produce cooling curves and temperature versus length curves for samples cooled at varying rates from different soak temperature. Figures 4.2 - 4.5 show a set of dilatometer records that were obtained on continuously cooling the specimens from 950°C austenitising temperature.

On cooling, the start of austenite transformation is readily detected as the thermal contraction of austenite is counteracted by the volume expension due to transformation. Figure 4.2 illustrates complete transformation to bainite even at the fastest cooling rate (600°C/min, Test N) and transformation to mixture of bainite, proeutectoid ferrite at the slowest cooling rate (0.3°C/min, Test X1), see Figure 4.5.

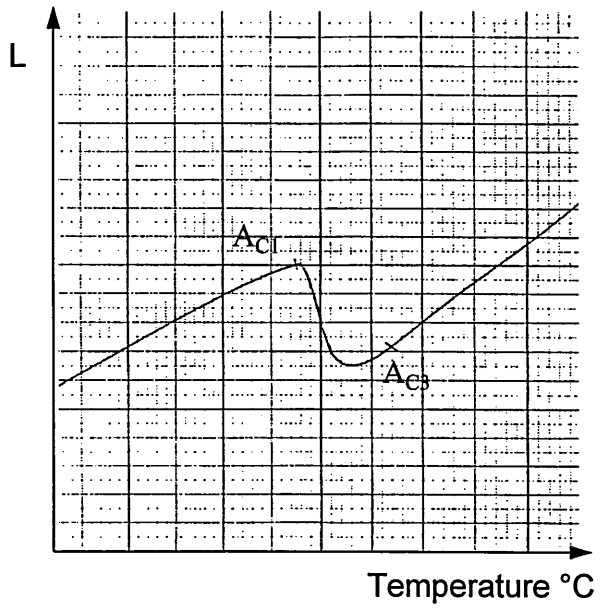

Figure 4.1 Dilatometer record obtained on linear heating the specimen at 2°C/min to determine A_{C1} and A_{C3}

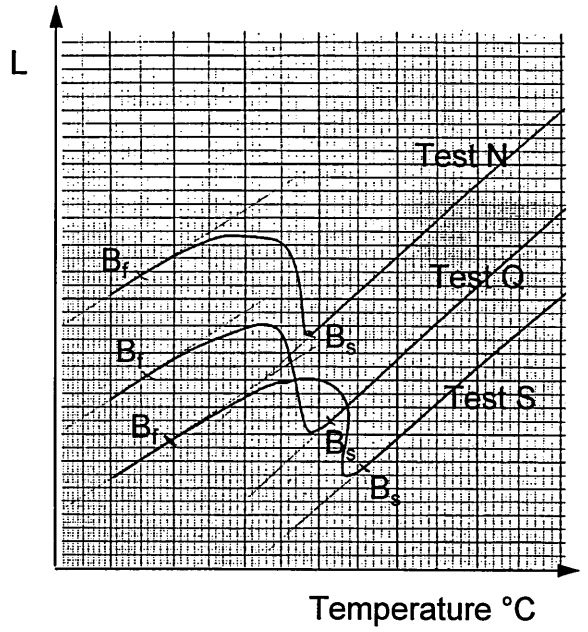

Figure 4.2 Dilatometer records obtained on continuously cooling the specimens from 950°C austenitising temperature

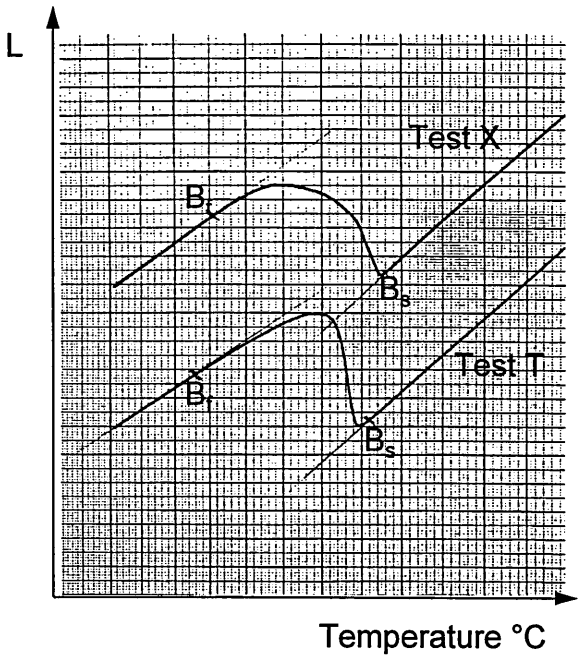

Figure 4.3 Dilatometer records obtained on continuously cooling the specimens from 950°C austenitising temperature

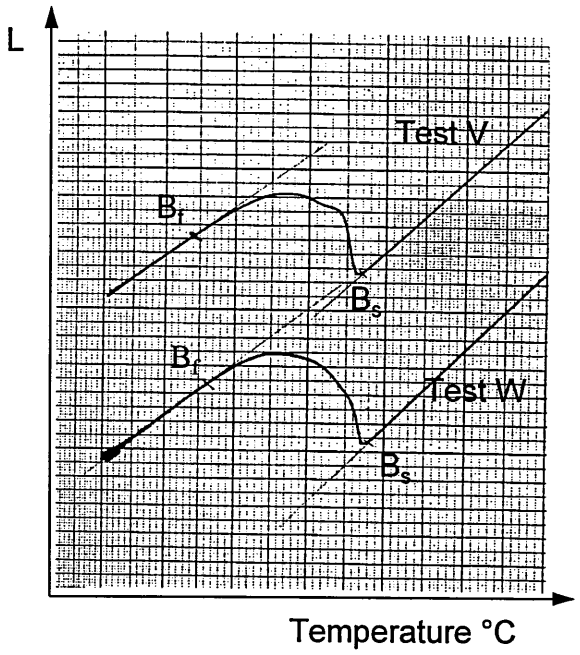

Figure 4.4 Dilatometer records obtained on continuously cooling the specimens from 950°C austenitising temperature

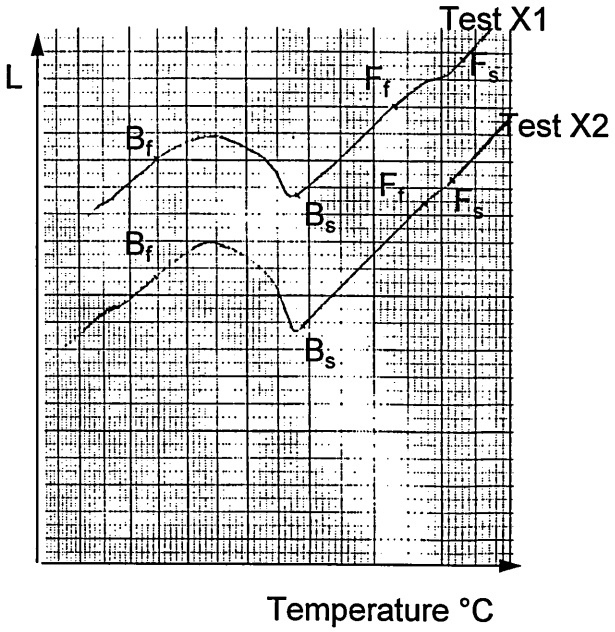

Figure 4.5 Dilatometer records obtained on continuously cooling the specimens from 950°C austenitising temperature

The results of the dilatometric work were summarized in the form of continuous cooling transformation (CCT) diagram, Figure 4.6 (austenitised at 950°C). The lower and upper critical temperatures, A_{C1} (790°C) and A_{C3} (870°C) are indicated. The cooling rates (°C/min) are written on the individual cooling curves which are labeled adjacently. The results of hardness (HV30) measurements on each "as cooled" dilatometer specimen are given at the ends of their respective cooling curves. The prior austenite grain size developed is also given in the diagram.

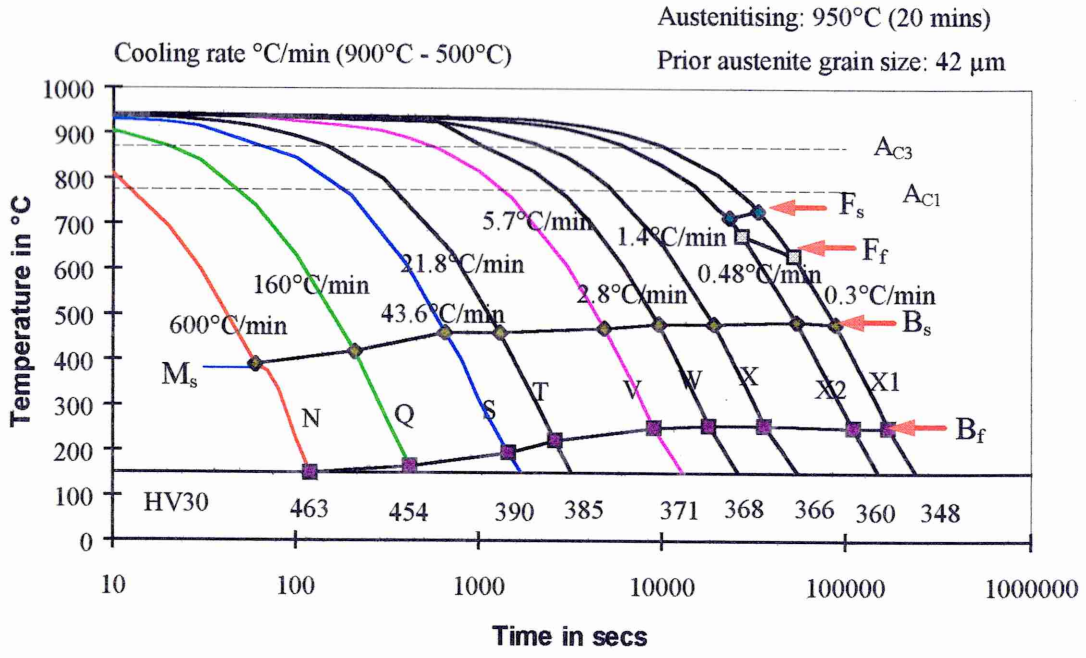

Figure 4.6 Continuous cooling transformation diagram for the 2CrMoNiWV rotor steel austenitised at 950°C for 20 mins

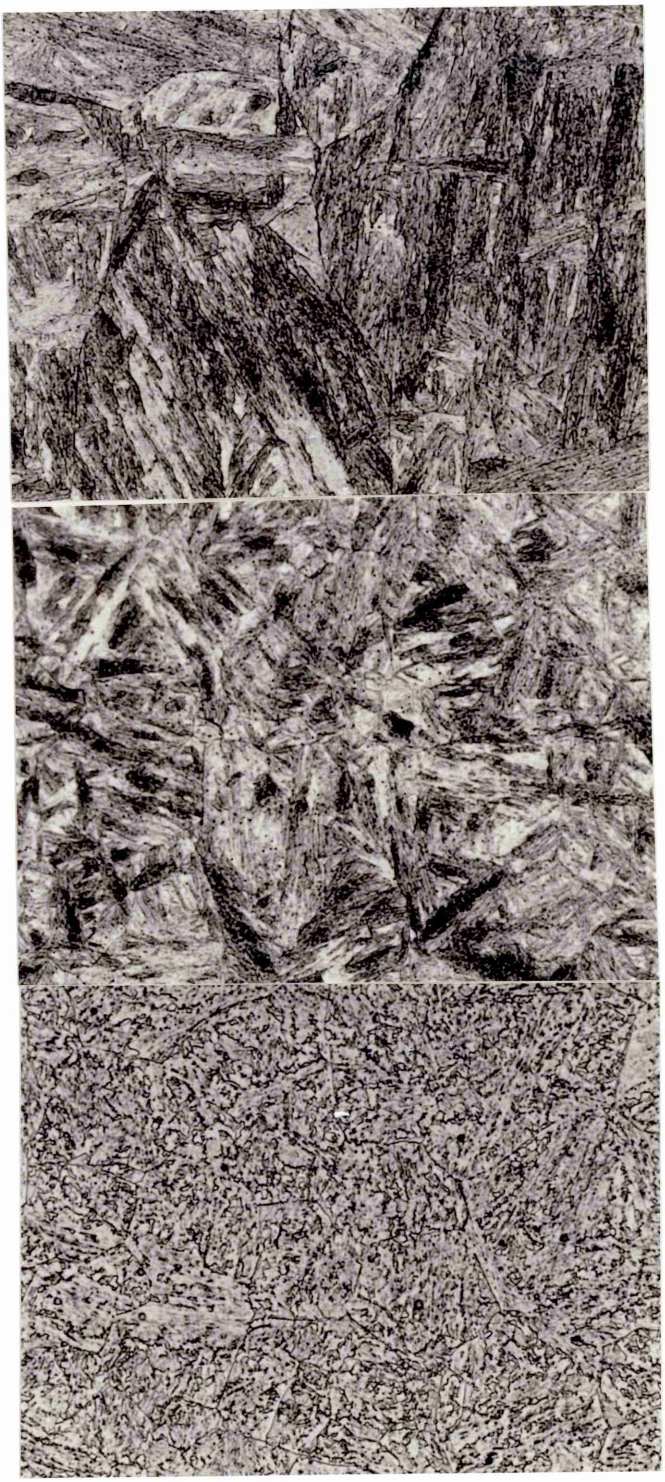

(a) 600°C/min
Test N

(b) 160°C/min
Test Q

(c) 43.6°C/min
Test S

Figure 4.7-1 Optical micrographs of specimens in different cooling rates austenitised at 950°C for 20 mins (600x)

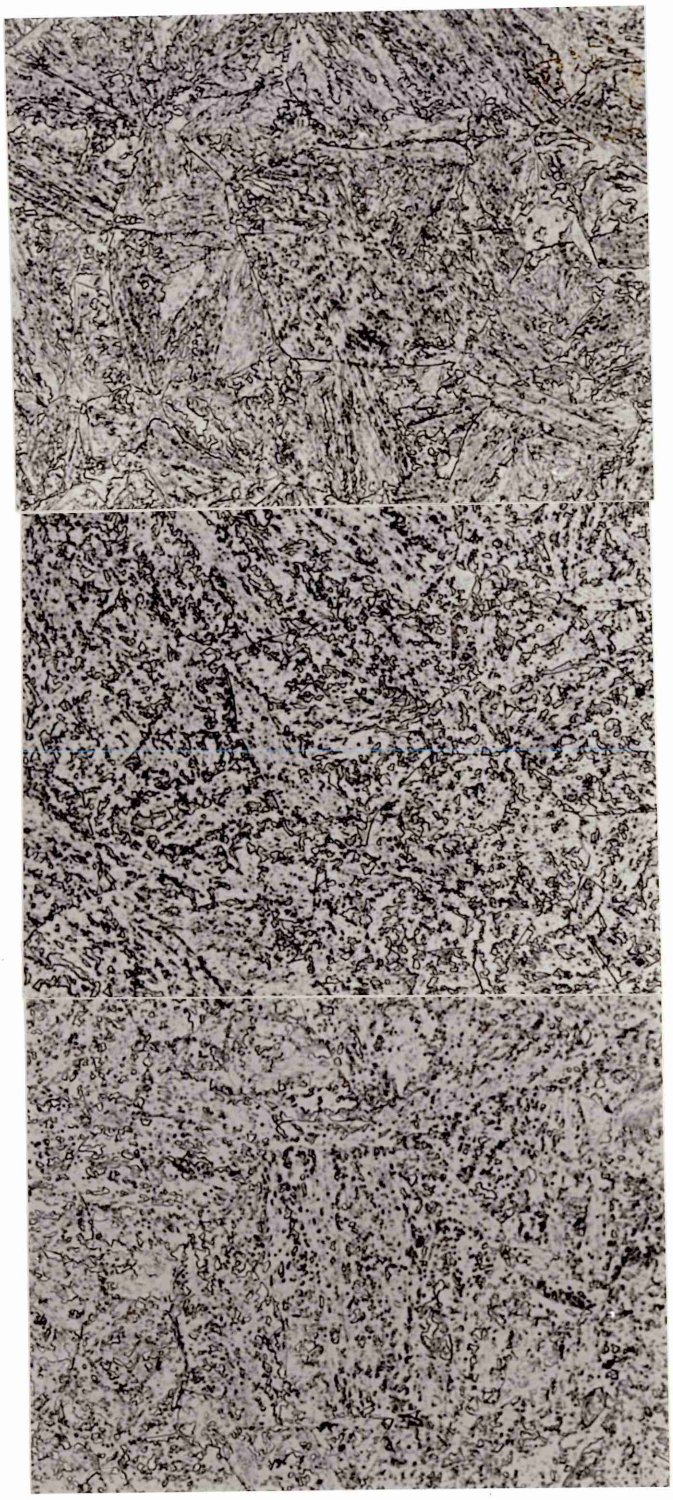

(d) 21.8°C/min
Test T

(e) 5.7°C/min
Test V

(f) 2.8°C/min
Test W

Figure 4.7-2 Optical micrographs of specimens in different cooling rates austenitised at 950°C for 20 mins (600x)

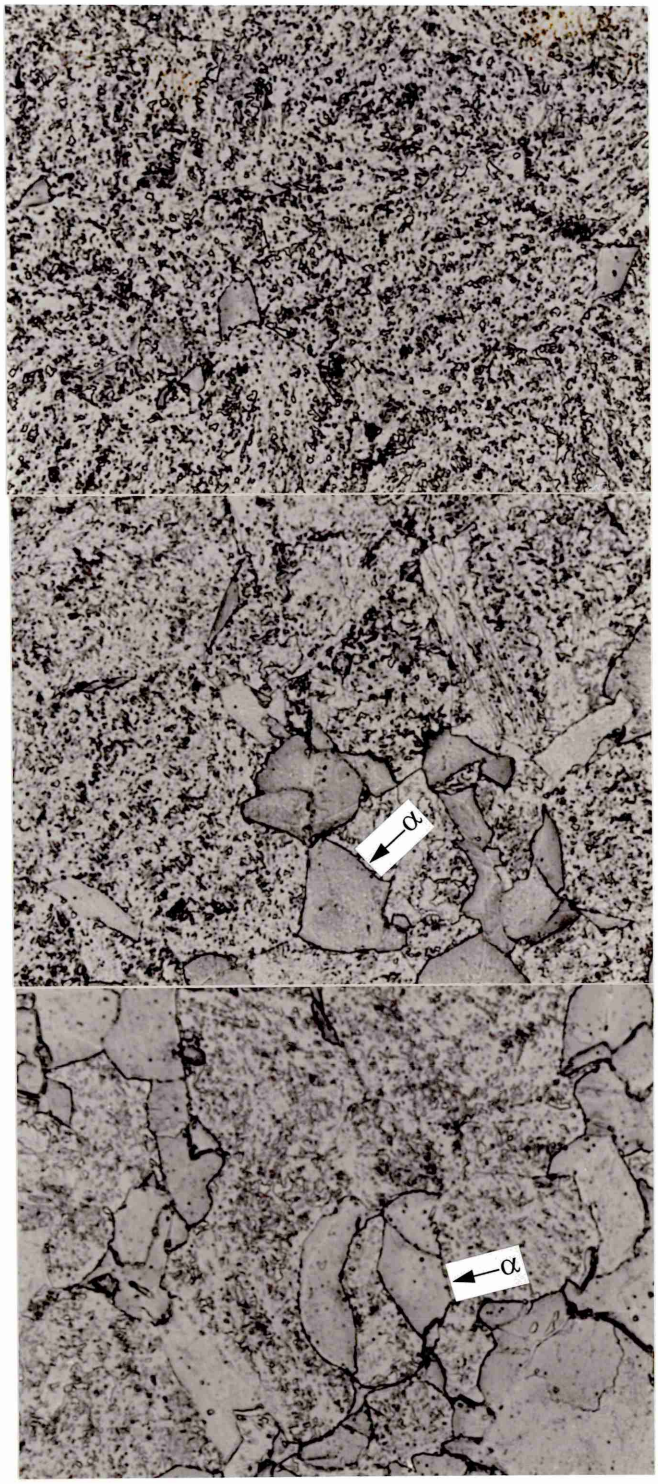

(g) 1.4°C/min
Test X

(h) 0.48°C/min
Test X2

(l) 0.3°C/min
Test X1

Figure 4.7-3 Optical micrographs of specimens in different cooling rates austenitised at 950°C for 20 mins (600x)

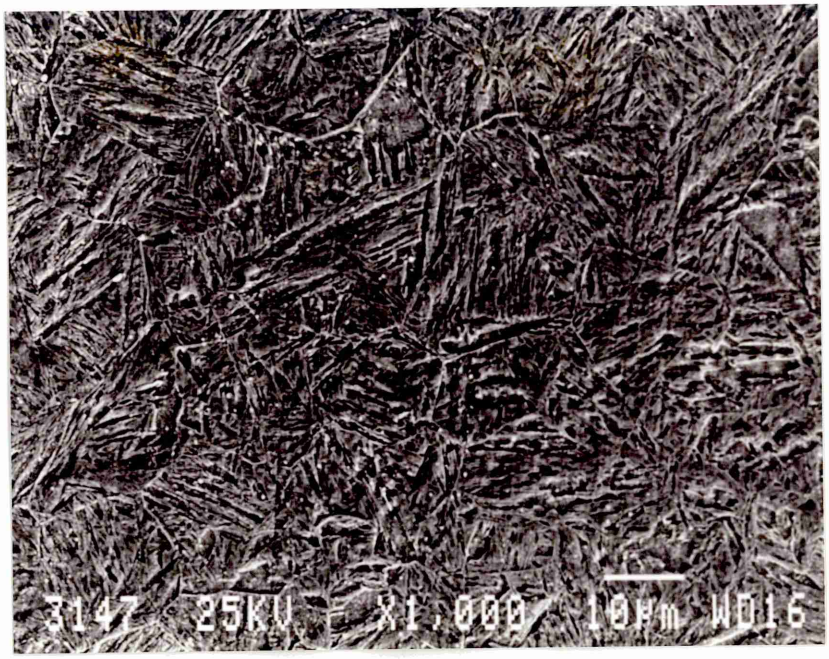

Figure 4.8 SEM micrograph showing the microstructure consisted of martensite with a few flecks of bainite, austenitised at 950°C for 20 mins and then cooled at 160°C/min

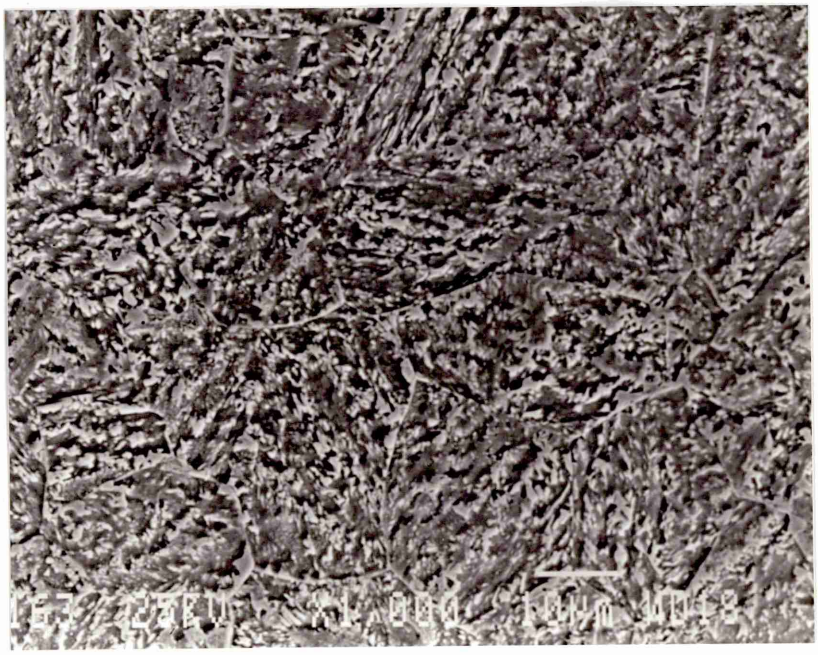

Figure 4.9 SEM micrograph showing the upper bainite microstructure, austenitised at 950°C for 20 mins and then cooled at 2.8°C/min

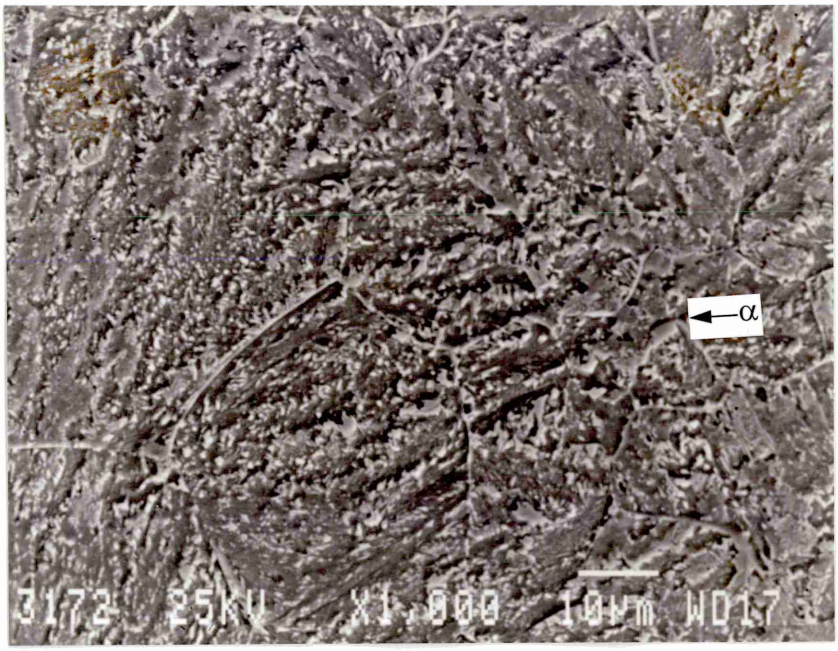

Figure 4.10 SEM micrograph showing the microstructure consisted of upper bainite and small amount of ferrite, austenitised at 950°C for 20 mins and then cooled at 0.48°C/min

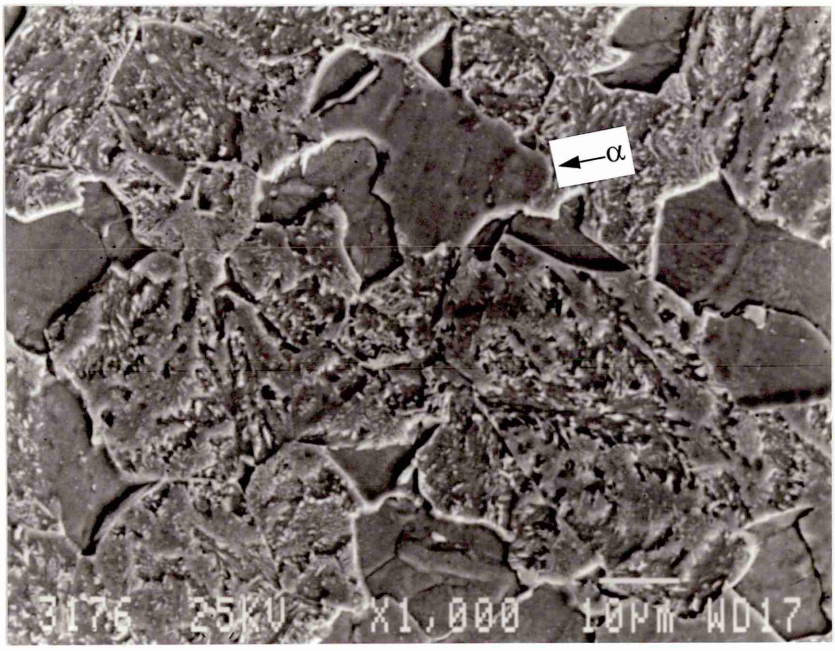

Figure 4.11 SEM micrograph showing the microstructure consisted of upper bainite and considerable volume fraction of ferrite, austenitised at 950°C for 20 mins and then cooled at 0.3°C/min

Alloying elements will influence the M_s temperatures of steels, and a number of equations have been developed to relate M_s to steel composition (Krauss, 1980). The equations developed by Andrews (1965) were based on measurements of M_s temperatures and compositions of a large number of steels of British, German, French, and American manufacturers. Andrews (1965) showed that 95% of measured M_s temperatures for the steels were within ± 25°C of the M_s temperatures calculated from their compositions according to the linear and product equations.

$$M_s\ (°C) = 539 - 423C - 30.4\ Mn - 12.1Cr - 17.7Ni - 7.5Mo \quad ...(linear)...(4.1)$$

$$M_s\ (°C) = 512 - 453C - 16.9Ni + 15Cr - 9.5\ Mo + 217(C)^2 - 71.5(C)(Mn) - 67.6(C)(Cr) \quad .....(product)...(4.2)$$

The M_s for this 2CrMoNiWV steel was calculated using Andrews' linear and product equations (4.1) and (4.2). The calculated M_s was 376°C and 377.5°C respectively, indicating good agreement with experimental result which was approximately 370°C. The slight difference between the calculated M_s and the experimentally obtained M_s might be in that Andrews' empirical equations did not take W addition into consideration.

After cooling, the specimens were metallographically examined to identify the microstructures associated with the various temperature ranges over which transformation occurred. Optical micrographs of specimens subject to different cooling rates are shown in Figure 4.7. At the faster cooling rates, 600°C/min to 160°C/min, the microstructure consisted of martensite with a few flecks of bainite, the hardness values were correspondingly high, see SEM micrograph Figure 4.8. The next five slower cooling rates, produced bainite microstructures, coupled with lower hardness value, as one of them shown in Figure 4.9. From the cooling rate of 0.48°C/min and slower, the microstructures

consisted of mixture of bainite and proeutectoid ferrite with an increasing volume fraction of proeutectoid ferrite, illustrated in Figures 4.10-4.11. The hardness level reduction reflected the amount of proeutectoid ferrite present.

4.3 Effect of Austenitising Temperature on Hardenability

From the study of austenitising treatment on prior austenite grain size, it was concluded that the austenite grain size of a steel depends both upon the temperature and time at the temperature above A_{C3} and has an important effect upon the transformation kinetics. A higher austenitising temperature 1000°C was used for dilatometric test from which another set of dilatometer records were obtained and a CCT diagram was constructed, see Figure 4.12.

When Figure 4.6 is compared to the diagram in Figure 4.12, it can be clearly seen that when the austenitising temperature is increased from 950°C to 1000°C, the proeutectoid ferrite nose moves towards the right, in other words, the hardenability of the steel is increased. From this fact, it could be concluded that one of the major factors influencing the continuous cooling characteristics of this steel is that of austenitising temperature. The reason for the increase in hardenability with increasing austenitising temperature is probably due to more carbides dissolving at higher temperature thus leading to more carbon being present in solution, and all other alloying elements will also play a full part in modifying the hardenablity.

It should be noted that prior austenite grain size between two austenitising temperatures with the same holding time is different. The higher austenitising temperature, the larger prior austenite grain size.

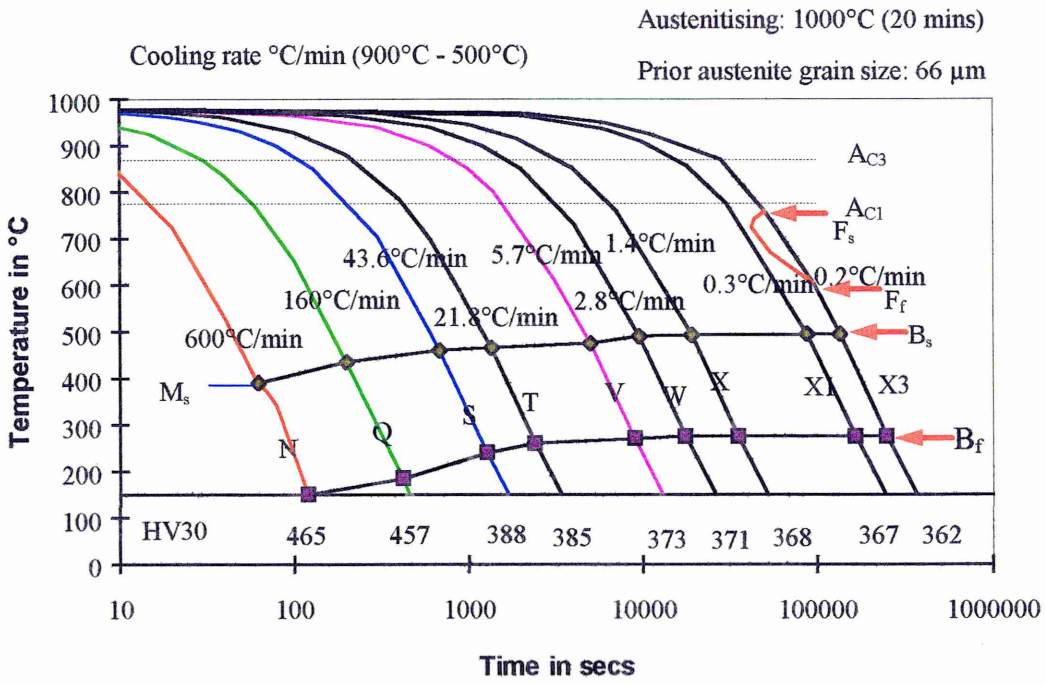

Figure 4.12 Continuous cooling transformation diagram for the 2CrMoNiWV rotor steel austentised at 1000°C for 20 mins

One of the most striking features of the CCT diagram for 2CrMoNiWV steel is the wide range of cooling rates over which bainite is the predominant transformation product from austenite. A convenient parameter for expressing this bainitic hardenability is the critical cooling rate for ferrite formation, *f'*. This is the slowest cooling rate at which the steel can be cooled and still attain a structure free of proeutectoid ferrite. The proeutectoid ferrite that forms at the slower cooling rate can be seen in Figure 4.10 and Figure 4.11. Figure 4.10 shows a rather characteristic feature of the bainitic microconstituent and proeutectoid ferrite just about to form. Figure 4.11 illustrates a large portion of proeutectoid ferrite (approximately 20% volume fraction) has already formed at the cooling rate of 0.3°C/min.

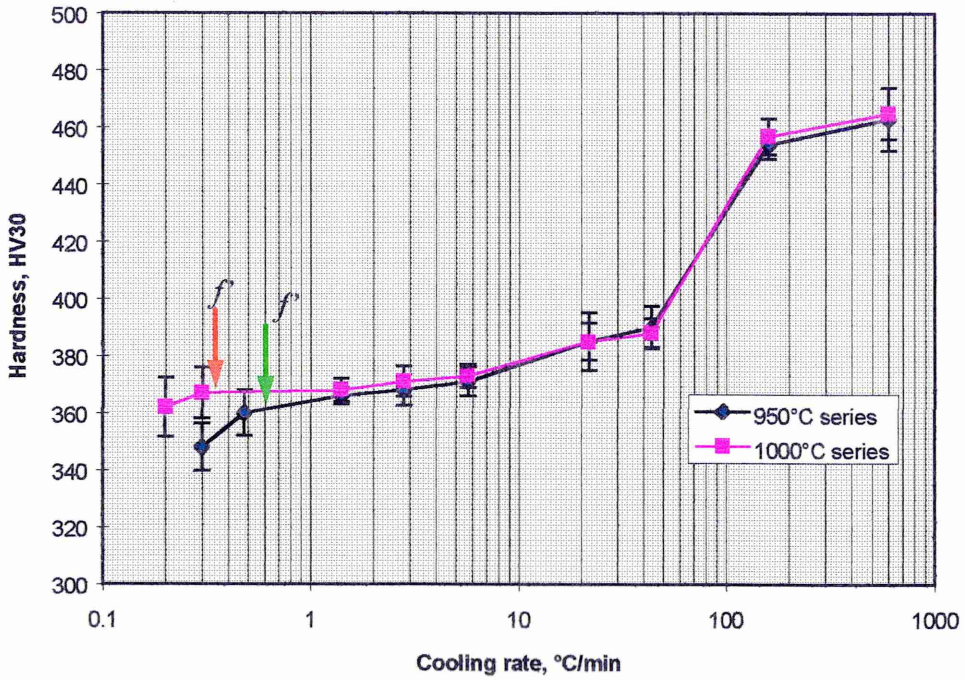

Figure 4.13 Hardness of as-cooled specimens as a function of cooling rates

The proeutectoid ferrite that forms on cooling at rates slower than *f'* affects the mechanical properties. This is illustrated in Figure 4.13 where hardness is plotted as a function of cooling rate. Beyond *f'* hardness decreases rapidly as the softer microconstituent, proeutectoid ferrite, becomes an increasing portion of the microstructure. Figure 4.13 also shows clearly the hardness droped dramatically at a critical cooling rate faster in 950°C series than in 1000°C series, this is attributed to the fact that the critical cooling rate, *f'*, in the 1000°C series was slower than the 950°C series, *i.e.* a larger volume fraction of proeutetoid ferrite formed at 950°C austenitising temperature than those formed at 1000°C austenitising temperature, cooling down at the same rate from austenite.

4.4 Comparison of Experimental Results and Theoretical Predictions

In this 2CrMoNIWV low alloy steel, the potential equilibrium reaction between Fe and other alloying elements have been investigated using the National Physical Laboratory's Metallurgical and Thermodynamic Data Bank (MTDATA) package (Davies *et al*, 1990). This computer package contains critically assessed thermodynamic data for a number of alloy systems. MTDATA allows the equilibria in multicomponent, multiphase systems to be calculated from a knowledge of the thermodynamic data for the subsystems. It is possible to calculate for a given temperature, pressure or volume, the phases by minimizing the Gibbs free energy of the system for specified component amounts. The main database used for the calculation in this work is the solution database created by the Scientific Group Thermodata Europe (SGTE). All calculations were made using the MULTIPHASE module of MTDATA.

Two cases were considered for thermodynamic calculations: (I) Using the actual composition of this 2CrMoNiWV steel, to predict the A_{C1}, A_{C3} and to see whether there are any phases existing in the austenite range. The operation of MTDATA was controlled through an easily learned user interface. The sequence of commands used in setting up the calculations is given in Appendix. (II) Without W addition in the system to repeat the calculation to see whether there are any differences in the austenite range. The sequence of operation of MTDATA was the same as Appendix, except the system excluded W.

Thermodynamic calculations were performed for each case with the same wide temperature range, in an attempt to know what equilibrium phases will form in service and temperature ranges as well. The calculation results

were almost the same in the austenite range, see Figures 4.14 and 4.15, which indicates 0.68 wt% W addition will not exert a significant effect on the thermodynamics in the austenitising temperature range. As carbide phases are always in small amounts in mass percentage, the ordinate was plotted in mass percentage logarithm scale. The calculated austenite start to form temperature A_{C1} is about 790°C and the calculated fully austenite temperature A_{C3} is about 870°C in Figures 4.14 and 4.15, which have very good agreement with the experimental results in Figures 4.6 and 4.13. However, taking account of the material in the "as-received" condition which was already tempered at 660-670°C for 30 hours, it can be reasonably deduced that in order to fully dissolve precipitated carbides during the solution treatment, a higher austenitising temperature than A_{C3} is required. Actually in practice, from the kinetic point of view the austenite temperature should be at least 50°C higher than the A_{C3} (Honeycombe, 1981).

It should be noted that in the austenite temperature range there is another FCC_A1 phase which finally disappears at about 970°C. In order to clarify what FCC_A1 stands for, mass fraction of component for the two FCC_A1 phases were demonstrated separately in Figures 4.16 and 4.17. Figure 4.16 shows FCC_A1 phase (1) is basically composed of Fe austenite with the bulk alloy composition. Figure 4.17 illustrates FCC_A1 phase (2) is V-rich carbide corresponding to V_4C_3 (referred as MC in this study) with face centered crystal structure and a few Mo, W, Cr, soluted in this carbide phase.

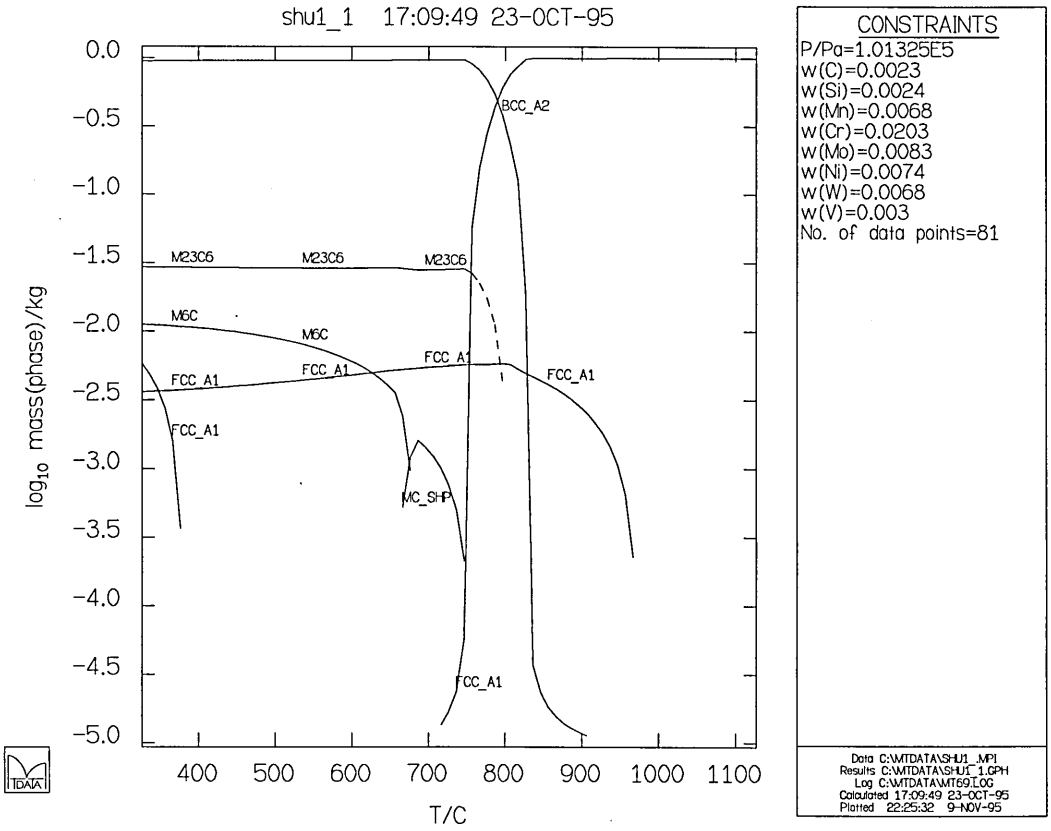

Figure 4.14 Thermodynamic calculation with actual composition

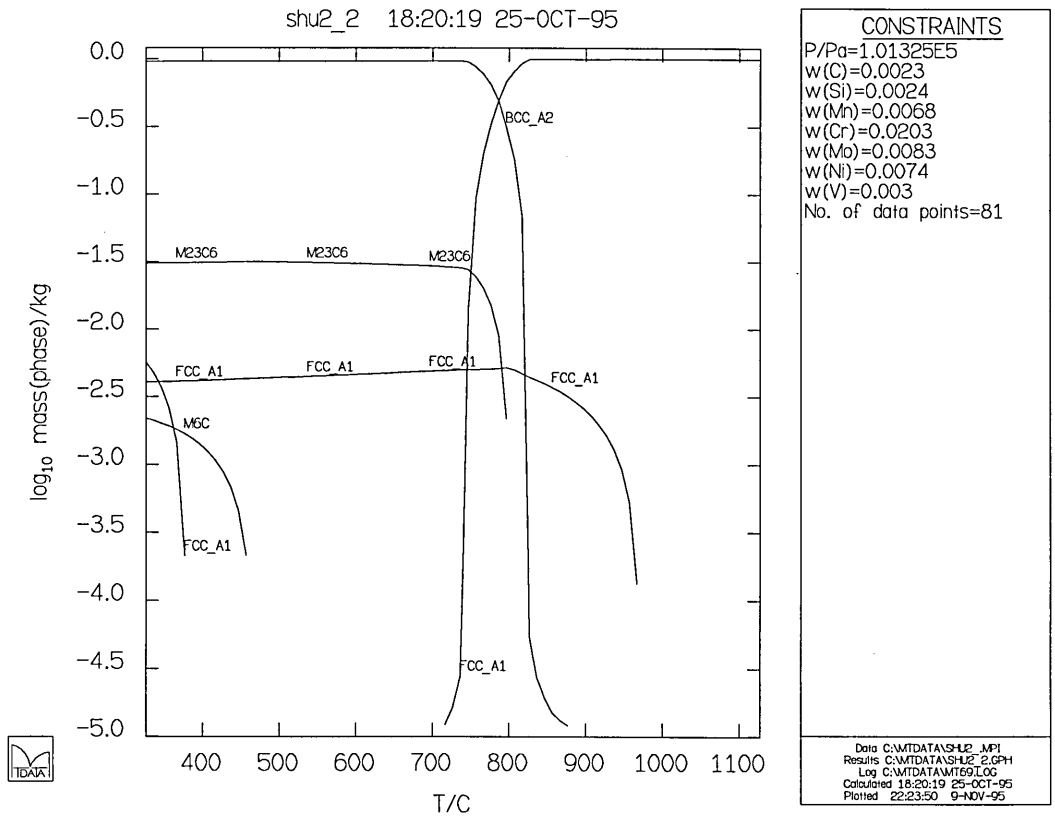

Figure 4.15 Thermodynamic calculation without W addition

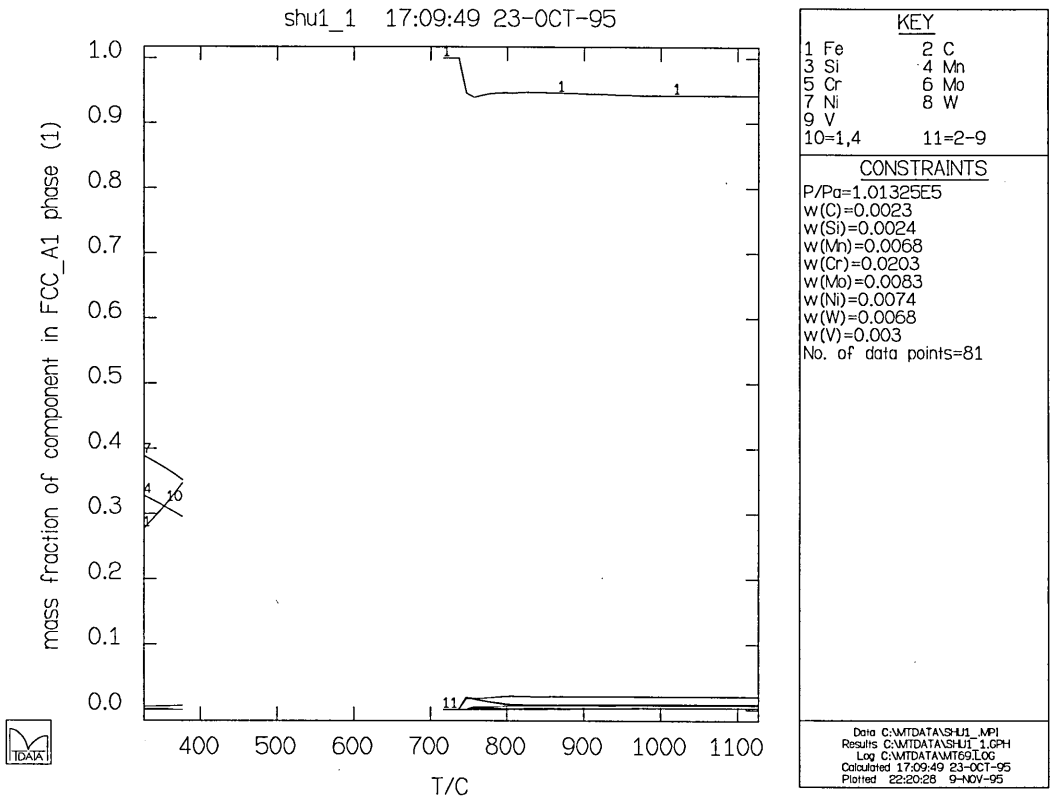

Figure 4.16 Mass fraction of component in FCC_A1 phase (1) as a function of temperature

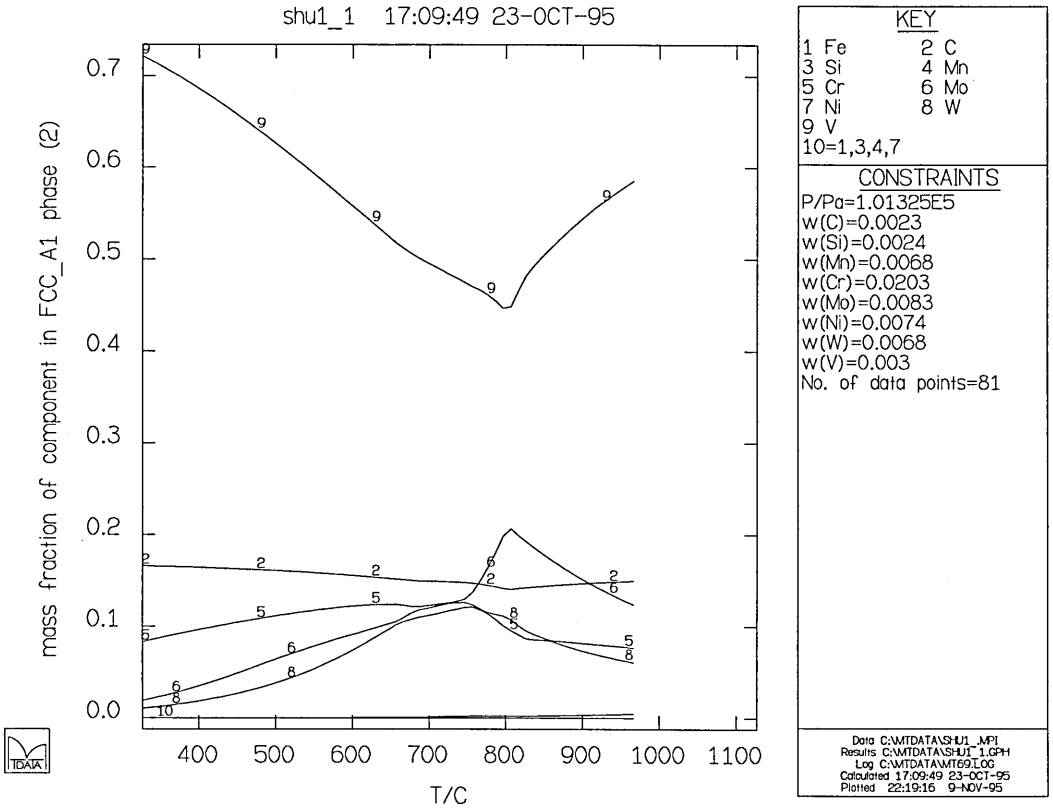

Figure 4.17 Mass fraction of component in FCC_A1 phase (2) as a function of temperature

4.5 Discussion and Conclusions

The mechanical properties of the 2CrMoNiWV rotor steel are dependent upon the rate of cooling of the material from the austenitising temperature and the degree of tempering. Increasing the austenitising temperature, will increase the austenite grain size whilst enabling more carbon to be present in the solution and therefore increase the bainitic hardenability of the material. It is generally accepted that the cooling rate from the austenitising temperature should be such that the structure transforms from austenite to bainite, as this structure after tempering possesses the most satisfactory creep and tensile strength while retaining adequate ductility (Bates and Ridal, 1963). Cooling rates which are too fast will result in the formation of martensite; those that are too slow allow sufficient time for proeutectoid ferrite to form. Both these constituents are recognized as imparting inferior creep properties to the material (Bates and Ridal, 1963). It is therefore necessary to ensure that the cooling rates across the diameter of a forging lie within the bainite range.

In practice, to manufacture larger rotors it was anticipated that greater hardenability would be required to produce upper bainite structure for the core of a rotor. From this point of view, the 2CrMoNiWV steel for application as steam turbine rotors should have sufficient hardenability to provide the appropriate microstructure and improved toughness compared with conventional CrMoV steel (Wiemann, 1991). This investigation confirmed that the 2CrMoNiWV steel has very high banitic hardenability, and thereby provided useful information in applying this steel as steam turbine rotor in diameters up to 1000 mm. The critical cooling rate for proeutectoid ferrite formation, f' defined as the slowest rate at which the material can be cooled and still result in a microstructure free of proeutectoid ferrite, is considered the parameter of great significance. In terms of the average cooling rate between 900 and

500°C, *f'* for 2CrMoNiWV steel is less than 1°C/min; this corresponds to the cooling rate at the center of a 1000 mm diameter rotor forgings during oil quenching (Strang, 1995).

Within a certain range of cooling rates the formation of predominant bainite recognized as essential to the good creep integrity and therefore cooling rate may be a more accurate parameter to be controlled in commercial practice.

According to equilibrium calculations, performed with MTDATA, there are no other intermediate phase in the actual temperature range for austenitisation, except a few V-rich carbides which should be fully dissolved at about 970°C. Therefore if austenitising temperature between 970-1000°C is chosen, all alloy elements will play full part in modifying the hardenability. This conclusion will be confirmed by TEM examination on thin foils and carbon extraction replicas of austenitised specimens in the following Chapter.

Chapter 5

HEAT TREATMENT OPTIMISATION

In most of ferritic low alloy steels, the high temperature properties such as creep strength, ductility and crack growth resistance depend critically on the structures produced during the initial heat treatment and on the type and morphological distribution of alloy carbides formed during subsequent tempering (Townsend, 1993). In order to obtain the best distribution of carbides by choosing the correct critical heat treatment which has to be chosen to maintain structure as far as possible during service (Strang, 1995). Extensive studies on the effect of various heat treatment trials on microstructural change and carbide evolution are discussed in this chapter. The observed carbide composition changes are found to be highly dependent on the position of the carbides within the microstructure and on the particle size. The transformation of alloy carbides from one type to the other is also studied. Consequently it is of considerable interest, both from an industrial and academic point of view, to investigate any changes in carbide characteristics with different heat treatments. A possible optimised heat treatment route for this 2CrMoNiWV steel was suggested following the systematic study.

5.1 Austenitising Treatment

Austenitising treatments were conducted at temperatures of 900, 925, 950, 975 and 1000°C for times of 1, 2, 5, 10, 20 and 50 hours followed by oil quenching to room temperature to study the effects of austenitising treatments on hardness and prior austenite grain size.

5.1.1 Hardness Test Results

Vickers hardness tests (Hv30) were conducted on all oil quenched specimens. As comparisons were to be made between different specimens, the same Vickers machine and same load (30 kg) was used. Nine readings were taken from each specimen to provide the mean and standard deviation for each condition of heat treatment. Specimens which were exposed for more than 20 hours at higher temperatures were found to be severely oxidised and Vickers pyramid ocular readings deviated greatly between the outside and centre of the specimens due to decarburisation. Thus for specimens exposed for 20 and 50 hours at 975 and 1000°C not only did the hardness dropped rapidly, but the standard deviations were significant. However, the Hv30 values for those exposed less than 10 hours were almost constant. No significant effect on hardness occurred in the austenitising temperature range of 900 to 1000°C with exposure times of up to 10 hours.

Accordingly it was decided to conduct all high temperature heat treatments with all specimens put in evacuated silica tubes under a low pressure argon atmosphere. In the experimental austenitising range the hardness Hv30 obtained varied between 360-460. Table 5.1 shows Vickers hardness test results after austenitising treatment followed by oil quenching. A graph was drawn showing the relationships between hardness, austenitising temperature and time, see Figure 5.1. From Table 5.1 and Figure 5.1, it can be concluded that increasing austenitising temperature increases the hardness of the material, but increasing austenitising time at higher temperature will result in the hardness dramatically drop.

From a theoretical viewpoint, time at temperature should be kept to a maximum to enable carbides back into solution and to obtain a homogeneous microstructure. However in practice, this condition is limited due to the

combined possibility of excessive scaling, austenite grain growth and associated decarburisation.

Table 5.1 Hv30 test results after austenitising treatment followed by oil quenching

Temperature	Austenitising time (hrs)					
°C	1	2	5	10	20	50
900	455.8 ±2.22	454.4 ±2.51	453.1 ±1.05	450.2 ±2.86	447.2 ±4.82	428.7 ±12.25
925	455.9 ±5.99	451.6 ±2.18	453.0 ±4.09	444.9 ±3.33	442.1 ±2.47	422.0 ±13.00
950	456.0 ±4012	450.4 ±3.97	447.4 ±3.47	449.8 ±4.18	438.4 ±4.36	416.7 ±15.12
975	458.4 ±4.07	454.8 ±4.68	448.3 ±7.07	443.1 ±5.21	434.6 ±7.83	389.2 ±12.04
1000	459.9 ±7.10	453.4 ±3.88	449.1 ±3.14	447.2 ±3.63	424.6 ±13.25	362.9 ±13.92

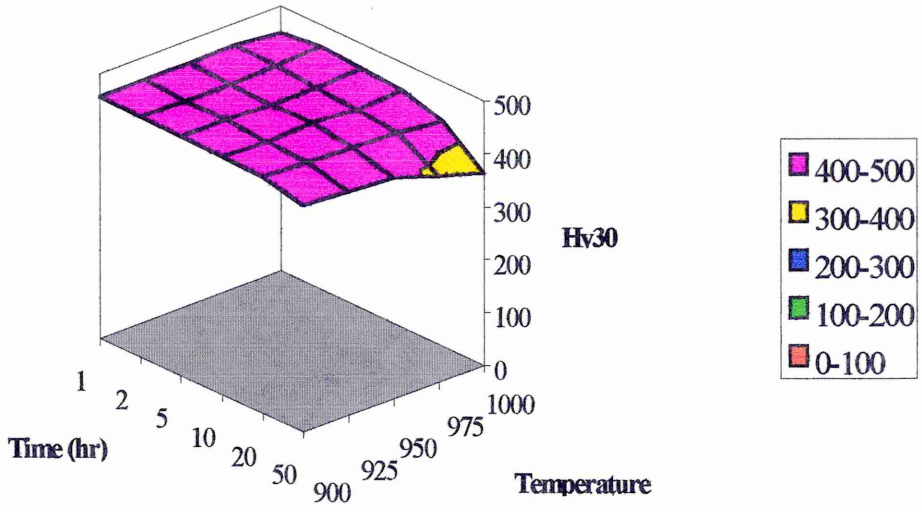

Figure 5.1 Effect of austenitising temperature and time on hardness

5.1.2 Prior Austenite Grain Size

One approach to improving the reliability and efficiency of turbine rotors has been to optimise both toughness and creep properties through control of prior austenite grain size.

It is well established that the toughness of steel can be improved through prior austenite grain size refinement (Roberts, 1970). However, large prior austenite grain size favours creep strength improvement. There have been a number of studies(Bates and Ridal, 1963) in which creep ductility and strength of CrMoV rotor steel have been measured for different prior austenite grain size. Unfortunately, however, other important parameters, such as carbide size and distribution, have also been simultaneously varied. Nevertheless, classical physical metallurgy indicates that, under typical service condition, steels with coarse grain size have lower creep rates and higher stress rupture strengths as compared to the same steel of finer grain size. A simple explanation for this is

that a coarse grained steel possesses less total grain boundary area for grain boundary sliding than a fine grained steel.

In order to study the effect of austenitising treatment on prior austenite grain size, many reagents and methods recommended by various references have been tried. Although clearly delineating grain boundaries for a specific low alloy steel is always a challenging problem for metallurgists, it was found in this investigation that several reagents and methods could be effectively used. The criterion for revealing the prior austenite grain boundaries is the least time consuming and it must be the true prior austenite grain size to be measured. Table 5.2 lists some of the effective etching techniques used in this case, along with a few relevant comments. In order to get a better revelation of grain size, some times several methods or combination of techniques have been tried.

It was also noticed that samples austenitised at higher temperatures and longer times were comparatively easier to reveal grain boundaries than those austenitised at lower temperatures and shorter times. The examination of the effect of austenitising temperature and time on grain size showed that with an increase in austenitising temperature and exposure time, grain sizes increased from about 40 μm to 70 μm.

Table 5.2 Summary of etching methods for revealing prior austenite grain boundaries

Methods	Comments
(1) CrO_3 + Phosphoric acid + H_2O	(a) Electrolytic etch, current and voltage may be vary on different heat treated samples (b) 15-30 minutes etch
(2) Villela's reagent and 2% Nital successive etching	(a) Least time consuming (b) Show grain boundaries as well as microstructure (c) Suitable only for those samples austenitised at higher temperature and longer exposure time
(3) Saturated aqueous solution of picric acid	(a) Time consuming (may last several hours) (b) May repeat polishing and etching several times
(4) Oxalic acid +H_2O_2 +H_2O	(a) Lightly tempering before etching (b) Room temperature etch
(5) Shaffe Meister's	(a) Quick etching (b) Show microstructure as well
(6) Vacuum grooving	(a) Re-heat treatment at austenitising temperature range (b) Need vacuum heating facility (c) May not reflect true prior austenite grain size
(7) $CuCl_2$ + picric acid	(a) Direct room temperature etch (b) 7-10 minutes etch (c) Wash in 50% ammonia solution

5.1.3 Carbide Dissolution

According to equilibrium calculations, performed using MTDATA (see Figure 4.9), there were no carbides or other intermediate phase in the experimental austenitising temperature range. The question was, however, if all particles could be dissolved within 5 hours. Some experiments were conducted at selected austenitising temperature and the micrographs from TEM examinations of these specimens by carbon extraction replicas are shown in Figures 5.2-5.3. Figure 5.2, shows no significant particles remained for the samples austenitised 975°C and 1000°C, which indicates that all carbides were dissolved above that experimental autenitising temperature range. However the grain size following austenitisation at 1000°C was obvious larger than the one austenitised at 975°C. Another experiment was carried out using an austenitising temperature of 950°C for 5 hours and then quenched in oil to minimise any precipitation during cooling to room temperature. Thorough examination of this specimen in TEM it was found that for the lower austenitising temperature a small number of spherical particles remained within the microstructure which were confirmed as MC (V_4C_3) carbides by convergent beam electron diffraction techniques, see Figure 5.3.

According to the experimental results and TEM examination, this steel should be austenitised for 5 hours at 975-985°C to ensure complete resolution of all carbide phases. Temperature above this range leads to grain growth and severe surface decarburisation in real commercial practice. For temperatures below 975°C there will be a risk for undissolved carbides.

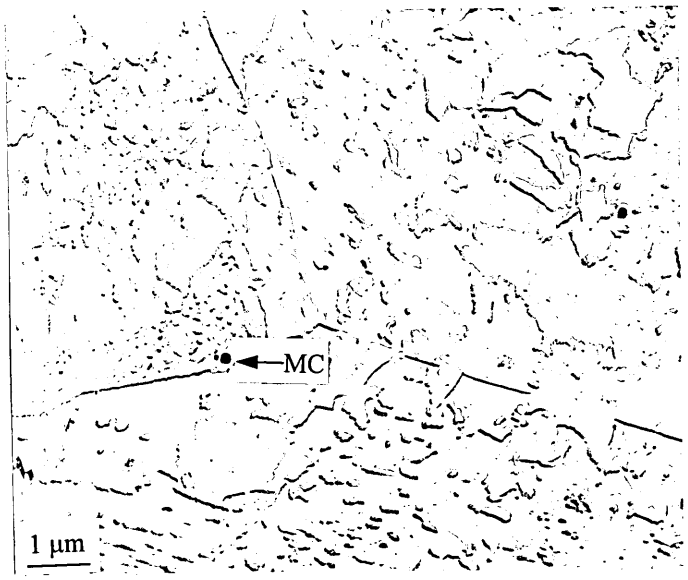

(a)

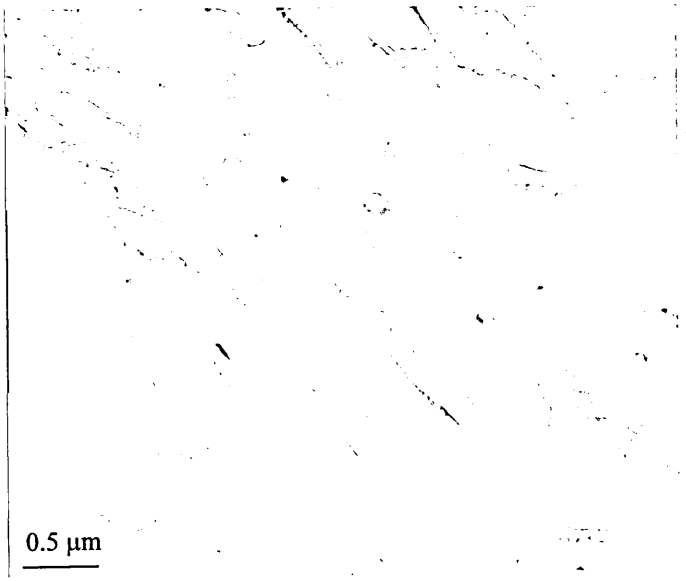

(b)

Figure 5.2 Austenitised at (a) 975°C for 5 hrs and (b) 1000°C for 5 hrs followed by furnace cooling showing particles almost fully dissolved

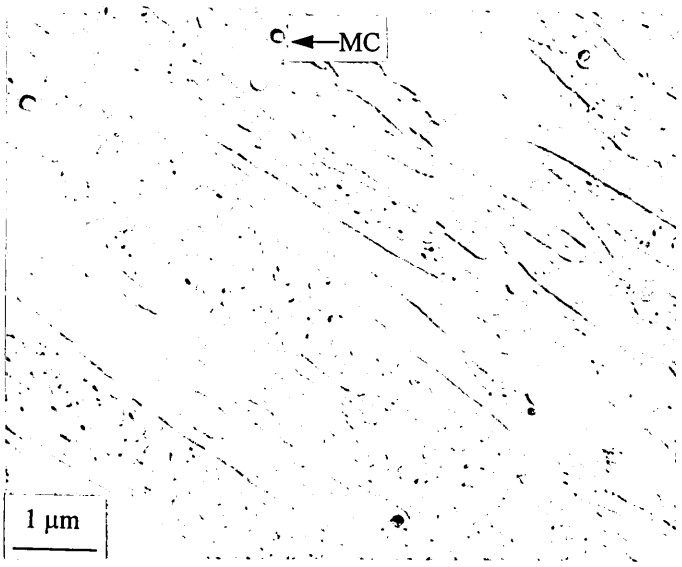

(a) TEM bright field image

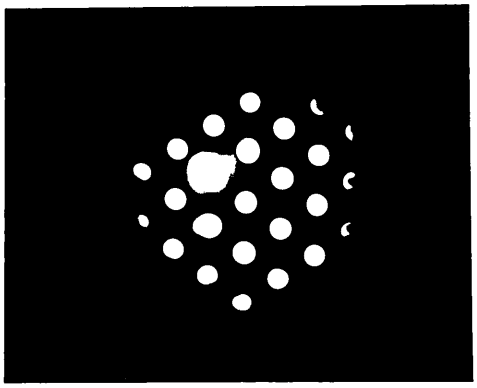

(b) Convergent beam diffraction pattern of one of undissolved particles

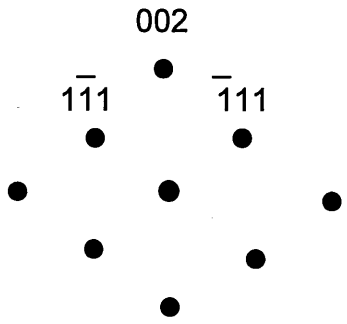

<110> MC

(c) Interpretation of CBDP (b)

Figure 5.3 Austenitised at 950°C for 5 hrs followed by oil quenching showing undissolved MC particles remained

5.2 Tempering Treatment

In order to enable alloy elements dissolving in solution during austenitising treatment without obvious grain growth, 975°C for 5 hours followed by furnace cooling was selected as the austenitising condition for this material. Several experiments were carried out aiming for controlled cooling rate to produce fully bainitic structure. It was found the rapid heating carbolite furnace (RHF) gives a furnace cooling rate around 10°C/min from 900-500°C and preliminary experiments demonstrated that this material austenitised at 975 °C for 5 hours followed by RHF furnace cooling could produce a fully bainitic structure. After austenitising at these conditions, specimens were tempered individually for times of 1, 2, 5, 10, 20, 50 and 100 hours at temperature of 600, 625, 650, 675 and 700°C followed by air cooling.

5.2.1 Hardness Test Results

Vickers hardness tests (Hv30) were carried out on all tempered specimens. In the furnace cooled condition, the mean Hv30 was 372±1.41 and hardness test results after tempering for up to 100 hours in the tempering range 600°C to 700°C are shown in Table 5.3. The effect of tempering temperature and time on the hardness of the bainitic microstructure is shown in Figure 5.4. Generally speaking, the higher the tempering temperature and/or longer tempering time, the lower the hardness of the specimens. It indicates that when a bainitic structure is heated it becomes possible for carbon held in the supersaturated solution to diffuse through the lattice and precipitate from solution in the form of carbides. The precipitation in the early stages are likely to harden the material. Figure 5.4 shows a obvious secondary hardening in the lower tempering temperature range. This must be due to the carbide forming

elements not only retard softening but also form fine alloy carbides that produce a hardness increase at relatively short tempering time. Later when precipitates have coarsened, the dislocation density within the matrix will be reduced and the strain within the lattice also relieved, which may cause the hardness of the steel to be reduced.

Table 5.3 Hv30 test results after tempering of specimens austenitised at 975°C for 5 hrs followed by furnace cooling at rate of about 10°C/min

Temperature	Tempering time (hrs)							
°C	0	1	2	5	10	20	50	100
600	372.0 ±1.41	421.8 ±3.03	416.8 ±2.77	410.4 ±3.29	404.2 ±3.19	397.4 ±2.97	373.8 ±4.09	354.2 ±1.79
625	372.0 ±1.41	415.6 ±1.34	413.0 ±1.41	409.0 ±4.85	392.4 ±2.61	378.6 ±1.67	342.6 ±0.89	308.2 ±0.84
650	372.0 ±1.41	407.0 ±3.81	385.0 ±2.83	368.4 ±1.67	339.8 ±2.28	302.4 ±1.52	269.0 ±1.00	249.2 ±0.45
675	372.0 ±1.41	388.6 ±1.67	368.8 ±1.10	330.8 ±1.79	301.2 ±1.79	273.6 ±1.52	238.2 ±0.84	222.6 ±0.89
700	372.0 ±1.41	333.4 ±1.82	304.0 ±0.50	265.0 ±1.22	242.4 ±0.89	222.4 ±0.55	199.8 ±0.45	187.0 ±0.71

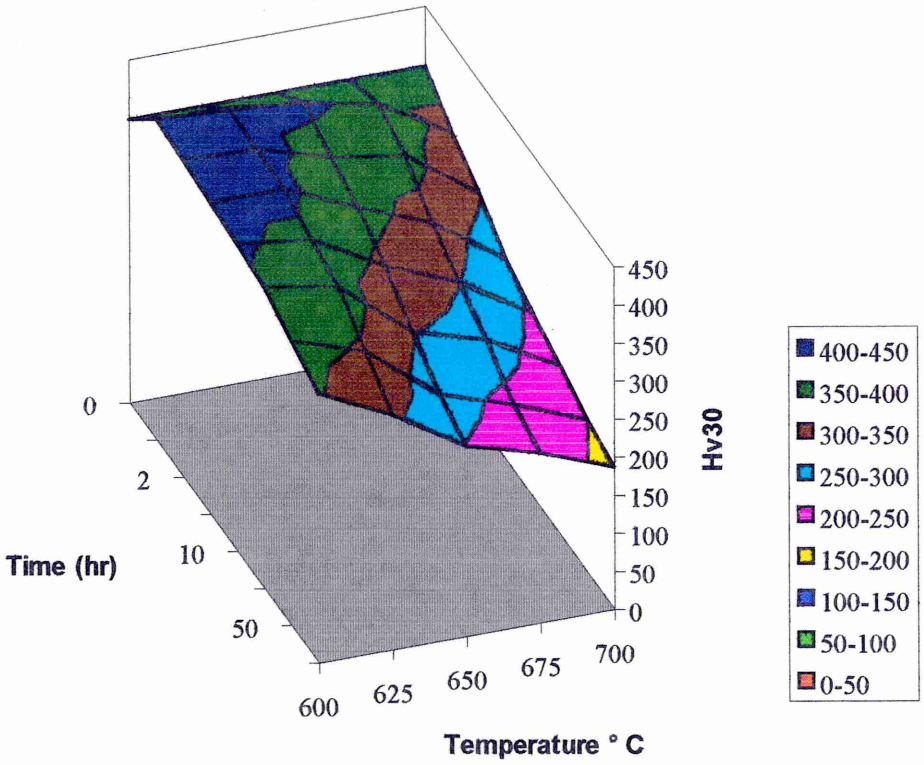

Figure 5.4 Effect of tempering temperature and time on hardness of bainitic microstructure

On obtaining a critical dispersion parameter, the strength of the steel reaches a maximum, and as the carbide dispersion slowly coarsens, the strength decreases. The process is both time and temperature dependent, so both variables are often combined in terms of the tempering parameter P, such as the Larson-Miller Parameter (LMP).

$$LMP = T (k + \log t)/1000 \quad \text{.....(5.1)}$$

where T is the absolute temperature and t the tempering time, while k is a constant which is about 20 for alloy steels (Honeycombe, 1981). HV can be plotted against the LMP to give one typical curve for this steel which is illustrated in Figure 5.5. These tempering treatments represent a variation in

LMP between 17.5 and 20.5, which covers a combination of tempering temperature range of 600°C to 700°C with exposure times from 1 hour up to 100 hours.

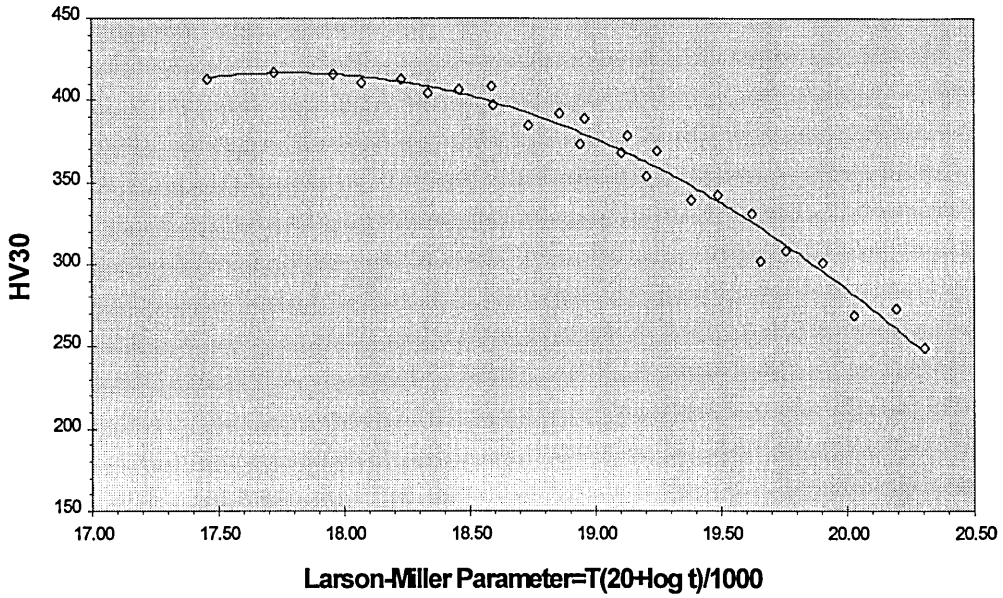

Figure 5.5 Tempered Hardness versus Larson-Miller Parameter

5.2.2 Morphologies of Tempered Bainite

All tempered specimens were preliminarily examined using a optical microscope. The observations showed that the microstructure of furnace cooled then tempered specimens exhibited microstructures with very fine dispersed carbides both within the matrix and on the prior austenite grain boundaries.

Selected results of the structural examination using SEM are illustrated in Figures 5.6-5.9 which give an impression of the real particle distribution and

size. Tempered bainitic structures with fine dispersed carbides both within the matrix and on the prior austenite grain boundaries are clearly shown. The chemical composition of the steel, tempering time and tempering temperature directly affect the phase constitution of the long-term tempered state. The character, mechanism and kinetics of carbide changes in crystal structure, chemical composition and size of carbide particles during tempering will be discussed in details in the Section 5.3.3 and Section 7.3.

5.3 TEM and EDX Examination

Theoretically, most of carbide phases can be identified uniquely using electron diffraction, but in practice this can be very difficult and time consuming when examining large numbers of small particles. The carbides were often too thick or too thin to provide reasonable diffraction data, and the diffraction patterns could sometimes be ambiguous. Using electron convergent beam diffraction pattern can be of great help in this aspect (Titchmarsh, 1979).

A frequently used alternative method in this type of research was based on EDX microanalysis. This technique for carbide phase identification was carried out in the TEM and permits chemical analysis to be made on individual carbide particles. Pilling and Ridley(1982) found that the carbides showed one of five characteristic X-ray spectra while these spectra were identified using diffraction techniques. Titchmarsh(1979) used a method based on EDX and diffraction patterns to produce some characteristic Mo/Cr and Fe/Cr count ratios which allow carbides to be identified rapidly.

Morphological differences can also act as a guide in the identification of carbides Pilling and Ridley(1982) suggested that there were four distinct carbide morphologies in 2.25%Cr-1%Mo specimens tempered at 700°C. The

clusters of needle shaped precipitates in the matrix was Mo_2C, globular grain boundary carbides were M_6C or $M_{23}C_6$ and rod shaped precipitates and small parallelogram shaped carbides were M_7C_3. But the shape of the particles alone is not a convincing method of identification.

5.3.1 Electron Diffraction and EDX

A full survey for each type of distinctive EDX spectrum in this steel was carried out using the convergent beam diffraction patterns from individual precipitate particles in replicas. The specimens covered a wide range of different tempering treatment conditions. Replicas for each tempered condition were placed in a double-tilt TEM holder allowing particles to be titled to align a low index zone axis with the optical axis of the microscope. This process was somewhat tedious, but pattern indexing was greatly facilitated during subsequent analysis. A characteristic X-ray spectrum was recorded from the same precipitate (Titchmarsh, 1978)

The spectra of the different carbides were quite distinctive as shown in Figure 5.10 and therefore can be used as "finger prints" for the identification of individual carbides, and this was confirmed by recorded convergent beam diffraction patterns as also shown in Figures. 5.10-1 to 5.10-3 with schematic interpretation. The carbide species in a commercial 2CrMoNiWV creep resisting steel could be identified from their EDX spectra according to the following rules:

(1). The spectrum with just one high peak corresponding to V was that of MC carbide.

(2). M_2C had high Mo and W peaks and the presence of significant peaks of Cr and V.

(3). M_3C had a spectrum with a high Fe peak and a high Cr peak.

(4). M_7C_3 was distinguished by the Cr peak higher than the other high peak for Fe.

(5). $M_{23}C_6$ had a spectrum with similar height of Fe and Cr peaks, Fe/Cr count ratio is about 1.

(6). M_6C had a spectrum with a high Fe peak and considerable high peaks for Mo and W.

The results of the TEM/EDX examination are shown in Table 5.4-5.8. Some selected long time tempering conditions up to 1000 hrs were added to determine final equilibrium carbide phase and carbide evolution process in this material. Precipitated carbide phases in the tempering conditions of low temperature and short times were basically M_3C with a few MC. M_7C_3 and $M_{23}C_6$ appeared at 600°C for 20 hrs. M_2C was found at 650°C after 20 hrs or 700°C after 5 hrs, meanwhile M_3C starts to disappear. At high temperature and longer time tempering, $M_{23}C_6$ becomes dominant at prior austenite grain boundaries, M_6C was also found. The concentration of C in the matrix was reduced by the precipitation of M_6C and the transformation from M_7C_3 to $M_{23}C_6$ was accelerated. The latter had a lower concentration ratio of C to metal than the former (Kuo, 1956). $M_{23}C_6$ and M_6C exist after a long time tempering as the stable precipitated phases, but MC, M_2C and M_7C_3 were also detected for sample tempered at 700°C for 500 hours.

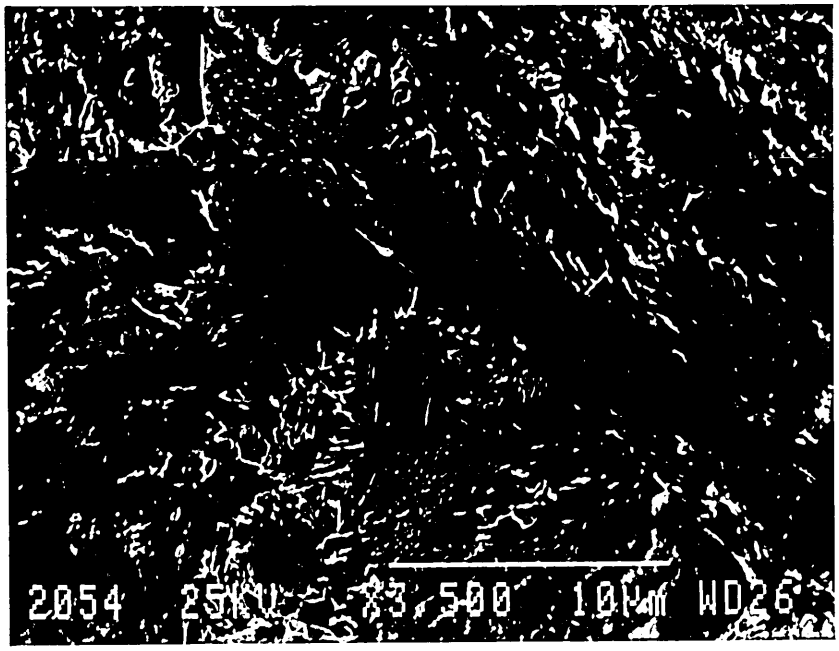

Figure 5.6 Austenitised at 975°C for 5 hrs followed by furnace cooling and then tempered at 600°C for 5 hrs

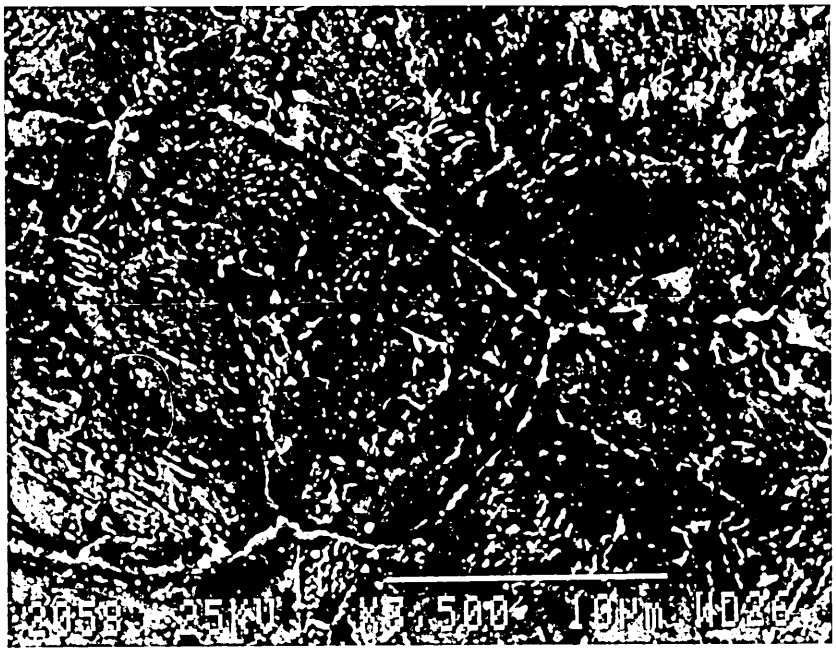

Figure 5.7 Austenitised at 975°C for 5 hrs followed by furnace cooling and then tempered at 650°C for 20 hrs

Figure 5.8 Austenitised at 975°C for 5 hrs followed by furnace cooling and then tempered at 700°C for 20 hrs

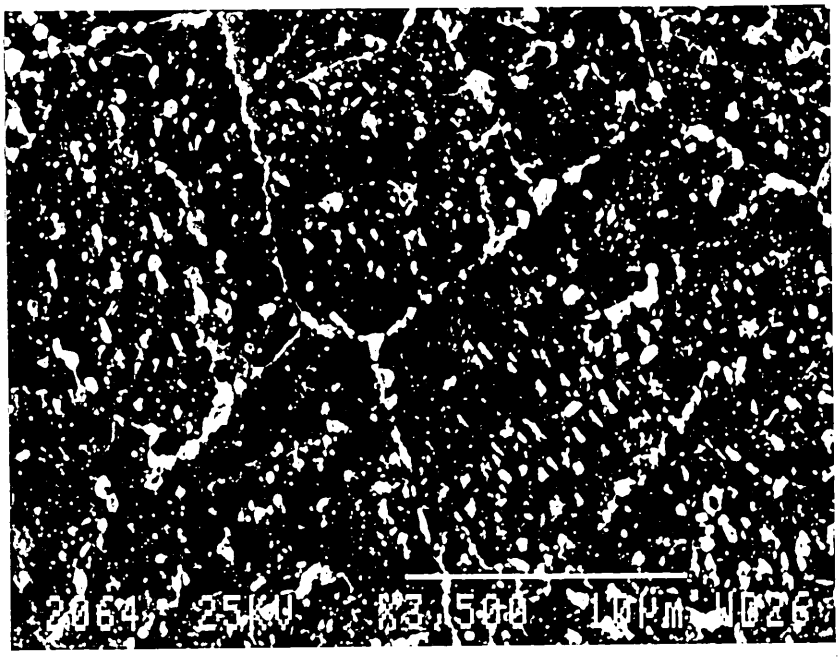

Figure 5.9 Austenitised at 975°C for 5 hrs followed by furnace cooling and then tempered at 700°C for 100 hrs

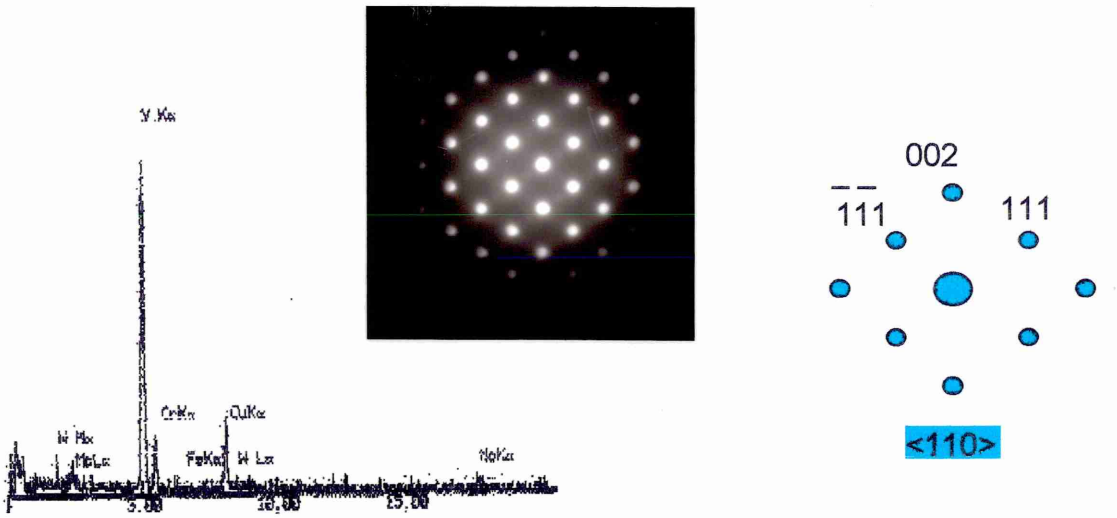

(a) MC

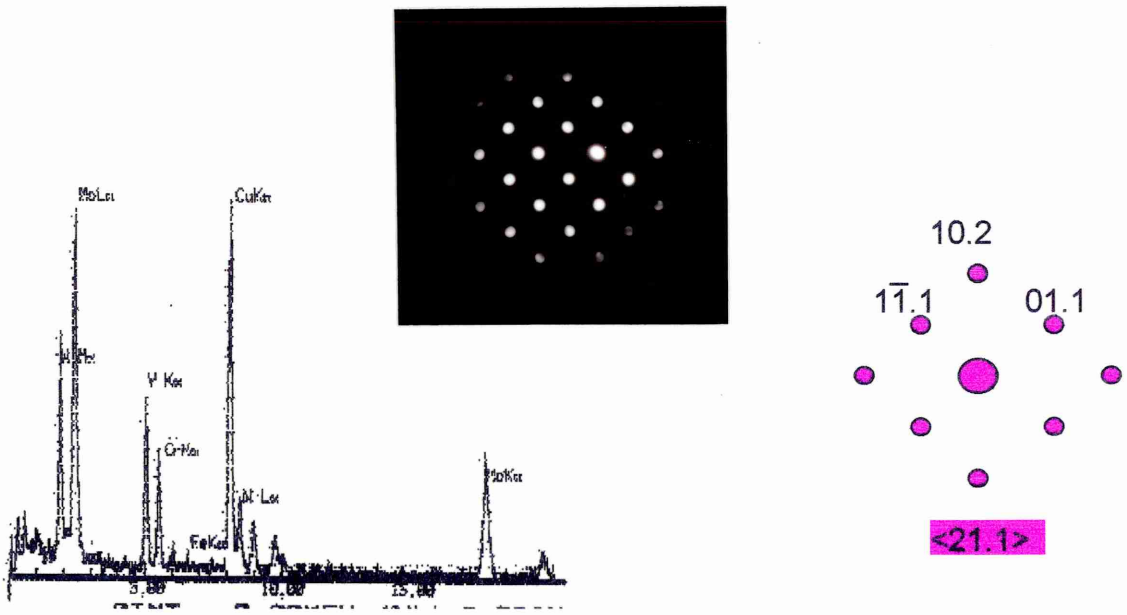

(b) M_2C

Figure 5.10-1 Characteristic X-ray spectra of carbides confirmed by their convergent beam electron diffraction patterns in 2CrMoNiWV steel

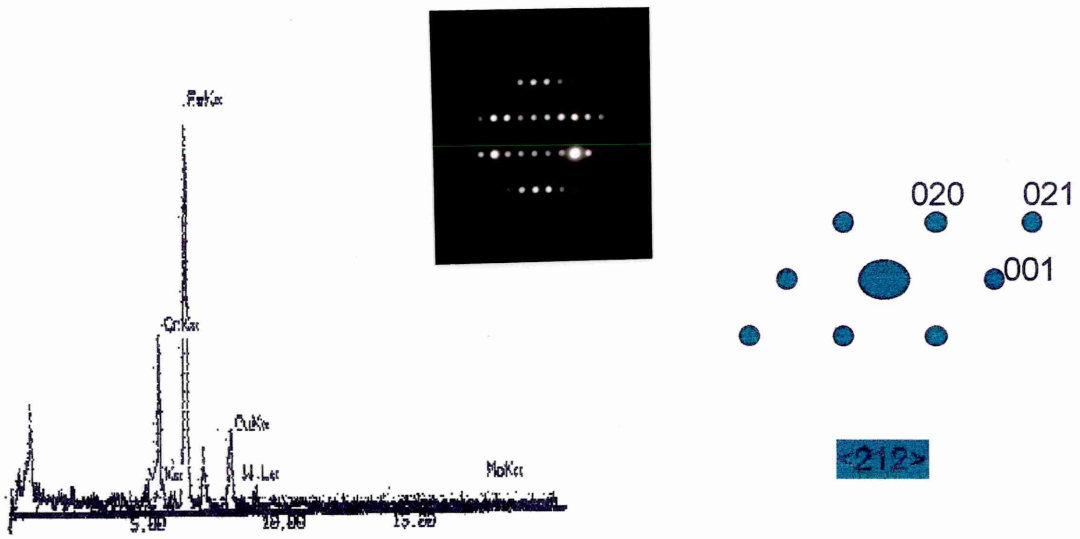

(c) M_3C

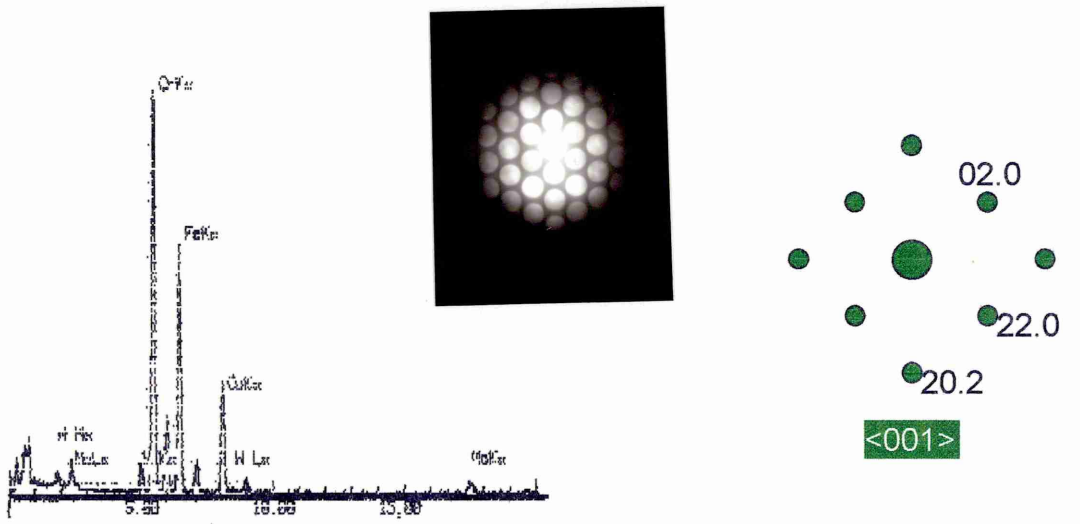

(d) M_7C_3

Figure 5.10-2 Characteristic X-ray spectra of carbides confirmed by their convergent beam electron diffraction patterns in 2CrMoNiWV steel

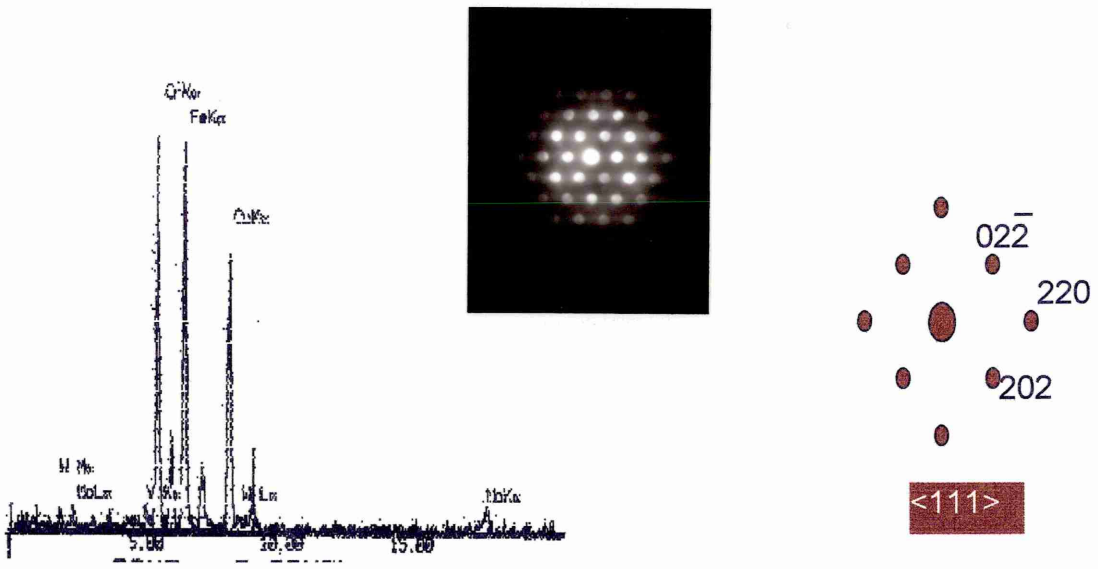

(e) $M_{23}C_6$

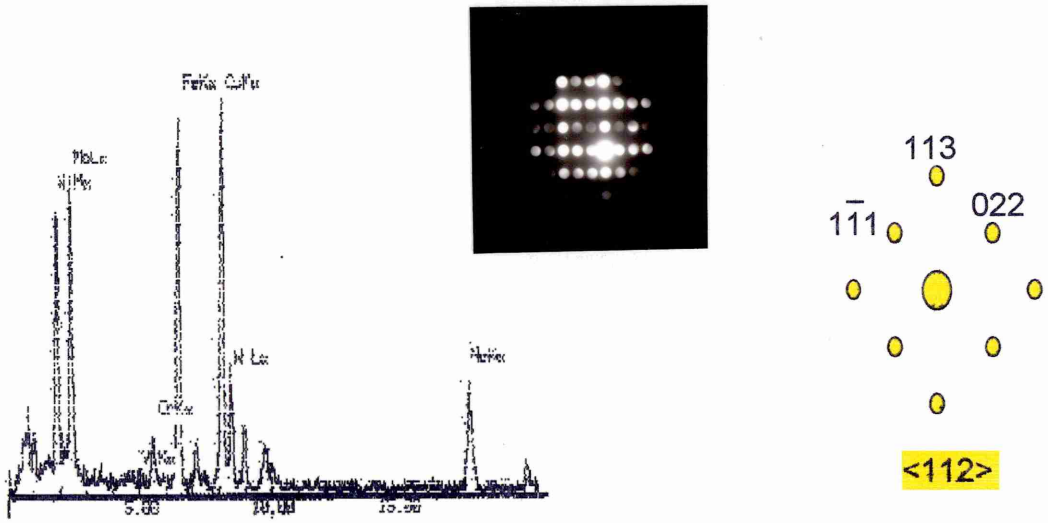

(f) M_6C

Figure 5.10-3 Characteristic X-ray spectra of carbides confirmed by their convergent beam electron diffraction patterns in 2CrMoNiWV steel

Table 5.4 Carbides found in samples austenitised at 975°C for 5 hrs followed by furnace cooling and then tempered at 600°C for various time by TEM/EDX

Sample code	Tempering Time (hr)	Carbides					
		MC	M_2C	M_3C	M_7C_3	$M_{23}C_6$	M_6C
F-600-1	1	Y		Y			
F-600-2	2	Y	--	Y	--	--	--
F-600-5	5	Y	--	Y	--	--	--
F-600-10	10	Y	--	Y	Y	--	--
F-600-20	20	Y	--	Y	Y	--	--
F-600-50	50	Y	--	Y	Y	Y	--
F-600-100	100	Y	--	Y	Y	Y	--
F-600-500	500	Y	Y	Y	Y	Y	--
F-600-1000	1000	Y	Y	Y	Y	Y	Y

Table 5.5 Carbides found in samples austenitised at 975°C for 5 hrs followed by furnace cooling and then tempered at 625°C for various time by TEM/EDX

Sample code	Tempering Time (hr)	Carbides					
		MC	M_2C	M_3C	M_7C_3	$M_{23}C_6$	M_6C
F-625-1	1	Y	--	Y	--	--	--
F-625-2	2	Y	--	Y	--	--	--
F-625-5	5	Y	--	Y	Y	--	--
F-625-10	10	Y	--	Y	Y	--	--
F-625-20	20	Y	--	Y	Y	Y	--
F-625-50	50	Y	--	Y	Y	Y	--
F-625-100	100	Y	Y	Y	Y	Y	--

Table 5.6 Carbides found in samples austenitised at 975°C for 5 hrs followed by furnace cooling and then tempered at 650°C for various time by TEM/EDX

Sample code	Tempering Time (hr)	Carbides					
		MC	M_2C	M_3C	M_7C_3	$M_{23}C_6$	M_6C
F-650-1	1	Y	--	Y	--	--	--
F-650-2	2	Y	--	Y	Y	--	--
F-650-5	5	Y	--	Y	Y	Y	--
F-650-10	10	Y	--	Y	Y	Y	--
F-650-20	20	Y	Y	Y	Y	Y	--
F-650-50	50	Y	Y	Y	Y	Y	--
F-650-100	100	Y	Y	Y	Y	Y	Y

Table 5.7 Carbides found in samples austenitised at 975°C for 5 hrs followed by furnace cooling and then tempered at 675°C for various time by TEM/EDX

Sample code	Tempering Time (hr)	Carbides					
		MC	M_2C	M_3C	M_7C_3	$M_{23}C_6$	M_6C
F-675-1	1	Y	--	Y	Y	--	--
F-675-2	2	Y	--	Y	Y	Y	--
F-675-5	5	Y	--	Y	Y	Y	--
F-675-10	10	Y	Y	Y	Y	Y	--
F-675-20	20	Y	Y	Y	Y	Y	--
F-675-50	50	Y	Y	--	Y	Y	Y
F-675-100	100	Y	Y	--	Y	Y	Y

Table 5.8 Carbides found in samples austenitised at 975°C for 5 hrs followed by furnace cooling and then tempered at 700°C for various time by TEM/EDX

Sample code	Tempering Time (hr)	Carbides					
		MC	M_2C	M_3C	M_7C_3	$M_{23}C_6$	M_6C
F-700-1	1	Y	--	Y	Y	--	--
F-700-2	2	Y	--	Y	Y	Y	--
F-700-5	5	Y	Y	Y	Y	Y	--
F-700-10	10	Y	Y	Y	Y	Y	--
F-700-20	20	Y	Y	Y	Y	Y	--
F-700-50	50	Y	Y	--	Y	Y	--
F-700-100	100	Y	Y	--	Y	Y	Y
F-700-500	500	Y	Y	--	Y	Y	Y
F-700-1000	1000	Y	--	--	--	Y	Y

5.3.2 Starting Bainitic Microstructure

The "as-received" microstructure was initially characterised in the TEM using carbon extraction replicas. The micrograph in Figure 5.11 illustrates that there was a complex precipitates co-existing in the "as-received" condition. The morphologies and sizes of carbides were very much different and they were identified as: MC -- a V-rich carbide, corresponding to the V carbide VC (V_4C_3) with fcc structure which dissolved limited amounts of other metallic elements; M_2C -- a Mo- and W-rich carbide, corresponding to hexagonal Mo_2C structure, which was capable of dissolving Cr, V and Fe; M_3C -- a Fe-rich carbide having the orthorhombic structure of cementite and this carbide took into solution very considerable amount of Cr; and M_7C_3 -- a Cr-rich carbide with the hexagonal structure of Cr_7C_3 which had a very high solubility for Fe.

A carbon extraction replica taken from the specimen austenitised at 975°C for 5 hours then furnace cooled (cooling rate about 10°C/min) is presented in Figure 5.12, in which almost no carbide precipitates can be observed except a trace of MC. This indicates that the austenitising treatment for 5 hours at 975°C was essentially adequate to dissolve all of the precipitates and take the carbides back into solution. It also evidently confirmed that the thermodynamic calculation performed with MTDATA in Chapter 4 was accurate. If the austenitising temperature is lower than 975°C, there will be a certain amount of MC remaining undissolved (Ref to Figure 5.3), but no other intermediate phase could exist at higher austenitising temperature.

Figure 5.13 shows a TEM thin foil micrograph of a furnace cooled specimen. Examination of the micrograph revealed that the microstructure was typical of bainite. The rejection of carbon from sheaves of upper bainite during growth was discussed in Chapter 2. As a consequence of this, the austenite matrix will become richer in carbon. In the later stages of transformation the

bainite growing from the enriched austenite may then decompose to lower bainite. Immediately tempering begins, the retained austenite starts to decompose to a mixture of ferrite and cementite. The alloy carbides will not initially form until longer tempering time or higher temperature owing to the large differences in the diffusion rates of carbon and substitutional solute elements.

5.3.3 Microstructural Evolution During Tempering

Changes in the microstructure during tempering were extensively studied under SEM using conventionally etched specimens and TEM on thin foils and carbon extraction replicas. SEM micrographs are presented in Figures 5.14 to 5.16 showing the general microstructural evolution and distribution of carbides. These SEM micrographs also clearly revealed that carbide coarsening was a function of tempering temperature and time. Due to different types of carbides co-existing for a long time and the different behaviour of precipitation, it was unnecessary to give specific particle size at each heat treated condition, but one conclusion was certain: particle size increased with the increase of tempering temperature and time. The interparticle spacing would increase with increasing of particle size and consequently the hardness will decrease. As an example, Figure 5.15 shows a micrograph of the specimen austenitised at 975°C for 5 hours followed by furnace cooling and then tempered at 650°C for 500 hours. Figure 5.16 shows a micrograph of the specimen with the same austenitising treatment but tempered at 700°C for 500 hours. The increase of particle spacing and particle growth was quite obvious if Figure 5.16 is compared with Figure 5.15. As a part of the effect of the difference in interparticle spacing and particle size, the Hv30 of the specimen tempered at 700°C for 500 hours dropped to 150, but the specimen tempered at 650°C for 500 hours remained 200.

A TEM image from a carbon extraction replica of the specimen tempered at 600°C for 1 hour is presented in Figure 5.17 in which illustrates only cementite precipitation with a few spherical particles due to undissolved MC in solution treatment. Cr-riched M_7C_3 and $M_{23}C_6$ are not formed until 20 hours tempering at 600°C, see Figure 5.18. The composition of the cementite was found to be different. It would appear that not all the cementite precipitates immediately following transformation, but that there was further precipitation as tempering proceeded; any cementite precipitating after tempering for some time may not have the same composition of formation. Detailed microanalyses from the cementite precipitates are discussed in Section 7.2.

A thin foil taken from the specimen tempered at 600°C for 5 hours was carefully examined under TEM. Figure 5.19 (a) shows that cementite precipitation had occurred with one orientation. Figure 5.19 (b) shows the dark field image corresponding to the (011) reciprocal lattice vector corresponding to a selected area diffraction pattern from one of the lenticular carbides.

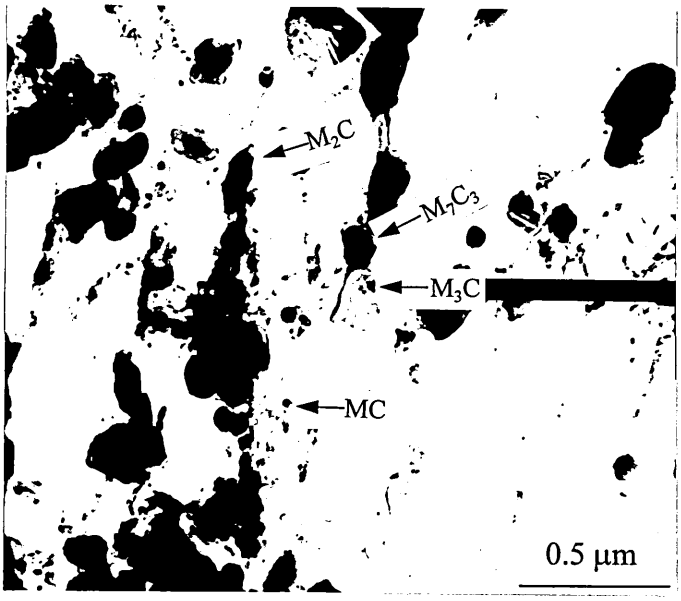

Figure 5.11 TEM micrograph taken from the "as-received" specimen showing four types of precipitates co-existing

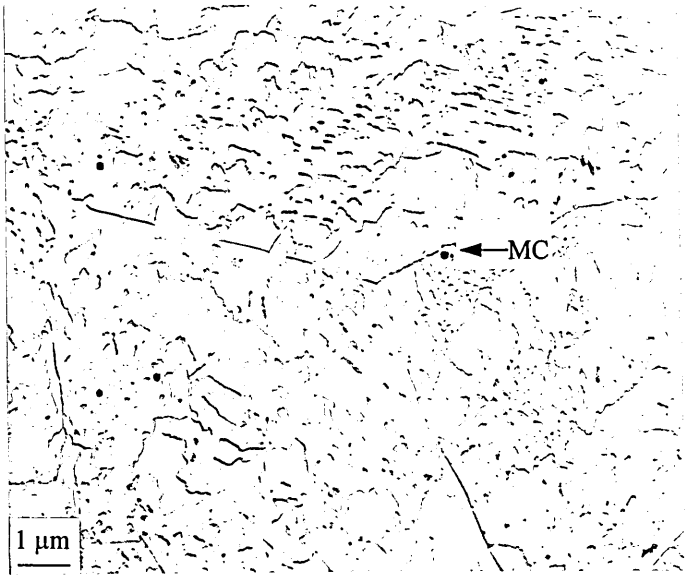

Figure 5.12 TEM carbon extraction replica micrograph taken from the as-furnace-cooled specimen austenitised at 975°C for 5 hrs illustrating that there were only a few carbides present

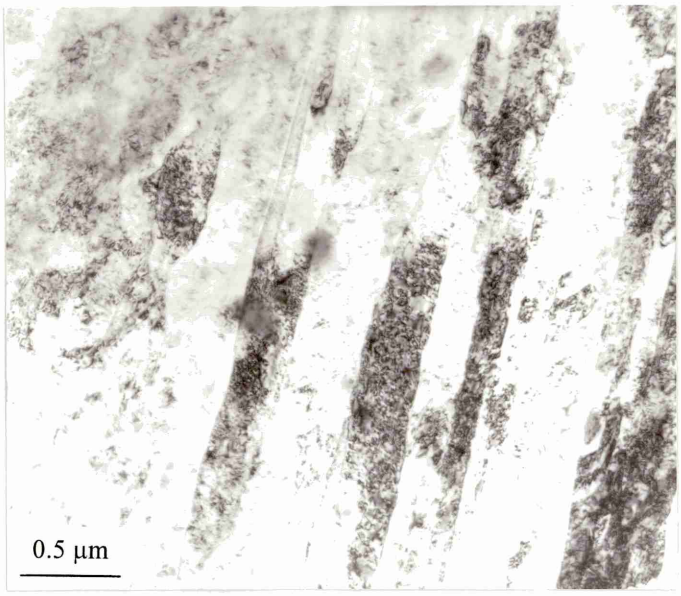

Figure 5.13 Austenitised at 975°C for 5 hrs followed by furnace cooling

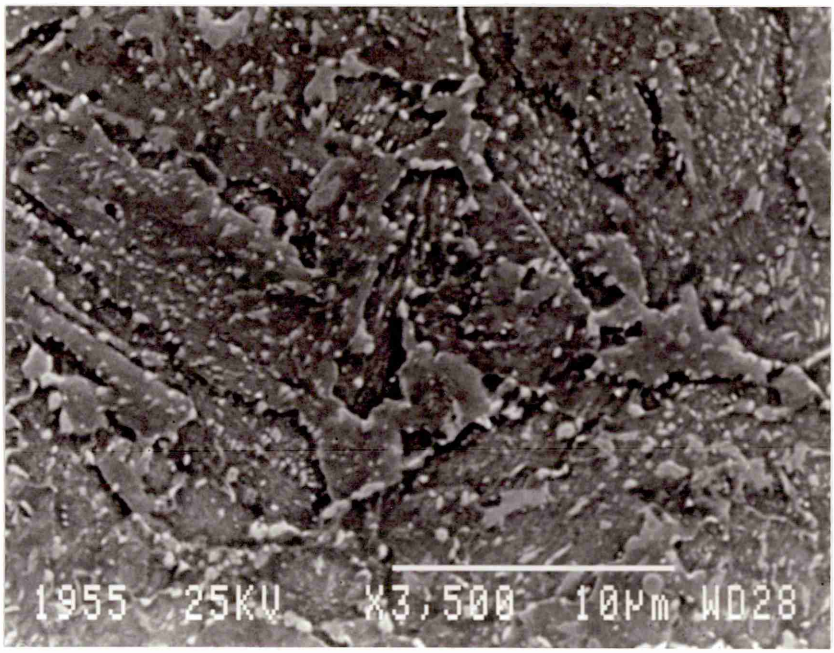

Figure 5.14 Austenitised at 975°C for 5 hrs followed by furnace cooling and then tempered at 700°C for 5 hrs

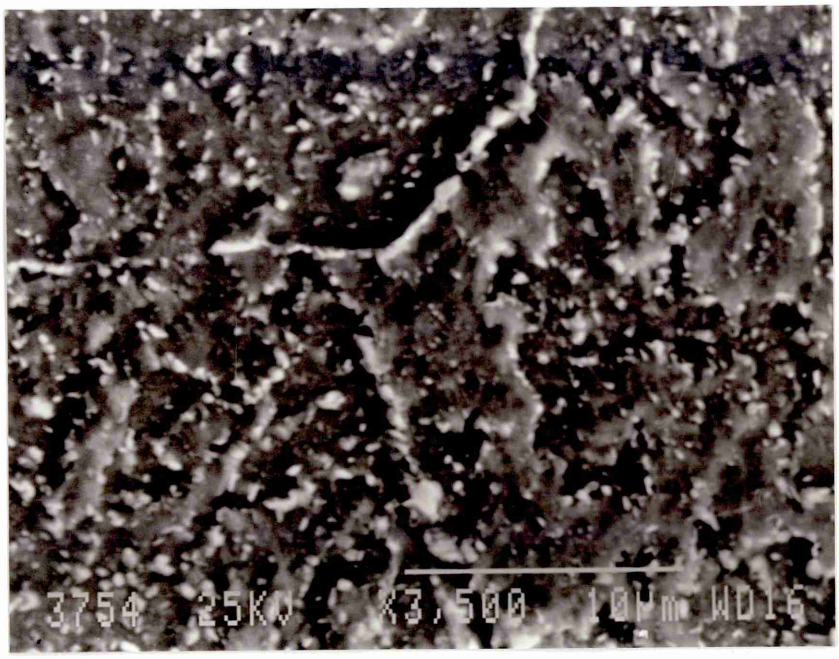

Figure 5.15 Austenitised at 975°C for 5 hrs followed by furnace cooling and then tempered at 650°C for 500 hrs

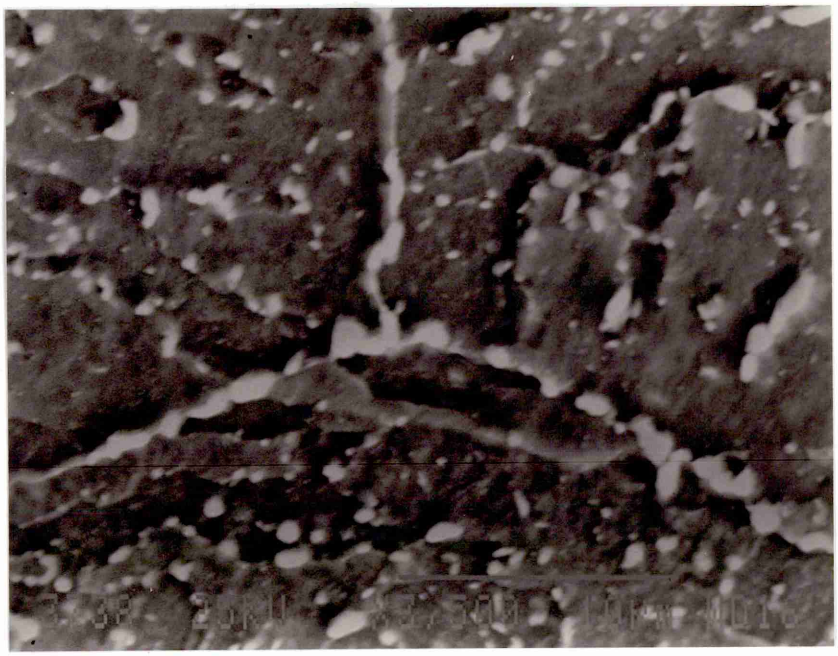

Figure 5.16 Austenitised at 975°C for 5 hrs followed by furnace cooling and then tempered at 700°C for 500 hrs

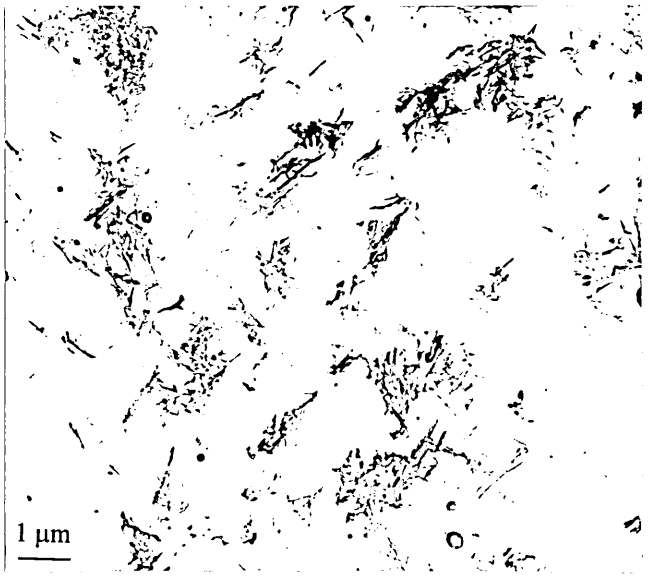

Figure 5.17 Carbon extraction replica micrograph of the specimen tempered at 600°C for 1 hr exhibiting the early stage of carbide precipitation

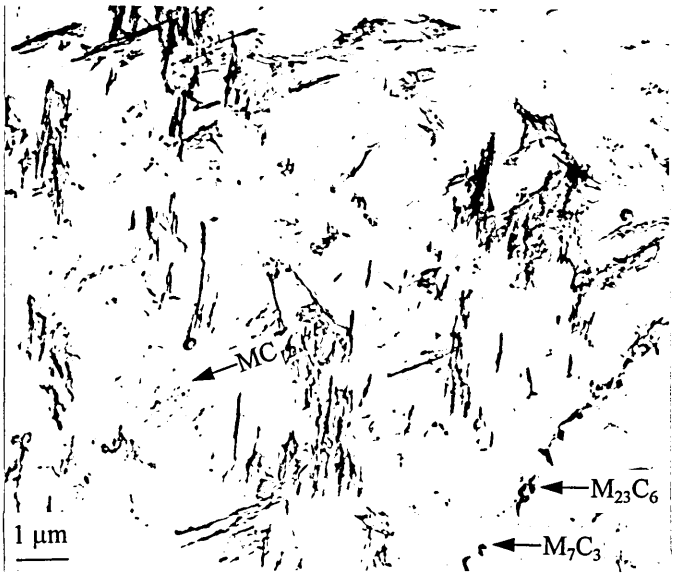

Figure 5.18 Carbon extraction replica micrograph of the specimen tempered at 600°C for 20 hrs illustrating further carbide precipitation

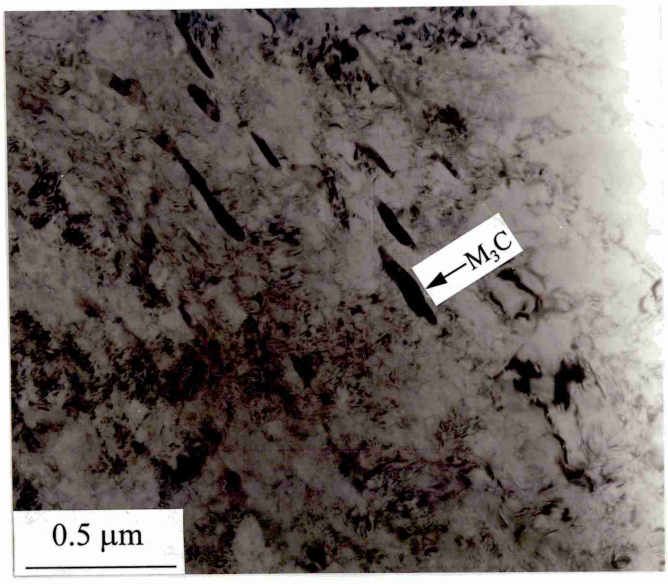

(a) Bright field image of a thin foil and M_3C precipitates

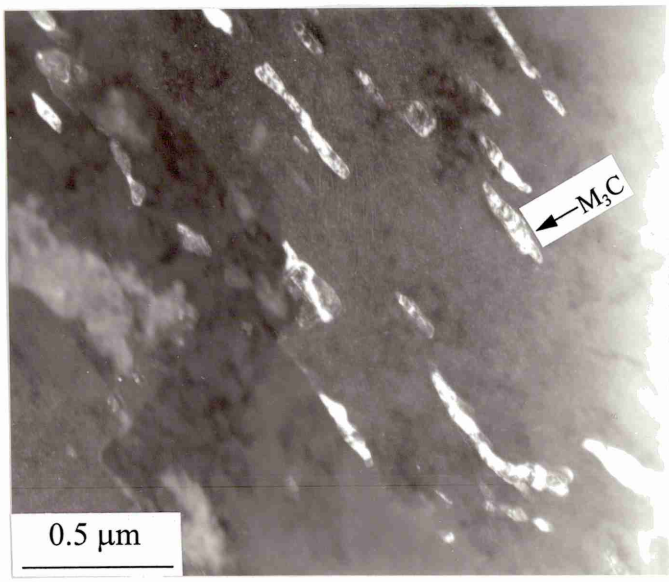

(b) Dark field image of carbide from (011) reflection of M_3C

Figure 5.19 TEM micrographs of furnace cooled sample after tempering at 600°C for 5 hrs

Figure 5.20 illustrates the microstructure following tempering for 100 hours at 600°C showing M_7C_3 and $M_{23}C_6$ carbide particles delineating the prior austenite grain boundaries while most of the cementite remained within the matrix.

All the cementite had dissolved in the specimen aged for 1000 hours tempered at 600°C, Figure 5.21. There was a slight enrichment of the M_7C_3 with respect to the Cr concentration with increasing tempering time.

Microstructural changes at 650°C were rapid compared to those at 600°C. This is illustrated in Figure 5.22 which shows extensive M_7C_3 and $M_{23}C_6$ precipitation after tempering for 20 hours taken from a carbon extraction replica. A thin foil made from the same specimen in Figure 5.23 clearly illustrates the microstructure with M_7C_3 precipitation mainly within matrix and $M_{23}C_6$ precipitation mainly at prior austenite grain boundaries.

Figures 5.24 shows a picture of carbide morphologies and size variations within a grain of a specimen tempered at 675°C for 50 hours in which the very fine precipitates were MC, rod types carbides were M_2C and parallelogram shaped ones were M_7C_3.

As the tempering proceeded to 20 hours at 650°C or above, some of the dispersed MC carbides grew one or two pairs of wings of M_2C to form the so called "H type" carbide. Figure 5.25 shows the typical early stage H-carbides with small wings grown on a MC plates. Figure 5.26 illustrates an H-carbide with long thin M_2C wings grown on a MC plate that appears to be lying flat. It has also been found that the M_2C carbides in the H-carbide wings were faulted and some MC particle appeared to be dissolving, Figure 5.27.

A TEM image from a carbon extraction replica of the specimen tempered at 700°C for 1 hour is illustrated in Figure 5.28 exhibiting the early stage of carbide precipitation. Figure 5.29 shows that further M_7C_3 carbide precipitation will be concomitant with the dissolution of cementite. It would seem that all the cementite precipitates immediately after tempering at 700°C and there was no further cementite precipitation as tempering proceeded.

Figure 5.30 shows the microstructure following tempering 20 hours at 700°C in which the microstructure consisted predominantly of M_7C_3 and $M_{23}C_6$. The M_3C had been completely replaced by M_2C with some larger M_7C_3, and $M_{23}C_6$ on the prior austenite grain boundaries. Some of M_3C with higher Cr either transformed to M_7C_3. A selected area electron diffraction pattern from an M_7C_3 particle is presented in Figure 5.31. Characteristic streaks from the presence of stacking faults in the structure are clearly visible. The result of thin foil examination for this specimen is presented as a montage in 5.32, all the cementite type carbides had dissolved and $M_{23}C_6$ carbides were predominant at grain boundaries.

When the cementite was saturated with alloy elements, whether it would be transformed into M_7C_3 or $M_{23}C_6$ seems closely related to the cooling rate from austenitisation. Some evidence from the TEM examination suggested that the $M_{23}C_6$ type carbide transformed from M_7C_3 "*in situ*". Figure 5.33 shows a electron convergent beam diffraction pattern observed from the specimen tempered at 700°C for 20 hours which can be fitted to both M_7C_3 <00.1> zone axis and $M_{23}C_6$ <111> zone axis, see also interpretation diagrams of CBDP in Figure 5.33 (b) and (c). The EDX spectrum was also corrected to analyse the composition of the precipitate which contained 42.09 mass%Cr, 39.88 mass%Fe, 3.40 mass%Mn, 6.97 mass%Mo, 4.93 mass%W, 2.72 mass%V. This composition again could be fitted either to M_7C_3 composition range or $M_{23}C_6$ composition range.

Interphase precipitation was found in specimens tempered at 700°C for 20 hours where small plates or rods nucleate at the austenite/ferrite interface which then moves to a new position where the nucleation cycle again occurs. This process can be repeated many hundreds of times within a particular austenite grain leading to a ferrite matrix with very fine banded dispersions, see Figures 5.34 and 5.35.

After tempering for 100 hours at 700°C the M_7C_3 precipitates have coarsened slightly (TEM thin foil montage Figure 5.36). The massive grain boundary carbides of either $M_{23}C_6$ or M_6C had also precipitated at the expense of some of the M_2C and M_7C_3 which had dissolved.

Figures 5.37 and 5.38 present the rearrangement of dislocations after tempering at 700°C for 20 hours and 100 hours. The translation of symmetrical low angle tilt boundaries are caused by the motion of dislocations which is prevented by the interaction between a dislocation and solute atoms. After a high temperature and long time tempering, this effect was reduced and therefore the creep rupture strength and hardness were bound to decrease.

Figure 5.39 (a) is a very interesting image from a carbon extraction replica made from the specimen tempered at 700°C for 100 hours. From this TEM micrograph much alloy carbide precipitation behaviour could be elucidated. First of all there are 5 types of carbides (MC + M_2C + M_7C_3 + $M_{23}C_6$ + M_6C) co-existing. Secondly typical morphologies and sizes of each carbide are exhibited together: the large ones are $M_{23}C_6$ and M_6C precipitated at grain boundaries, one of them was identified as $M_{23}C_6$ and the other was M_6C by electron diffraction pattern, see Figure 5.39 (b) and (c); the medium size carbides exhibiting parallelogram shape within the matrix were M_7C_3, see Figure 5.39 (d); M_2C precipitated in distinct Widmanstätten array and very fine MC presented as interphase precipitation. Thirdly it showed that near prior austenite grain boundaries there were MC and M_2C depleted zones which

could be explained as due to V soluted in $M_{23}C_6$ as a stabiliser and Mo, W entered into M_6C for its massive growth needs; Finally it demonstrated the difficulty in generalising the particle size, even though an approximation of particle size growth trend could be obtained, in reality the particles size could not be used alone as an accurate criterion to judge the thermal history of the steel.

An interesting discovery in this work was that the nucleation of M_7C_3 in the fast cooled specimens was much more than the slow cooled specimens. For instance, the specimen austenitised at 975°C for 5 hours followed by oil quenching then tempered at 650°C for 20 hours, consisted of about 65% M_7C_3, 15% $M_{23}C_6$, 10% M_3C, 5% M_2C and 5% MC, see Figure 5.40; whereas the specimen austenitised at the same condition but followed by program controlled cooling at 1°C/min then tempered at 650°C for 20 hours, consisted of about 15% M_7C_3, 65 % $M_{23}C_6$, 10% M_3C, 5% M_2C and 5% MC, see Figure 5.41. This is probably due to the different precipitation behaviour between lower and upper bainite (Honeycombe, 1981).

It was found that the carbide type was very sensitive to position within a given microstructure. After a short period of tempering MC dominates within the bainitic sheaves, whereas mixtures of M_3C and M_7C_3 were to be found at the bainitic sheaves boundaries. This was probably because far less carbon was available within the upper bainitic sheaves, whereas the sheaves boundaries were the sites for cementite precipitation during the growth of upper bainite. More carbon was usually available in the vicinity of the sheaves boundaries from dissolved cementite or carbon-enriched retained austenite, which could stimulate the formation of a variety of other alloy carbides.

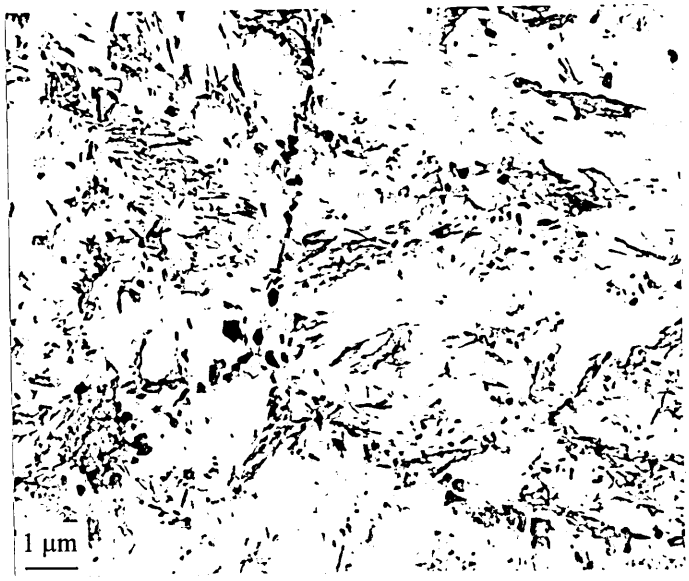

Figure 5.20 Carbon extraction replica micrograph of the specimen tempered at 600°C for 100 hrs exhibiting carbides delineating boundaries

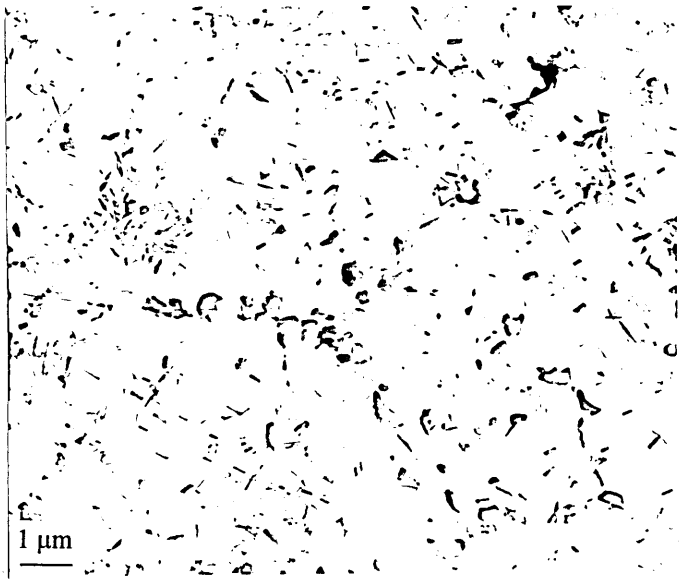

Figure 5.21 Carbon extraction replica micrograph of the specimen aged at 600°C for 1000 hrs illustrating all the M_3C had dissolved

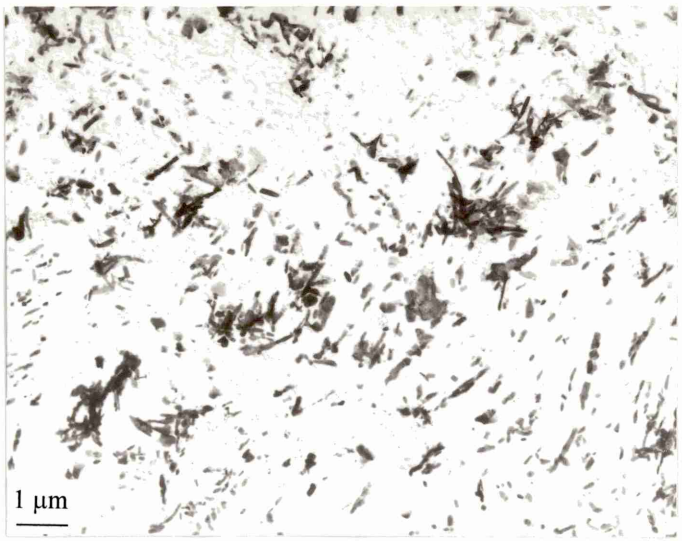

Figure 5.22 Carbon extraction replica micrograph of the specimen tempered at 650°C for 20 hrs showing extensive M_7C_3 and $M_{23}C_6$ precipitation

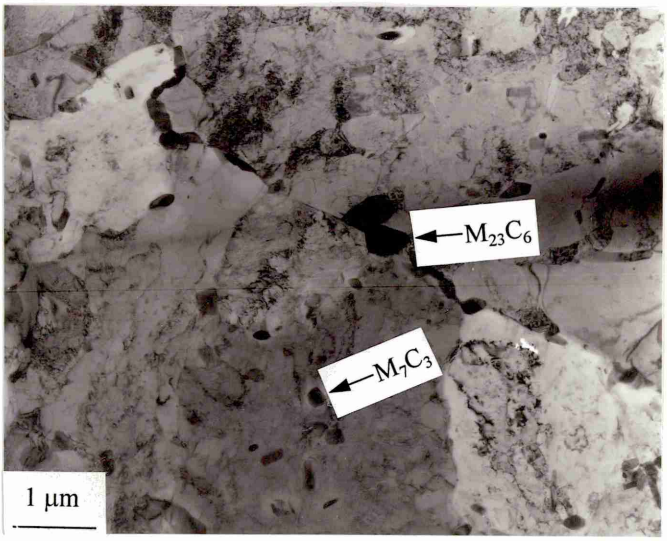

Figure 5.23 TEM thin foil micrograph of the specimen tempered at 650°C for 20 hrs illustrating M_7C_3 precipitated mainly within matrix and $M_{23}C_6$ mainly precipitated at boundaries

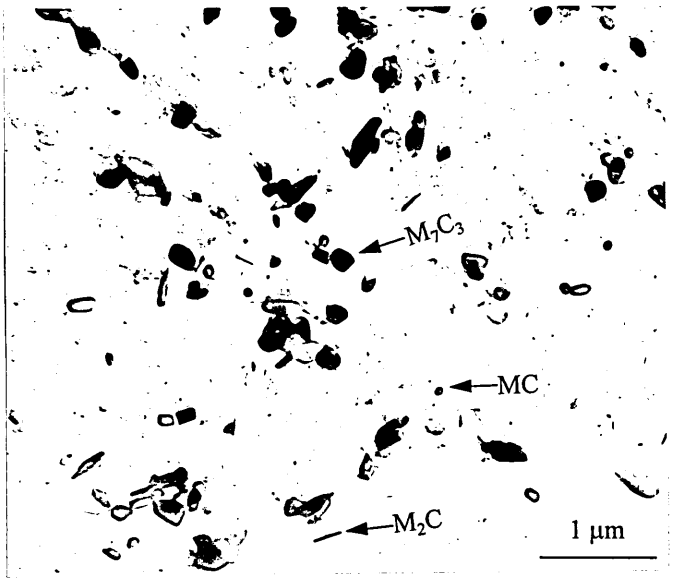

(a)

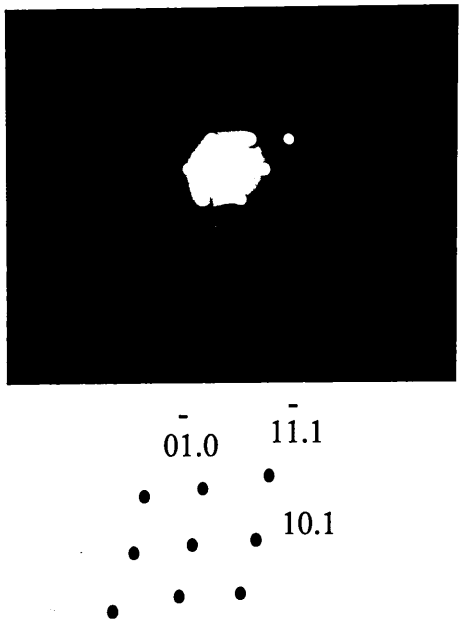

(b) <10.1> CBDP of M_2C carbide

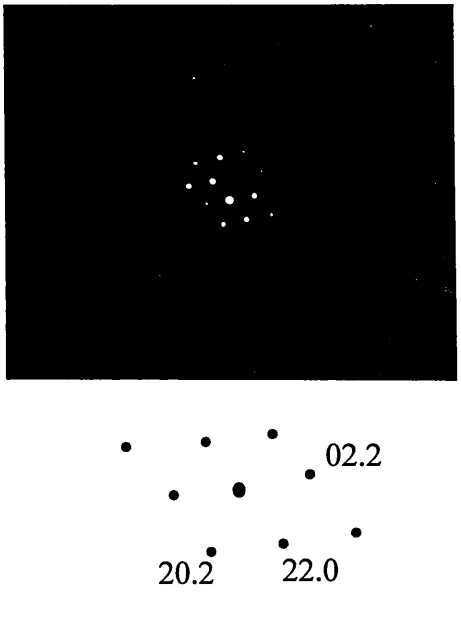

(c) <00.1> CBDP of M_7C_3 carbide

Figure 5.24 (a) Carbon extraction replica micrograph of the specimen tempered at 675°C for 50 hrs illustrating MC + M_2C + M_7C_3 co-existing within the matrix;
(b) A CBDP from one of rod type carbide and
(c) A CBDP from one of parallelogram shaped carbide

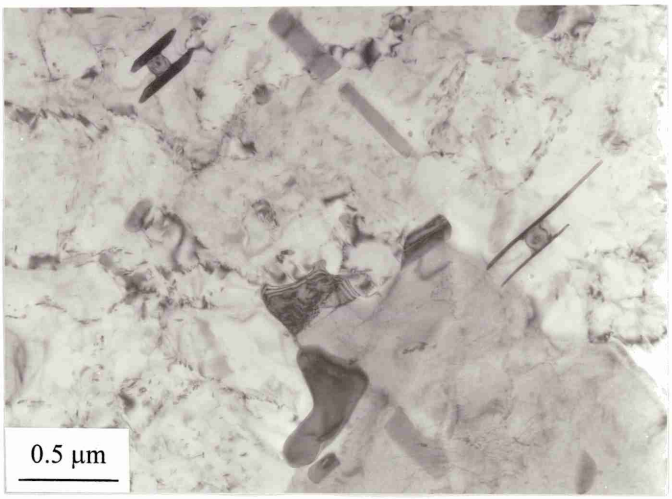

Figure 5.25 Typical early stage H-carbides with small wings grown on a MC plates

Figure 5.26 long thin M_2C wings grown on a MC plate

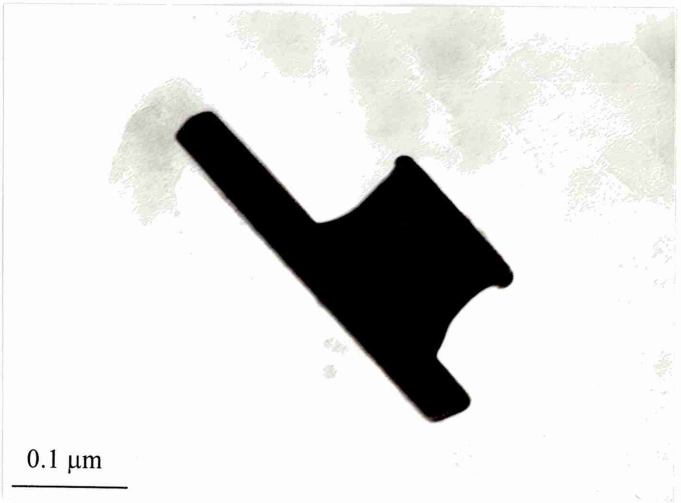

Figure 5.27 H-carbide wings were faulted and MC appeared to be dissolving

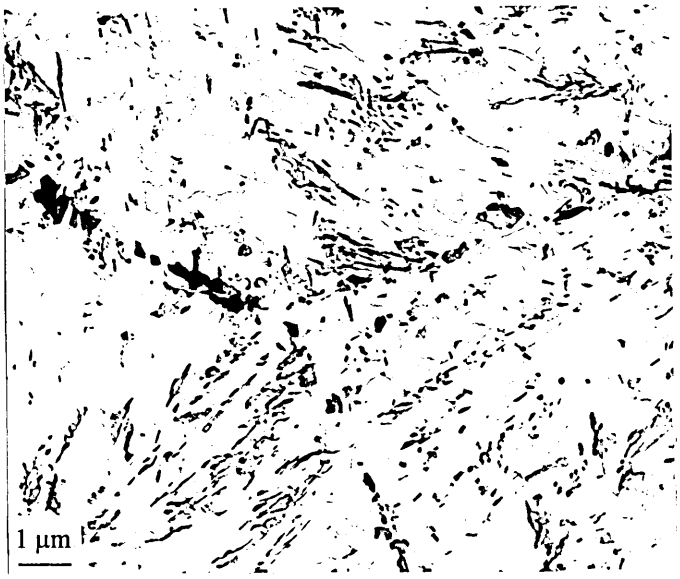

Figure 5.28 Carbon extraction replica micrograph of the specimen tempered at 700°C for 1 hr exhibiting the early stage of carbide precipitation

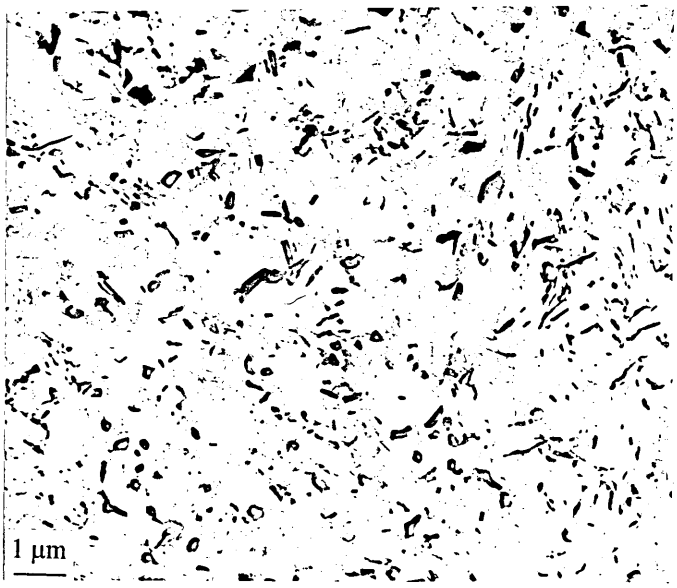

Figure 5.29 Carbon extraction replica micrograph of the specimen tempered at 700°C for 5 hrs illustrating M_7C_3 carbide precipitation and M_3C has begun to dissolve

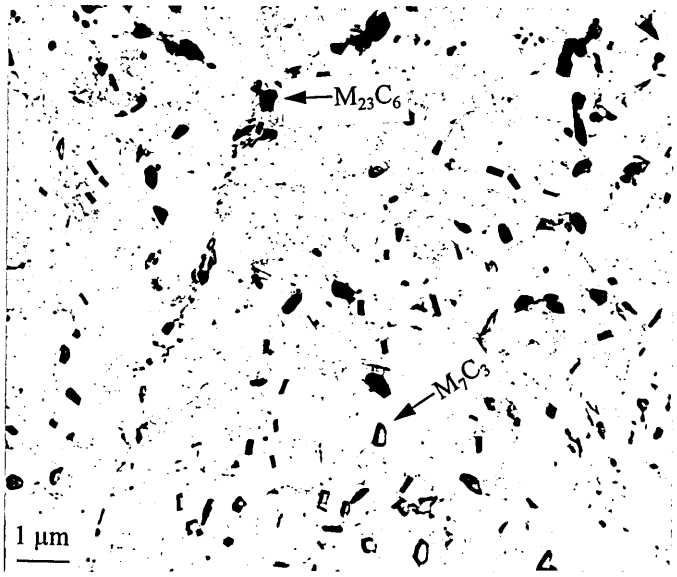

Figure 5.30 Carbon extraction replica micrograph of the specimen tempered at 700°C for 20 hrs illustrating the structure consists predominantly of M_7C_3 and $M_{23}C_6$

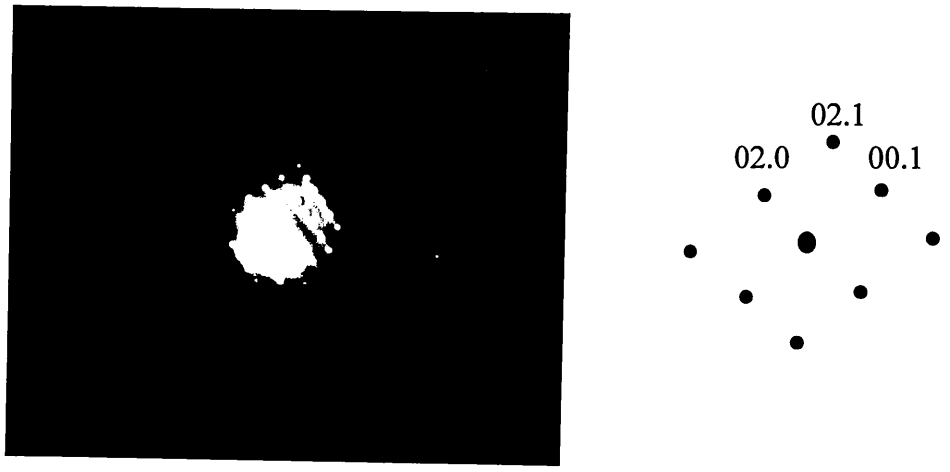

(a) (b) <10.1>

Figure 5.31 (a) <10.1> electron diffraction pattern of M_7C_3 with characteristic streaks and (b) interpretation of (a)

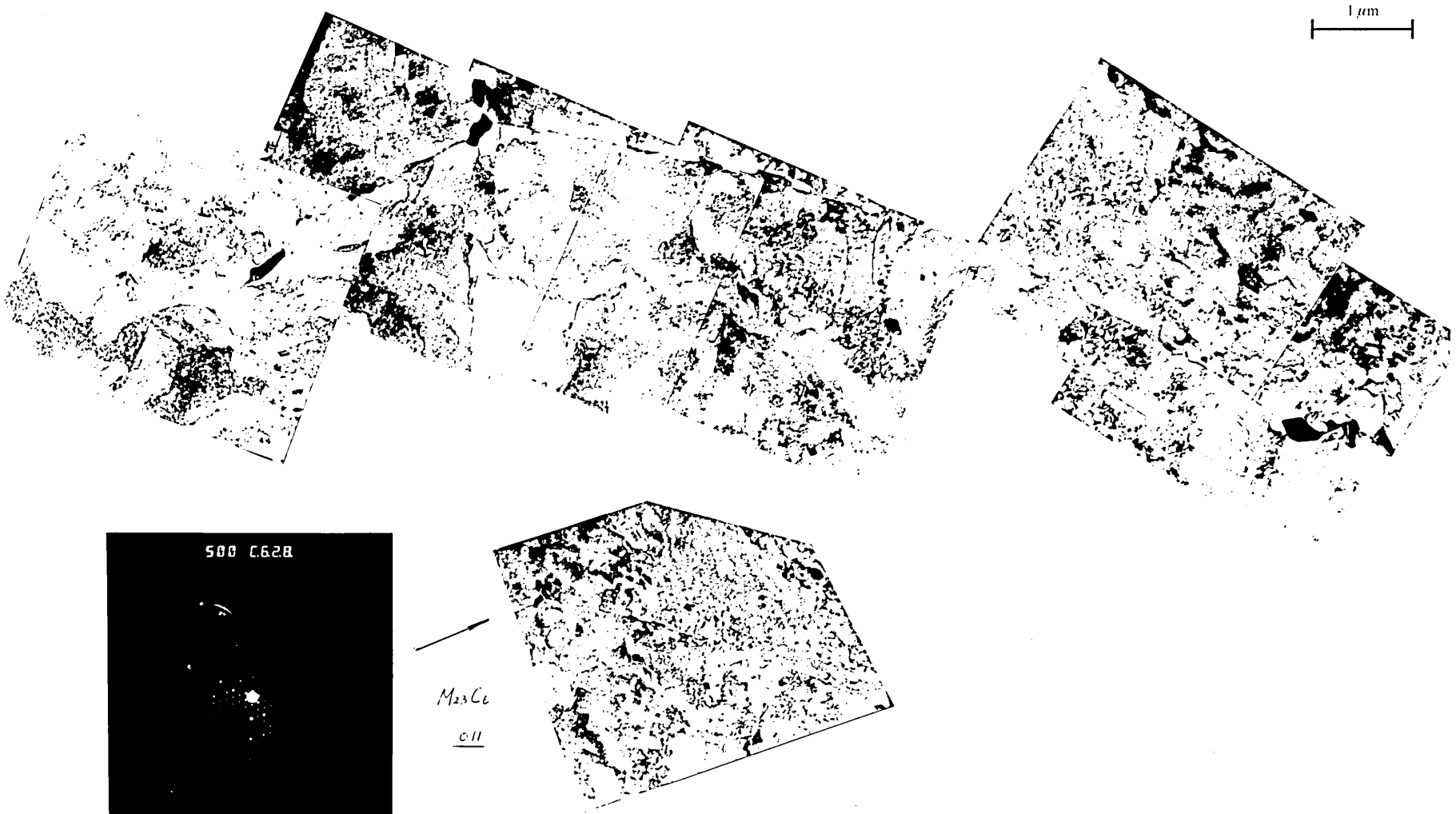

Figure 5.32 TEM montage taken from the specimen tempered at 700°C for 20 hrs showing all the M_3C had dissolved and $M_{23}C_6$ carbides were predominant at grain boundaries

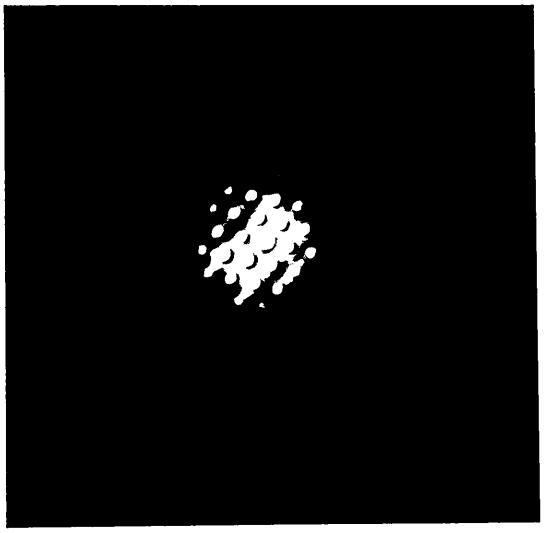

(a) An electron convergent beam diffraction pattern

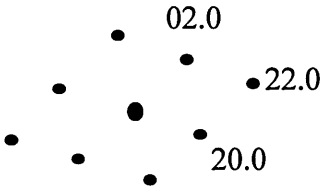

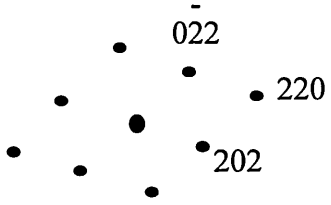

(b) <00.1> of M_7C_3 carbide

(c) <111> of $M_{23}C_6$ carbide

Figure 5.33 (a) An electron convergent beam diffraction pattern taken from the specimen tempered at 700°C for 20 hrs can be fitted to both (b) M_7C_3 <00.1> pattern and (c) $M_{23}C_6$ <111> pattern

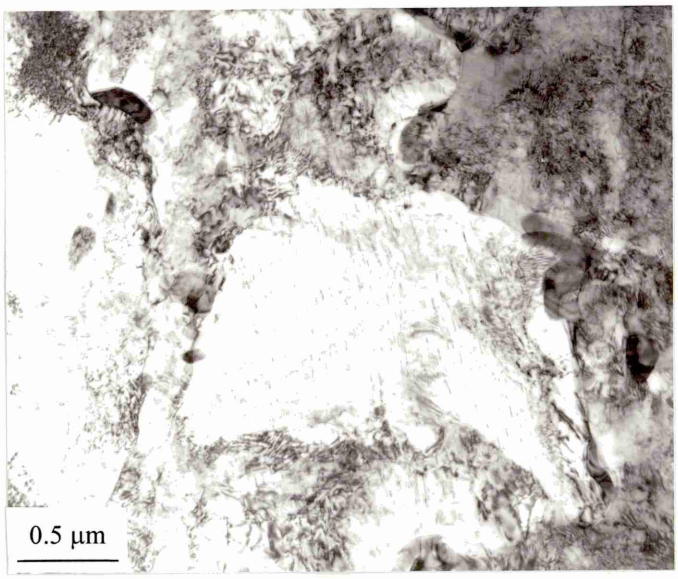

(a) TEM bright field image of interphase precipitation within a grain

(b) TEM dark field image of interphase precipitation within a grain

Figure 5.34 TEM thin foil micrographs of the specimen tempered at 700°C for 20 hrs showing interphase precipitation mechanism

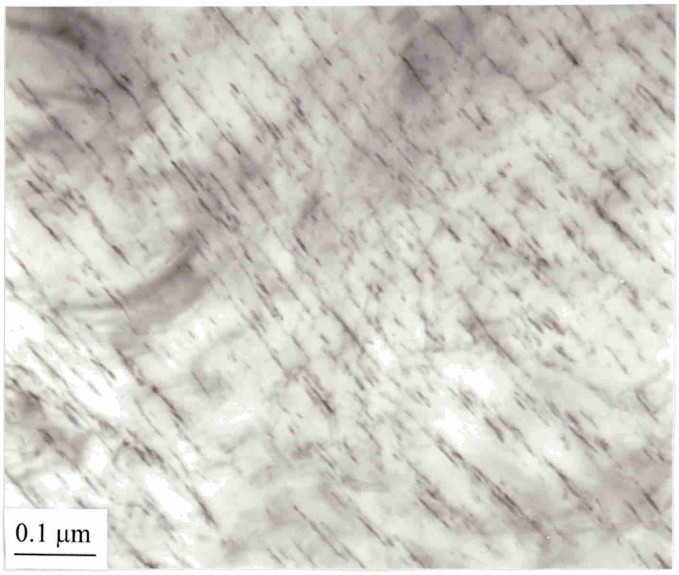

(a) TEM bright field image of interphase precipitation at high magnification

(b) TEM dark field image of interphase precipitation at high magnification

Figure 5.35 TEM high magnification micrographs of the specimen tempered at 700°C for 20 hrs showing interphase precipitation mechanism

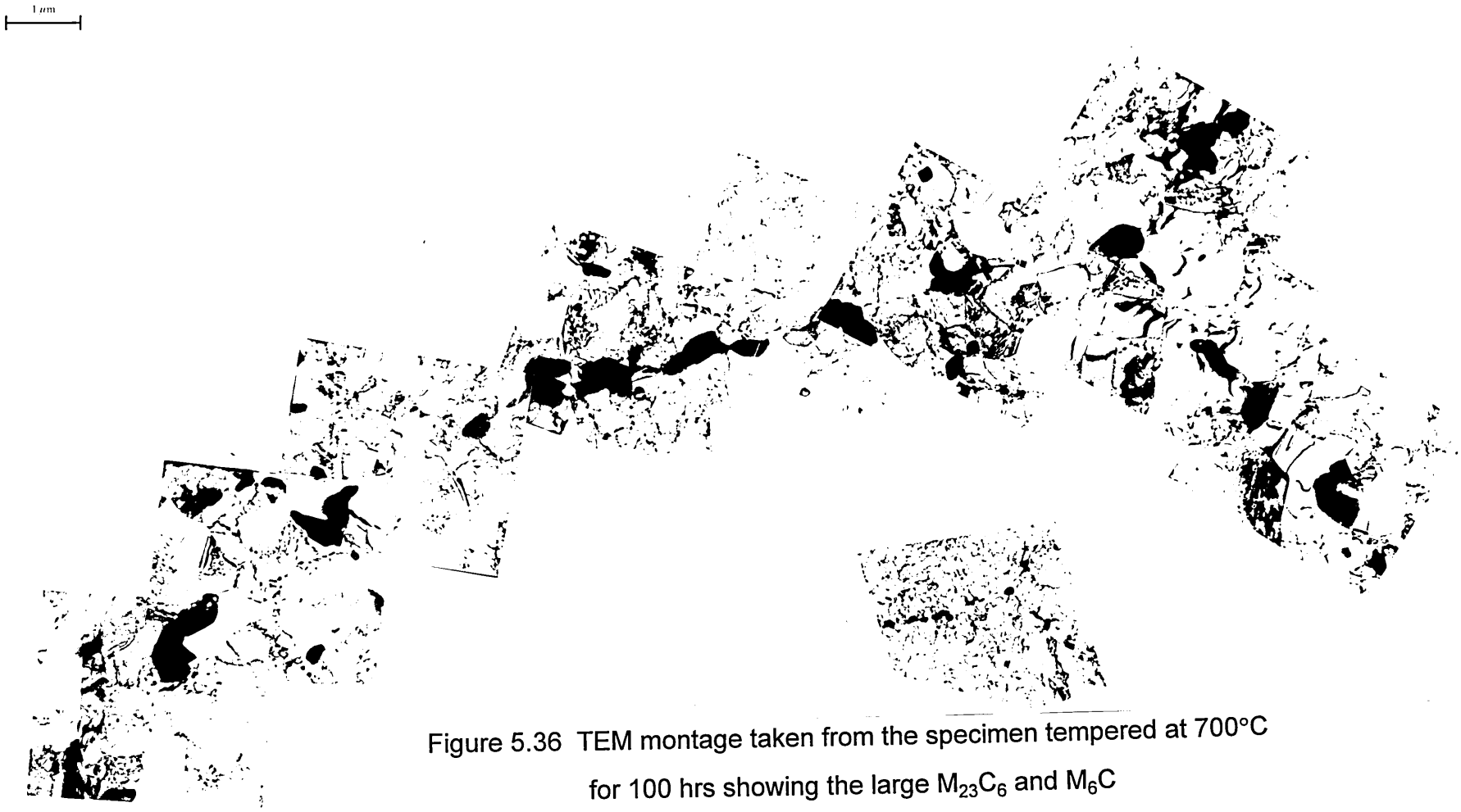

Figure 5.36 TEM montage taken from the specimen tempered at 700°C for 100 hrs showing the large $M_{23}C_6$ and M_6C carbides precipitated at grain boundaries

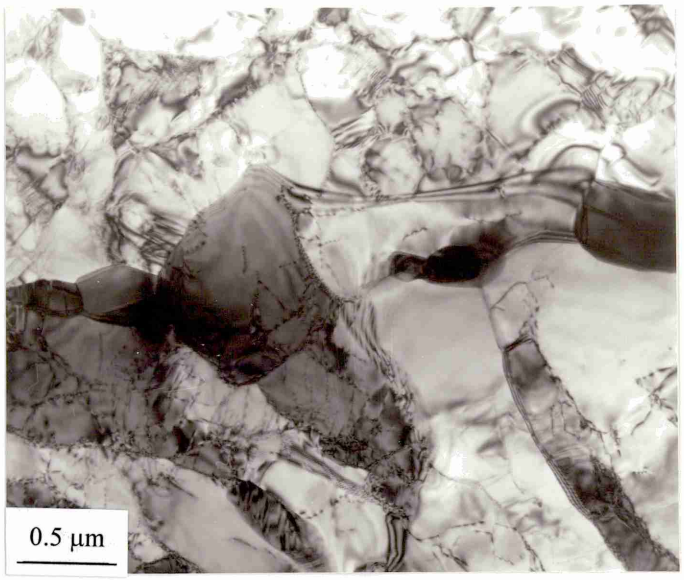

Figure 5.37 TEM thin foil micrograph taken from the specimen tempered at 700°C for 20 hrs

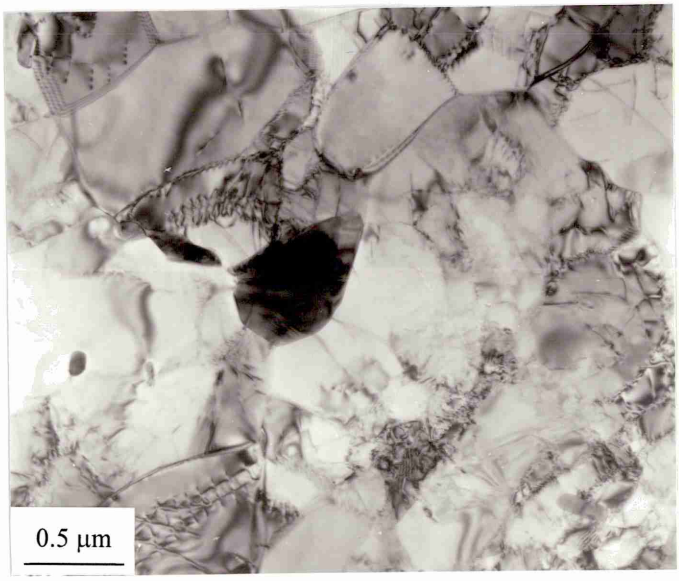

Figure 5.38 TEM thin foil micrograph taken from the specimen tempered at 700°C for 100 hrs

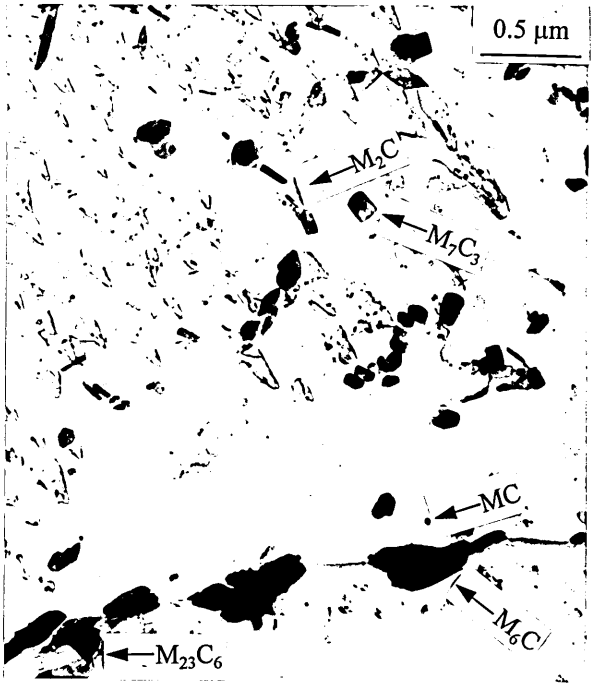

(a) Five types of carbides co-exist

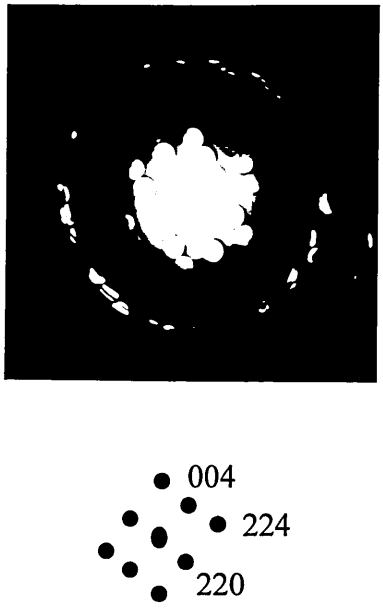

(b) <110> of $M_{23}C_6$ carbide

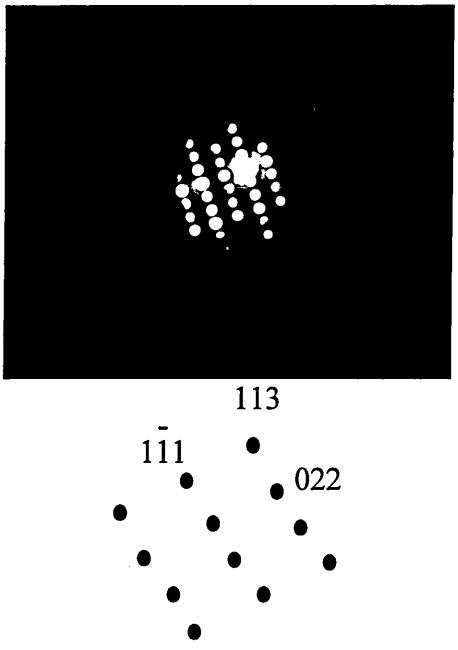

(c) <112> of M_6C carbide

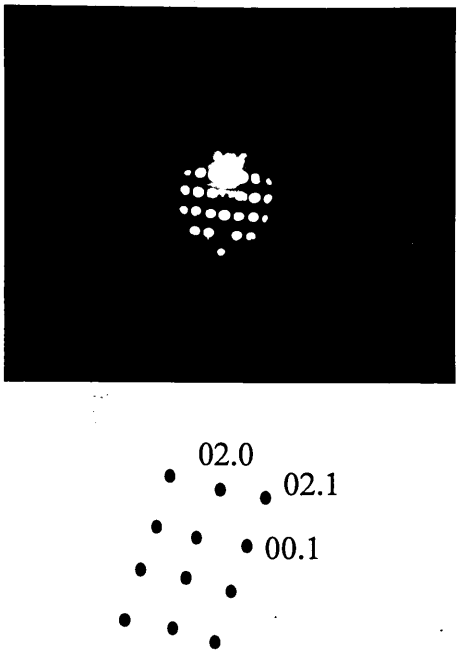

(d) <10.0> of M_7C_3 carbide

Figure 5.39 TEM micrographs taken from the specimen tempered at 700°C for 100 hrs showing MC + M_2C + M_7C_3 + $M_{23}C_6$ + M_6C co-existing

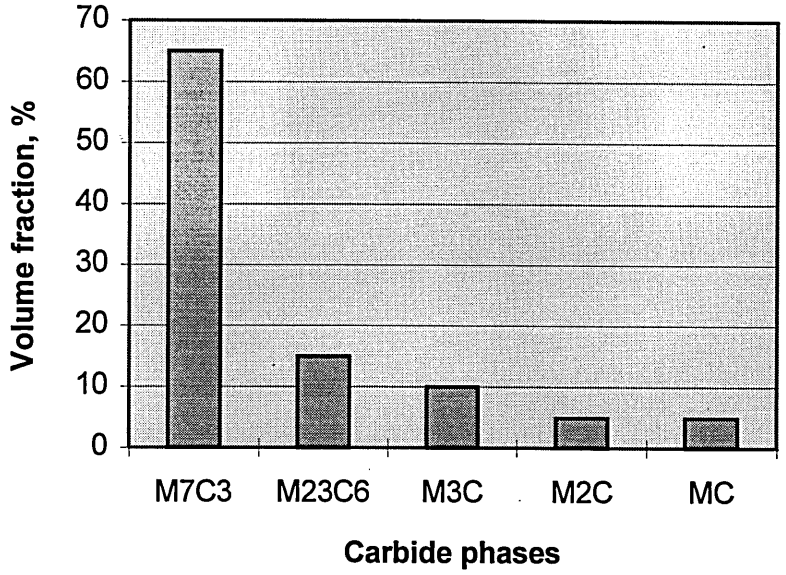

Figure 5.40 Volume fraction of the carbides in the specimen austenitised at 975°C for 5 hrs followed by oil quenching then tempered at 650°C for 20 hrs

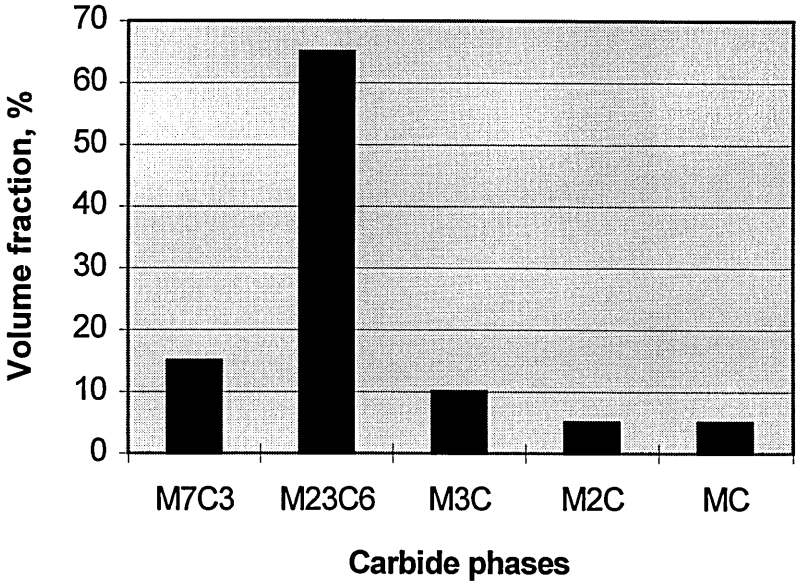

Figure 5.41 Volume fraction of the carbides in the specimen austenitised at 975°C for 5 hrs followed by program controlled cooling at 1°C/min then tempered at 650°C for 20 hrs

5.4 Heat Treatment Optimisation

The essential part of this research is to set up an optimised heat treatment route based upon the studies on microstructure and creep properties of the commercial 2CrMoNiWV rotor steel. By comparing different microstructure and carbide dispersion produced at various heat treatment conditions and correlating them with physical properties, an optimised heat treatment route shall be suggested to commercial heat treatment conditions.

5.4.1 Optimum Heat Treatment Trial

Microstructure examinations on specimen austenitised at 975°C for 5 hrs found that a prior austenite grain size was approximate 60 μm and almost no precipitates remained after this solution treatment condition (Figure 5.2). Hardness test on tempered specimen at 675°C for 20 hrs was 274 (Table 5.3), which is similar with the hardness of "as-received" sample (Hv30 = 235). A possible optimum heat treatment trial route was chosen as follows: Austenitising at 975°C for 5 hrs following by furnace cooling with a rate of approximate 10°C, then tempering at 675°C for 20 hrs following by air cooling.

Creep rupture tests on trial heat treated specimens were carried out at GEC Alsthom with the consideration of comparing commercial 2CrMoNiWV production material test data under the same test conditions. The creep strength of trial heat treated specimens were significantly higher than commercial production material, which is illustrated in Figure 5.42.

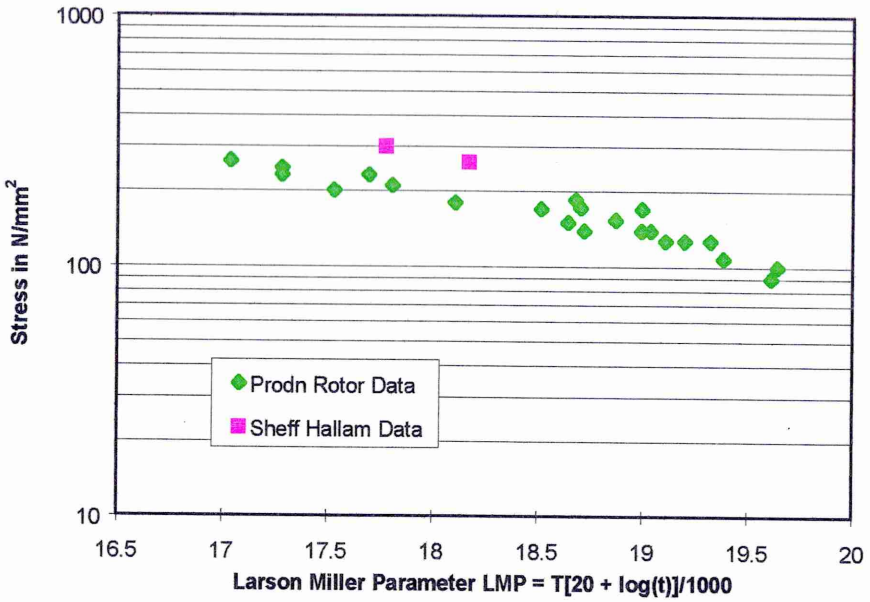

Figure 5.42 Larson Miller Parameter plot of the 0.2% creep strain data on the 2CrMoNiWV rotor material

5.4.2 Optimum Heat Treatment Suggestion

For good creep properties it is essential to obtain certain amount of a stable cubic carbide of structure, and a state as finely dispersed as possible. It appeared that V carbide forms preferentially to Cr, Mo and W carbide for this range of composition. The heat treatment should also be designed to increase the effective amount of V carbide and to avoid the early formation of alloy carbides other than V carbide.

With the view of experimental heat treatment characteristic may differ from commercial heat treatment conditions, some adjustments have to take into account. Based on all available experimental and theoretical data with comprehensive consideration, a possibly optimised heat treatment route for

production rotor forgings is suggested as follows: Austenitising at 980°C for 10 hours following by oil quenching, then tempering at 675°C for 20 hours.

5.5 Discussion

The mechanical properties of ferritic steels are controlled in part by the inherent strength of the matrix and in part by the way in which deformation of the matrix is affected by its interaction with carbide particles precipitated during heat treatment. The 2CrMoNiWV steel had been subjected to various heat treatment trials , and also contained a variety of carbides and these would have specific effects upon the deformation behaviour of the steel. It was found that 975°C was the appropriate austenitising treatment temperature because it could dissolve almost all alloy carbides present in this steel, bring alloying elements back into solution even the very strong carbide formers such as V were present, and largely overcome the influence of variation in forging and previous thermal history. The prior austenite grain size was about 60 μm in the specimen austenitised at 975°C for 5 hours. High austenitising temperature (about 105°C higher than actually measured A_{C3} in this heat treatment trial) ensured solution of the carbides and their correct precipitation in subsequent heat treatment which depends on cooling rate, tempering time and temperature. The type, amount, and distribution of these carbide phases which would have a profound influence on the high temperature service properties.

Tempering which affects the microstructure is extremely important. At the tempering temperature of 700°C, coarsening of carbides occurred, which will be accompanied by a marked decrease in creep and rupture properties (Bates and Ridal, 1963). To obtain the required room temperature mechanical properties and the best combination of creep strength and ductility, it would appear that the tempering temperature should be in the range 670°C to 680°C.

5.5.1 Microstructural Characteristics

During tempering, as changes in the size, spacing and form of the carbide particles occurred, the density of dislocations within the grains decreased accordingly. The individual dislocations observed within the grains were almost invariably found to be pinned at carbides, suggesting a gradual loss of creep resistance as particle coarsening takes places and carbides loose their pinning effects. Moreover, growth of grain boundary carbides leads to the progressive formation of particle-free zones adjacent to the boundaries (Figures 5.37 and 5.38). The extensive development of precipitate-free zones supports the view that deformation in the grain boundary zones controls the creep behaviour of ferritic steels under service conditions (Honeycombe,1985).

Tempering involves the diffusion of carbon to lattice defects and precipitation of carbides, the decomposition of retained austenite and recovery processes which will vary with alloying additions. Strong carbide forming elements such as Cr, Mo, V and W were present in sufficient concentration in this steel, and their carbides would be formed in preference to cementite. Nevertheless during tempering of the steel, alloy carbides do not form until the temperature range 500-600°C is reached. Since below this temperature the metallic alloying elements cannot diffuse sufficiently rapidly to allow alloy carbides to nucleate. The metallic elements substitute for iron, in contrast to carbon which moves through the iron lattice interstitially, with the result that the diffusivity of carbon is several orders of magnitude greater in iron, than those of metallic alloying elements. Consequently higher temperatures are required for the necessary diffusion of the alloying element atoms prior to the nucleation and growth of the alloy carbides. That is why the tempering conditions below 600°C in this investigation were eliminated.

The disappearance and rearrangement of dislocations and the translation of symmetrical low angle tilt boundaries were caused by the motion of dislocations which was prevented by the interaction between a dislocation and solute atoms. As a result, the change in microstructures was delayed and a high level of creep rupture strength and hardness could be maintained. However, after a high temperature and long time tempering, this effect was reduced and thereby the creep rupture strength and hardness will decrease.

Although dislocations were almost invariably found to be pinned at carbides, indicating the relevance of particle hardening under the conditions studied, indirect evidence suggested that the matrix characteristics were also important. This was inferred from measurements of the interparticle spacing in relation to the hardness of the experimental range of various tempered conditions. The hardness decreased with increasing particle spacing as expected for particle strengthened alloys (Figures 5.15 and 5.16)

It is generally recognised that all the creep resistant alloys depend primarily on finely dispersed particles for their strength and that interparticle spacing is an important factor controlling the movement of dislocation (Townsend, 1993). This 2CrMoNiWV steel can enter service in a metallurgical condition in which the major phase changes accompanying the decomposition of austenite are complete and the precipitation of alloy carbides well advanced. However, the steel is in highly active metastable condition and further carbide precipitation, accompanied by changes in composition and coarsening will occur throughout high temperature operation. During high temperature exposure solid state diffusion can occur and the particles coarsen to reduce their overall surface free energy and for a given volume fraction this coarsening is accompanied by an increase in the mean interparticle spacing. These changes will invariably lead to changes in the properties of the steel and in general to a weakening of the structure.

5.5.2 Carbide Precipitation and Evolution

The major carbides formed during tempering were M_3C, MC (V_4C_3), at longer tempering times, M_7C_3, M_2C and $M_{23}C_6$, and finally M_6C would form. For thermodynamic reasons, only the most stable carbides could exist finally in a system. If the environment was not changing, the holding of a specimen for increasing time at a given temperature should allow transformations to move the whole system towards equilibrium. The reason that the equilibrium phase was not formed at the beginning was due to there being a long sequence of carbide transformation before the equilibrium carbide was achieved. The carbide evolution will depend on the chemical composition of the steel, the crystal structure of the carbide, the temperature and the atomic diffusivities of alloying elements.

5.5.2.1 The Formation of M_3C and its Composition Change

M_3C is an Fe-rich carbide having a orthorhombic structure, consequently it is often referred to as Fe_3C. This carbide can take into solution very considerable amounts of other elements. M_3C was first formed during the tempering process for it has a low alloy content due to the low diffusivity of the substitutional alloying elements. As Fe cementite (Fe_3C) is less stable than the alloy cementite (M_3C) for its much higher free energy, the alloy elements, especially Cr, substitute for Fe gradually. At early stage of tempering, the cementite consists of almost no other alloy elements but Fe, but before it transforms to Cr-riched M_7C_3 and/or $M_{23}C_6$ the composition of the M_3C could have reached approximately 78 at.% Fe, 15 at.% Cr, 2.5 at.% Mn, 1.5 at.% Mo, 1.5 at.% W and 1.5 at.% V in its solution. The average composition of M_3C can also be expressed as $(Fe_{2.33}Cr_{0.45}Mn_{0.08}Mo_{0.05}W_{0.05}V_{0.04})C$. It is obvious that Cr is highly soluble in M_3C; up to one fifth of the Fe atoms may be replaced by Cr.

Alloy carbides of the M_3C type are more thermodynamiclly stable than Fe_3C (Senior, 1988), suggesting that a strong thermodynamic driving force for alloy partitioning to M_3C exists. The coarsening of cementite in this steel was greatly retarded by the presence of other alloying additions, especially Cr. Coarsening and coalescence of M_3C occurred as its composition was changing.

It was noticeable that the EDX measurement data on carbides had large errors at the short tempering times, which can be taken as an indication that the true coarsening process of carbides has not yet become fully operative.

5.5.2.2 M_7C_3 and $M_{23}C_6$ Carbides

The reason to form M_7C_3 and/or $M_{23}C_6$ carbides with higher Cr, Mo and W after a period of tempering is that when Cr was high in M_3C, it would be more stable if it transformed into Cr-based carbides. On the other hand, the diffusivities of Mo and W were lower than other alloy elements in ferrite and they were not very soluble in M_3C. It would not be easy for Mo and W to diffuse into M_3C until M_7C_3 and $M_{23}C_6$ carbides had been formed. The Cr content of cementite increased before the formation of M_7C_3 and $M_{23}C_6$. The reaction from $M_3C \Rightarrow M_7C_3$ was explained by Kuo (1953) that the concentration of Cr in M_3C was the first stage until a saturation value was achieved and then the structure change of $M_3C \Rightarrow M_7C_3$ was accompanied by an abrupt increase in the concentration of Cr.

There is considerable disagreement in the literature over the nature of the $M_3C \Rightarrow M_7C_3$ transformation which takes place in tempered steels containing additions of Cr. The mechanism has been variously described as "*in situ*" (Pickering, 1958) and as a mixture of "*in situ*" and separate nucleation (Seal and Honeycombe, 1958). Kuo (1953) has pointed out separate nucleation would be unlikely in a matrix already impoverished in Cr. Most of the

M_3C would change to M_7C_3 at an early stage of transformation but small amount of M_3C directly changed to $M_{23}C_6$. Detailed composition measurements were made on carbon replicas from this steel tempered isothermally in the range 550 - 700°C and the results are listed in Table 7.1. The average compositions were corresponding to $(Cr_{3.5}Fe_{2.58}Mn_{0.3}Mo_{0.32}W_{0.1}V_{0.2})C_3$ and $(Fe_{10.5}Cr_{9.5}Mo_{0.8}W_{0.7}Mn_{0.5}V_{1.0})C_6$. Cementite which formed in the steel showed an accumulation of Cr increasing with tempering time. The maximum level of Cr detected was about 20 mass%, but afterwards measurements became unreliable because of the close proximity of carbide of the type $M_{23}C_6$. It seems the maximum level of Cr in cementite would appear to be approximately 20 mass%. Any further increase would lead to instability and transformation to M_7C_3 with Cr content of approximately 40 - 50 mass% or to $M_{23}C_6$ with Cr content of approximately 35 - 45 mass%. The results indicate that the $M_7C_3 \Rightarrow M_{23}C_6$ transformation was an independent process involving both nucleation and growth. During TEM examination $M_{23}C_6$ was observed to nucleate at the same time as M_7C_3, but mainly at grain boundary sites. Perhaps one of the interesting discoveries was that nucleation of M_7C_3 in the fast cooled specimens was more than the slow cooled specimens. The reason for this phenomenon might be explained because the fast cooled specimen contained more retained austenite and it would be much easier for the nucleation of M_7C_3 since there would be more carbon available in the carbon-enriched retained austenite regions during tempering.

It is difficult to envisage the nucleation of M_7C_3 or $M_{23}C_6$ at sites other than regions of high Cr concentration. The accumulation of Cr is therefore interpreted as providing substantial evidence for the nucleation of M_7C_3 or $M_{23}C_6$ at dissolving M_3C sites. It would be expected that M_7C_3 nucleation events would take place at the M_3C-matrix interfaces and $M_{23}C_6$ would precipitate first at grain boundary regions where enhanced diffusion effects produced greatest concentration of substitutional alloying elements. This interpretation is perfectly in accord with the electron microscopic studies

(Section 5.3.3) in which M_7C_3 was observed mostly in the matrix whilst $M_{23}C_6$ preferentially precipitated at grain boundaries.

An effort has been made to detect "*in situ*" transformation from M_7C_3 to $M_{23}C_6$ by electron convergent beam diffraction patterns from individual carbide particles. A single particle giving patterns characteristic of both phases is shown in Figure 5.33 which indicates that transformation mode from M_7C_3 to $M_{23}C_6$ "*in situ*" was also possible.

5.5.2.4 M_6C Carbide

The EDX microanalysis data showed that the M_6C was Mo and W rich carbide, in the various tempering conditions had an relatively fixed composition. It did not appear to change with the tempering time. It had the atomic ratio close to 40.5 at.% Fe, 33 at.% Mo, 18 at.% W, 7 at.% Cr, and 1.5 at.% V, corresponding to $(Fe_{2.4}Mo_{2.0}W_{1.1}Cr_{0.4}V_{0.1})C$. The M_6C particles formed at grain boundaries and grew very rapidly at the expense of all the surrounding carbides. The nucleation of M_6C often occurred on $M_{23}C_6$, in addtion to nucleation on prior austenite grain boundaries. M_6C is unlikely to be present in "as tempered" condition but may form during extended tempering.

5.5.2.5 MC and M_2C Carbides

It is clear that the deformation of ferritic steels at elevated temperatures is influenced primarily by the type and dispersion of carbide phases and to a lesser degree by solid solution strengthening of the ferrite (Woodhead and Quarrell, 1965). Of the commonly used alloying elements, V is the most effective in promoting creep resistance by a dispersed carbide MC. V carbide, with a simple cubic crystal structure, exerts a beneficial influence on the creep

resistance of these bainitic steels because it occurs in a very finely divided state (interphase precipitation, see Figures 5.34-5.35) and resists coalescence and growth at elevated temperatures; whereas other carbides are much larger and have a much greater tendency to growth at these temperatures. The precipitation of MC, corresponding to $(V_{0.82}Cr_{0.05}Fe_{0.07}Mo_{0.04}W_{0.02})C$ as average composition, always occurs directly from the tempered bainite matrix and is not associated with the previous formation of any other phase. The hexagonal carbide M_2C, with average composition of $(Mo_{0.9}W_{0.35}V_{0.31}Cr_{0.3}Fe_{0.03}Mn_{0.01})C$, promotes creep resistance but is not as growth resistant as the cubic carbides at the highest service temperature (*i.e.* ~ 565°C) at which ferritic steels are applicable.

The strong carbide formers Mo and W were restricted in $M_{23}C_6$ carbide before M_6C was formed. It therefore formed its own carbide M_2C wherever possible. It has been found that when alloy additions are dissolved in Mo_2C carbide, especially W, its parameters will change and c/a will increase from 1.57 to about 1.60 (Wong and Dunlop, 1984), getting closer to the ideally closed-packed lattice. When H-type carbides were first formed, they have a high Mo and W content. Mo, together with W, and V diffused into each other's carbides, or M_2C grew with increasing V content from the centre MC and Mo, W from the matrix and probably from some dissolved M_3C (Carruthers and Collings, 1981). Eventually, MC and M_2C carbides co-existed, dissolving each other to a great amount and being more stable as a result of containing Mo, W and V. Williams and Wilshire (1981) investigated these H-type carbides more thoroughly. They suggest that a high incidence of H-type precipitation would be expected only in normalised and tempered material with large V carbides which were associated with dislocations in the ferrite regions or, more significantly, in samples in which large spherical V carbide particles had developed during service. Norton and Strang (1969) observed that H-type carbides formed in 1CrMoV rotor steels when the Mo/V ratio was over 2.5. Since Mo_2C (a = 3.00Å, c = 4.72Å) and W_2C (a = 2.98Å, c = 4.71Å) were probable completely soluble

each other, when (Mo + W)/V = 5.03 in this steel, H-type carbides would be expected. Actually, it was observed in this study that H-type carbides formed as $(Mo, W)_2C$ wings on small regular plates of MC (see Figures 5.25 - 5.27).

Additions of Ni and Si in this steel may effect the kinetics of the tempering process but do not affect the types of carbide formed.

5.5.2.6 Evolution of Carbides

In steels, the pure binary carbides do not generally occur as there is always some solubility of virtually all the alloying elements in the various carbide phases; in some cases these solubilities may be very extensive (Woodhead and Quarrell, 1965). The proportion of each carbide precipitated varied with tempering time and temperature, extended tempering producing coarsening of boundary carbides. When the cementite was saturated with Cr, it transformed to M_7C_3. This result was in agreement with other workers results (Baker and Nutting, 1959; Pilling and Ridley, 1982). However, it was found that some of the cementite also directly transformed to $M_{23}C_6$ at the early stage of transformation.

The atomic ratio of alloy element to carbon or to Fe is usually an intrinsic factor for the carbide transformation sequence. It has been shown by Kuo (1953) that in Cr steels the Cr content of the cementite increases with tempering time and temperature, due to diffusion, so that beyond a certain time the hexagonal carbide $(Cr, Fe)_7C_3$ replace the Cr enriched cementite. It has been confirmed by EDX microanalysis that in the M_7C_3 carbide about half of the metallic atoms were Cr.

$M_{23}C_6$ was characterised by its higher Cr, Mo and W contents compared with those in M_3C. After the $M_{23}C_6$ formed, the Cr content increased with

tempering time from 20 mass% up to 45 mass% while Mo and W contents from 3 mass% up to 8 mass%. Certainly, the overall steel composition will affect the equilibrium level. Theoretically, Cr can substitute all of the Fe in $M_{23}C_6$ and it did not because of the low Cr content in the steel, even though the Cr content was doubled to conventional 1CrMoV rotor steels. On the other hand, C content and the presence of other alloying elements were also the relevant restrictions. A small amount of Mo and W entered into the $M_{23}C_6$ carbides during tempering.

It could be deduced that the nucleation of M_6C takes place at the existing carbide particles, which might explain why only a few particles were formed and why they grew so rapidly meanwhile also producing MC and M_2C depleted zones around M_6C carbides (see Figure 5.39). The long time tempering results suggest that M_6C is an equilibrium phase.

The equilibrium state in tempered alloy steels is not, in general, reached by a simple precipitation and growth of the equilibrium carbides from the matrix. This fact has been explained by many other workers. However, it is still impossible to give specific temperatures for these carbide evolution processes because the effects of time and temperature are interrelated.

Efforts have been made to understand the saturation problem. It had to be decided what caused the saturation. A conventional thermodynamic sketch was first conceived for the situation as in Figure 5.42.

When the alloy content C was lower than C2 (*e.g.*C1), phase A was more stable than B, while C > C2 (*e.g.* C3), B would be more stable. Calculation has been done with the experimental data and the Gibbs energy of $M_{23}C_6$ was much lower than M_3C within the range of the experimental data. For example, the free energy of M_3C calculated with the carbide composition in sample tempered at 700°C was -39.46 KJ/mol and the Gibbs energy of $M_{23}C_6$

for the same sample was -44.99 KJ/mol respectively. Even though the entropy of mixing was not taken into account, it still implied that the Gibbs energy difference between $M_{23}C_6$ carbide and cementite was the driving force for the transformation of M_3C to $M_{23}C_6$ but not the controlling factor for the saturation of cementite.

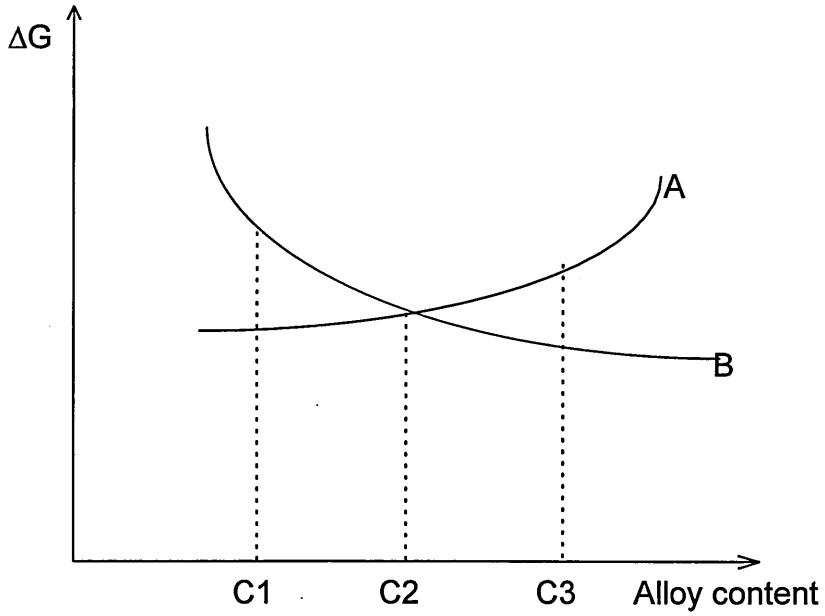

Figure 5 4.2 Supposed situation for the phase transformation from A to B

A further attempt was made to compare the electron microanalysis data with the original steel composition. Alloy cementite were all of much lower Gibbs energy than the Fe cementite and there was no special site for Cr in cementite. There is no doubt that thermodynamically Cr can substitute for all the Fe in cementite. The only restriction would be the alloy content of the steel itself. The ratio to the carbon and the ability to partition between cementite and ferrite of the alloy elements will limit the saturation level. It can be concluded

that the alloy contents in cementite were dependent on the ratios of alloying elements to carbon rather than to the absolute content of the steel.

When the cementite was saturated with alloy elements, it transformed into M_7C_3 or $M_{23}C_6$ which are closely connected with the cooling rate from austenite. During TEM examination of carbon extraction replica (Figure 5.33), It was found that the $M_{23}C_6$ type carbide transformed from M_7C_3 "*in situ*". The "*in situ*" transformation of $M_{23}C_6$ to M_6C carbide has been observed by Kuo and Jia (1985). They found the parallel orientation relationship between these two carbides. Kuo and Jia explained this transformation in CrMoV steel with a fair match on (001) Figure 5.43, after introducing a small relative translation along one of the cube directions. The present work confirmed that it is a reasonable approach, because the high Mo and W content (about 8 mass%) did introduce some distortion into the lattice structure.

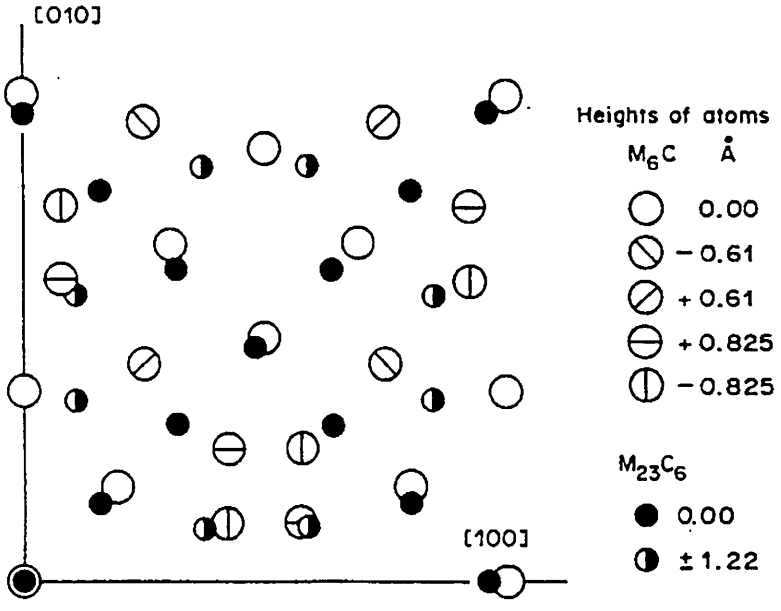

Figure 5.43 Schematic diagram showing the matching of metal atoms on $(001)_{M6C}$ and $(001)_{M23C6}$ and the nearby layers following a parallel orientation relationship (after Kuo and Jia, 1985)

Because the small Mo, W rich M_2C was precipitating during tempering, the amount of Mo and W retained in the big carbides was limited and it would have the effect of stabilising the $M_{23}C_6$ carbides to longer times.

After a systematic investigation on all specimens tempered at different conditions (see Tables 5.4-5.8), it could be concluded that the probable carbide precipitation sequences in this steel is as follows:

$$\text{Matrix} \Rightarrow MC + M_3C \Rightarrow MC + M_3C + M_7C_3 \Rightarrow MC + M_3C + M_7C_3 + M_{23}C_6 \Rightarrow$$
$$MC + M_2C + M_7C_3 + M_{23}C_6 \Rightarrow MC + M_2C + M_7C_3 + M_{23}C_6 + M_6C \Rightarrow$$
$$MC + M_2C + M_{23}C_6 + M_6C \Rightarrow MC + M_{23}C_6 + M_6C$$

It is generally agreed that improved creep resistance results from the presence of a stable, fine dispersion of carbide particles. Although the factors which make such a dispersion possible are complicated by the separate effects of composition, structure and morphology, the required microstructure with possible optimised high temperature properties suitable for large diameter rotor forgings were expect to be attainable by austenitising at 975°C for 10 hours following by oil quenching, then tampering at 675°C for 20 hours following by air cooling. For the austenitising temperatures below 975°C, there will be a risk of undissolved carbides remaining which means carbon could not be fully taken into solution (Figure 5.3). However, for austenitising temperatures above 975°C, there will be a tendency to decrease rupture ductility and to increase notch sensitivity (Strang, 1995). The oil quenching step after austenitisation ensures that the cooling rates from the rim to the core of a large diameter rotor are within the range of 600°C/min to 0.5°C/min and thus to produce a fully bainitic microstructure after solution treatment (Figures 4.5 and 4.11). The relatively higher tempering temperature and longer time, 675°C for 20 hours, were chosen to gain fine dispersions of stable carbides (Figure 6.10) and a more homogeneous microstructure without large and therefore detrimental

precipitates such as M_6C growing rapidly at grain boundaries. The preliminary creep test results (Figure 5.42) showed that specimens heat treated by this optimised condition (Table 5. 9) gave significant higher creep strength than commercial heat treatment practice.

Table 5.9 Comparison of commercial and new optimised heat treatment conditions

	Austenitising temperature °C	Time (hrs)	Quenching media	Tempering temperature °C	Time (hrs)
Commercial treatment	940 - 950	16	oil	660 -670	30
Optimised treatment	975	10	oil	675	20

Chapter 6

INNOVATIVE CARBIDE EXTRACTION AND XRD STUDY

6.1 Introduction

A major part of the effort in this study involves defining the correlation between creep integrity and a wide range of microstructural features, and establishing procedures for quantifying these features in large diameter rotors. The alloy elements in 2CrMoNiWV rotor steel will influence the constitution in two primary ways: by solid solution strengthening and/or by carbides or other phases formation. In this context the ability to extract carbides by effective methods offers an important contribution to the overall characterisation of microstructures, particularly when used in conjunction with X-ray diffraction (XRD) analysis.

6.2 Innovative Carbide Extraction Method

Conventionally, bulk extraction of carbides was prepared either by pure chemical dissolution or electrolytic dissolution of the alloy matrix. Chemical methods, in which the tempered steel was preferentially attacked, leaving the carbides as residues. Typical of these methods was the use of potassium dichromate and sulphuric acid; Electrolytic methods, in which the steel is made the anode in an electrolytic cell, the ferrite matrix again being preferentially attacked. The electrolyte is usually 5% aqueous hydrochloric acid or 5-10% hydrochloric acid in methanol. Most publications in this regard favour

electrolytic extraction of carbide precipitates. The range of electrolytes applicable to a variety of steels was reviewed by Andrews and Hughes (1958), but despite the increasing use of the technique in microstructural studies, no standard procedures have been established for the specific case of low alloy creep resisting steels (Stevens and Lonsdale, 1987). Indeed, some workers have recognised the possibility of incomplete extraction (Leitnaker *et al*, 1975) whilst in another study (Wada and Bliss, 1983) the identification by TEM of a carbide type M_2C that was not detected by XRD. Recognition of these factors cast doubt on the efficiency of the extraction method.

The extent to which this was achieved depends on variables that were both electrochemical or chemical in origin and physical separation of the extracted phases from the liquid by filtering or centrifugalization. Electrochemical variables include the composition and strength of electrolyte (pH value) and the conditions of voltage or current density (temperature of electrolyte), these determine the efficiency by which the dissolution of the alloy matrix occurs, whilst leaving the carbide precipitates intact. Following extraction, chemical dissolution of the precipitates in the electrolyte may occur, for which the relevant variables are the properties of the electrolyte, the temperature and the time of the extraction process. The above parameters were initially investigated by the material at as-received condition. However the XRD result contradicted to the EDX results in that M_3C type carbide could not be found in XRD pattern, which cast doubt on acid dissolution of the precipitates during extraction process. Assuming the electrolytic extraction was carried out with adequate care, it might still be possible to use a solvent which dissolved Fe-based cementite type particles, but not the other carbide phases. For extraction of carbide precipitates to be of value for the overall microstructural characterisation of low alloy steels it is essential to obtain a full yield of all carbide types. Hence if identification is the primary aim, it is better to obtain carbide extraction as efficiently and as completely as possible with the simplest apparatus and methods.

An innovative idea was inspired by making carbon extraction replica during which needs initial light etch to make the carbides stand out from the polished matrix surface. Based on this phenomenon, a sample was deeply etched by 6% nital and carbides could be clearly observed under SEM. However, when the sample was scanned by XRD, the trace only had a strong Fe peak.

A certain amount of experimentation was carried out to find the optimum conditions. It was found that by deeply etching in Villela's reagent for 24 hours gave a layer of carbide residues which remained on metal surface. The metal block was then picked up from Villela's reagent without touching the surface and immersed into alcohol for several minutes. After being dried under 50°C, all the carbide residues were deposited on sample surface and ready for XRD examination.

6.3 XRD Analysis and Theoretical Predictions

The X-ray diffraction technique is reasonably established and the computer controlled X-ray diffractometer may be used when two or more phases co-exist if identification is the primary objective. A typical XRD pattern, obtained from a sample in the "as-received" condition is shown in Figure 6.1. The analysis result from this pattern compared favourably with the conclusions from EDX examination. As many as six constituents have been identified in one sample by such patterns. Even very small amounts of constituents are still detectable and with highly crystalline phase the limit of detection is under 2% of the residue.

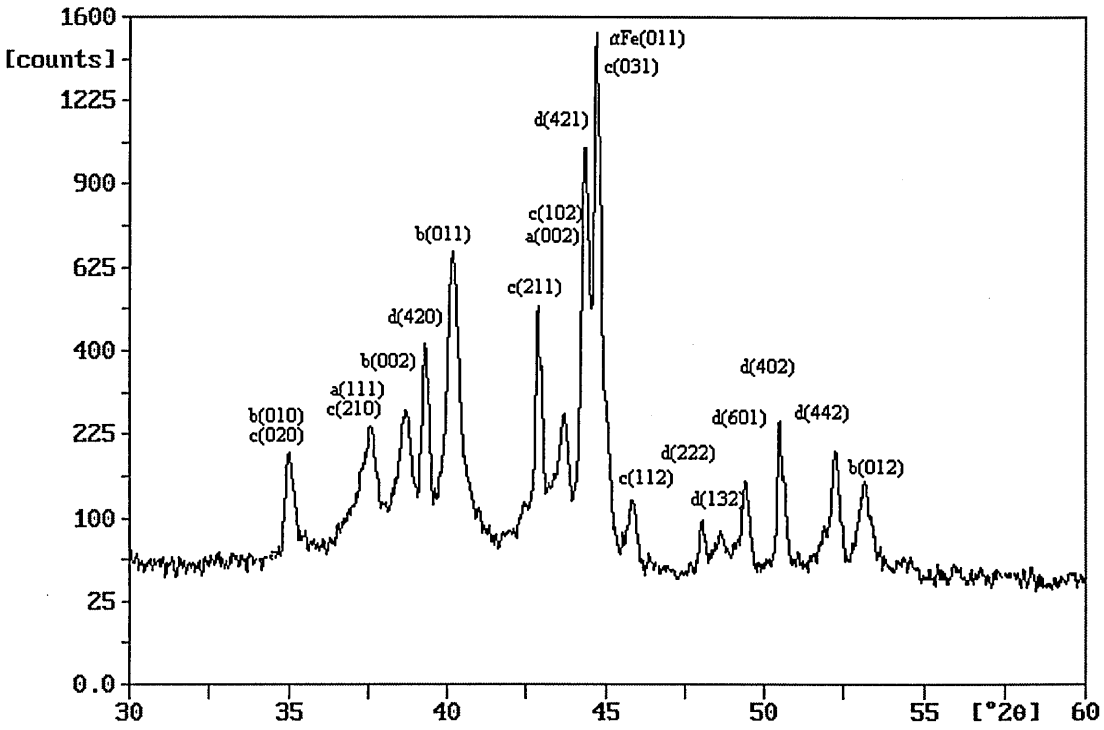

Figure 6.1 X-ray diffraction pattern of "as-received" specimen:

a - MC, b - M_2C, c - M_3C, d - M_7C_3

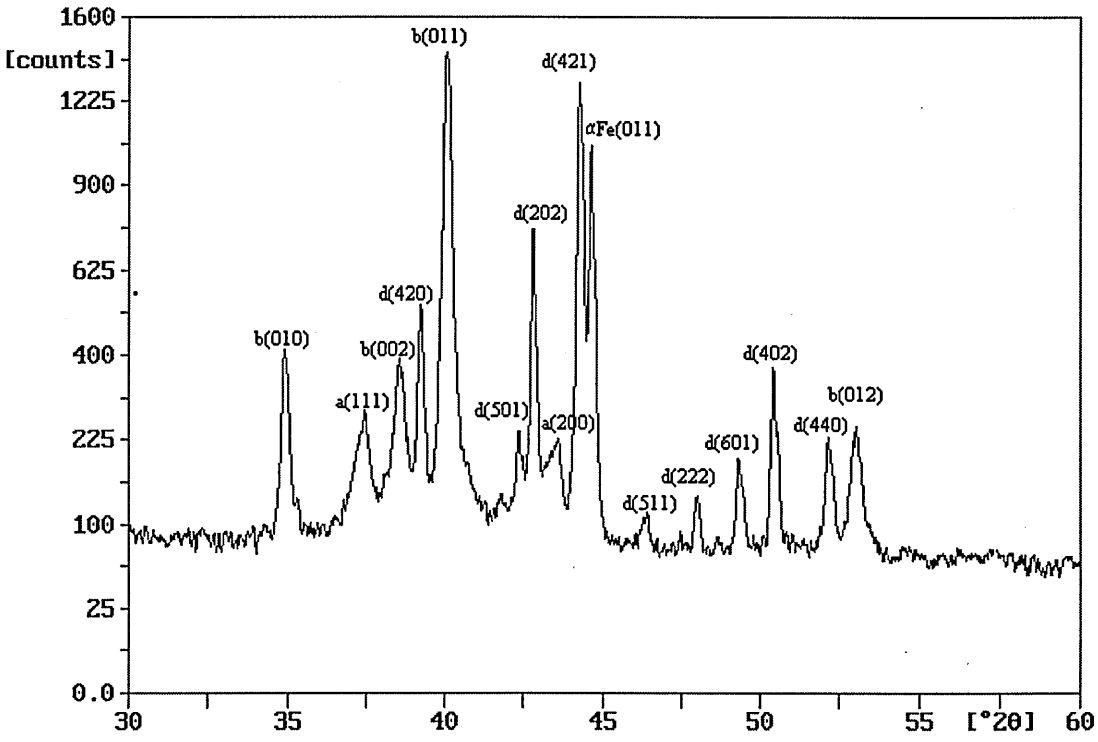

Figure 6.2 X-ray diffraction pattern of "as-received" specimen aged at 650°C for 500 hrs: a - MC, b - M_2C, d - M_7C_3

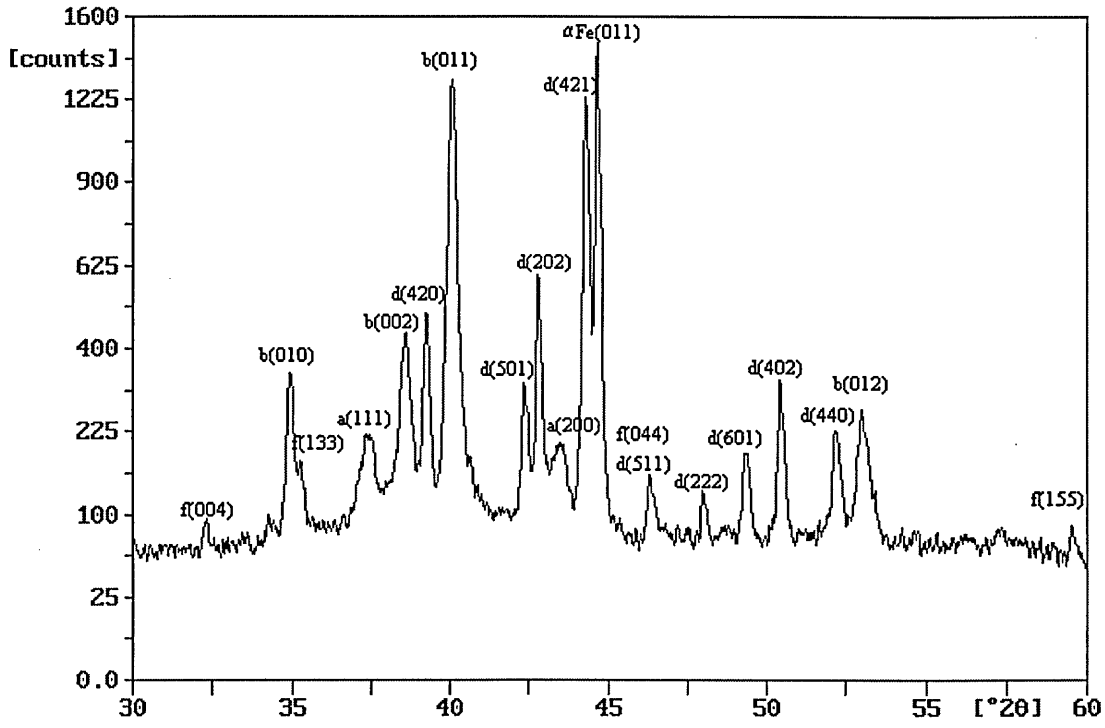

Figure 6.3 X-ray diffraction pattern of "as-received" specimen aged at 650°C for 1000 hrs: a - MC, b - M_2C, d - M_7C_3, f - M_6C

Figure 6.2 shows an XRD pattern of the "as-received" specimen aged 650°C for 500 hours in which M_3C has totally disappeared and M_2C has become the main carbide. Whereas Figure 6.3 illustrates an XRD pattern of as-received specimen aged at 650°C for 1000 hours in which M_6C started to form while M_2C was still dominant.

The information obtained from the X-ray diffraction examination becomes more significant from the practical metallurgical point of view when it is considered in relation to the properties of the material. From the present study point of view, the interests are mainly in the constitutional aspects. There are a number of interesting problems associated, in particular, with the sequences of carbide reactions at different heat treatment conditions, some stages of which are found in this steel containing only Cr, other reactions depending on the presence of Mo, W, V and Cr together.

In this study, the furnace controlled cooling of 10°C/min to room temperature was taken as the most fundamental and basic starting point for carbide precipitation processes or reactions. The carbides found after tempering times up to 100 hours at temperatures between 600°C and 700°C are selectively shown in Figures 6.4-6.7. It can be seen from these figures that the identified carbide species are in very good agreement with what was found by EDX examinations. X-ray diffraction analyses for specimens tempered at 700°C for 500 hours and 1000 hours are presented in Figure 6.8 and 6.9, respectively. In the spectra for the specimen tempered for 500 hours at 700°C, the {420}, {202} and {402} peaks from M_7C_3 are clearly visible, whereas these peaks have disappeared after tempering for 1000 hours at 700°C. The {420}, {202} and {402} peaks are strong visible peaks for M_7C_3, because the most intense {421} peak overlaps with the most intense {333} peak of $M_{23}C_6$.

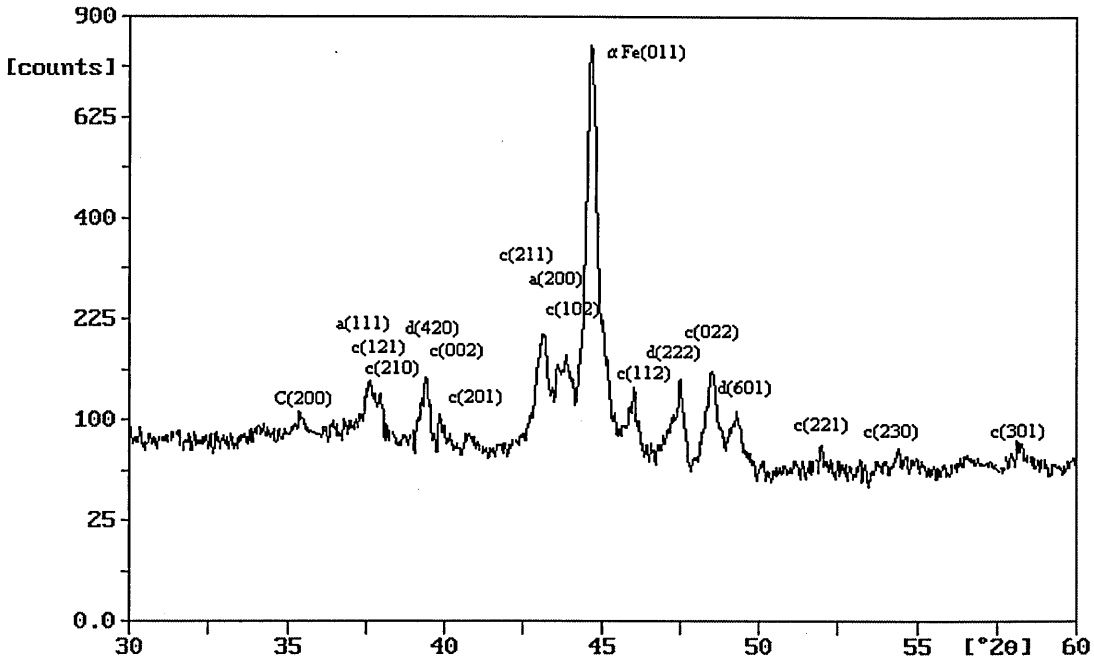

Figure 6.4 X-ray diffraction pattern of specimen tempered at 600°C for 5 hrs: a - MC, c - M_3C, d - M_7C_3

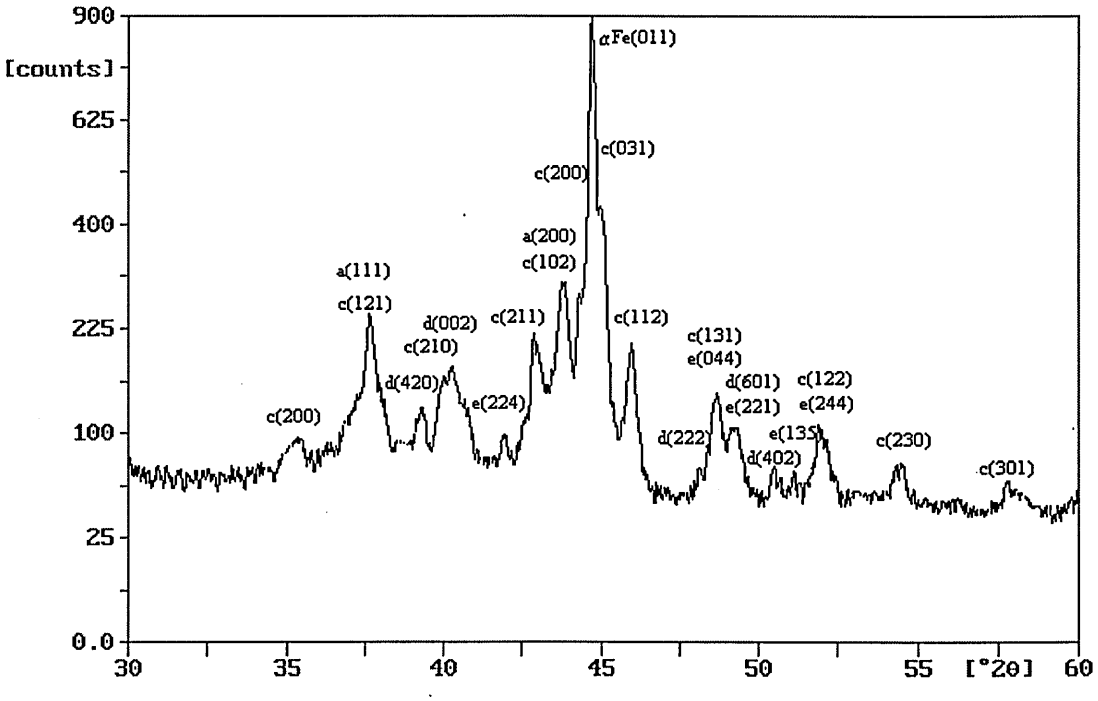

Figure 6.5 X-ray diffraction pattern of specimen tempered at 600°C for 20 hrs: a - MC, c - M_3C, d - M_7C_3

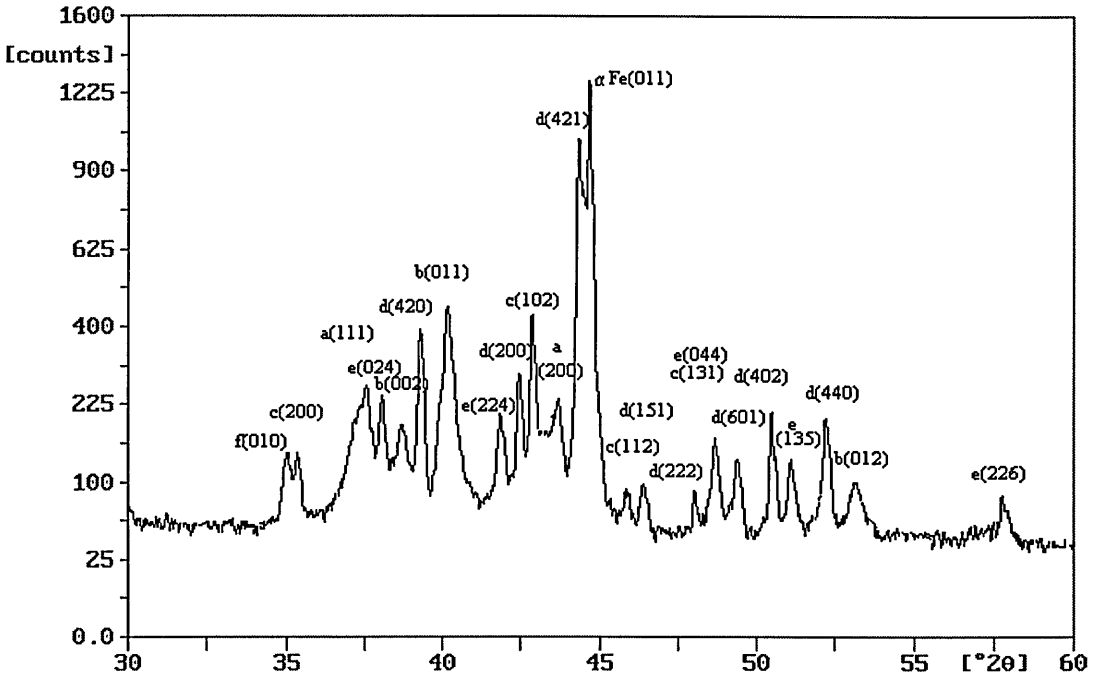

Figure 6.6 X-ray diffraction pattern of specimen tempered at 700°C for 20 hrs: a - MC, b - M_2C, c - M_3C, d - M_7C_3, e - $M_{23}C_6$

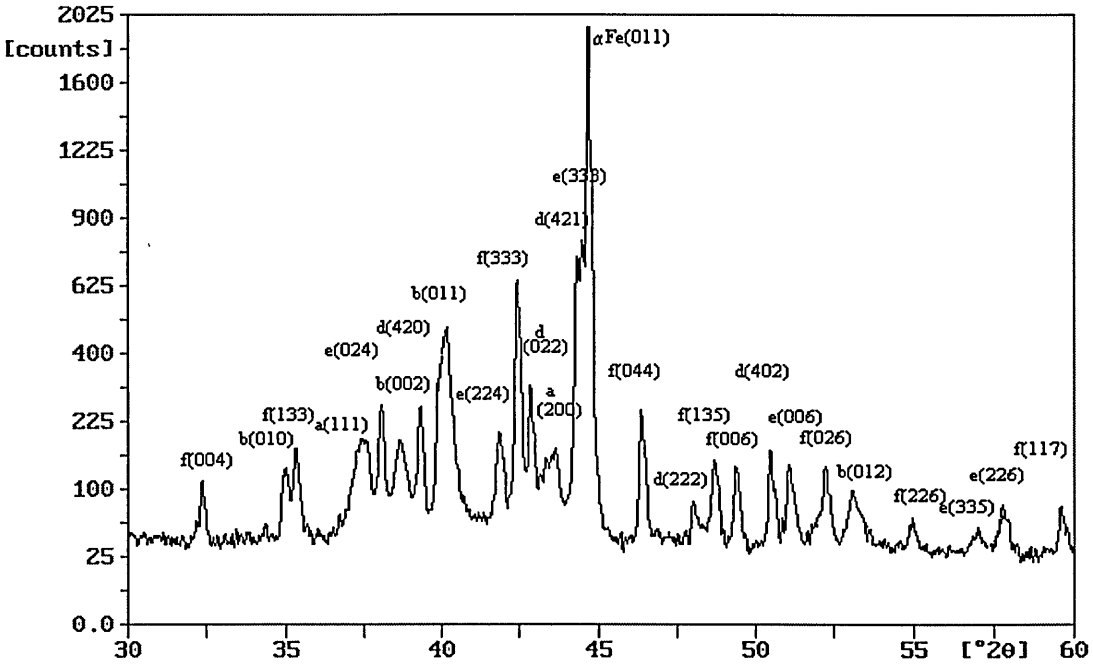

Figure 6.7 X-ray diffraction pattern of specimen tempered at 700°C for 100 hrs: a - MC, b - M_2C, c - M_3C, d - M_7C_3, e - $M_{23}C_6$, f - M_6C

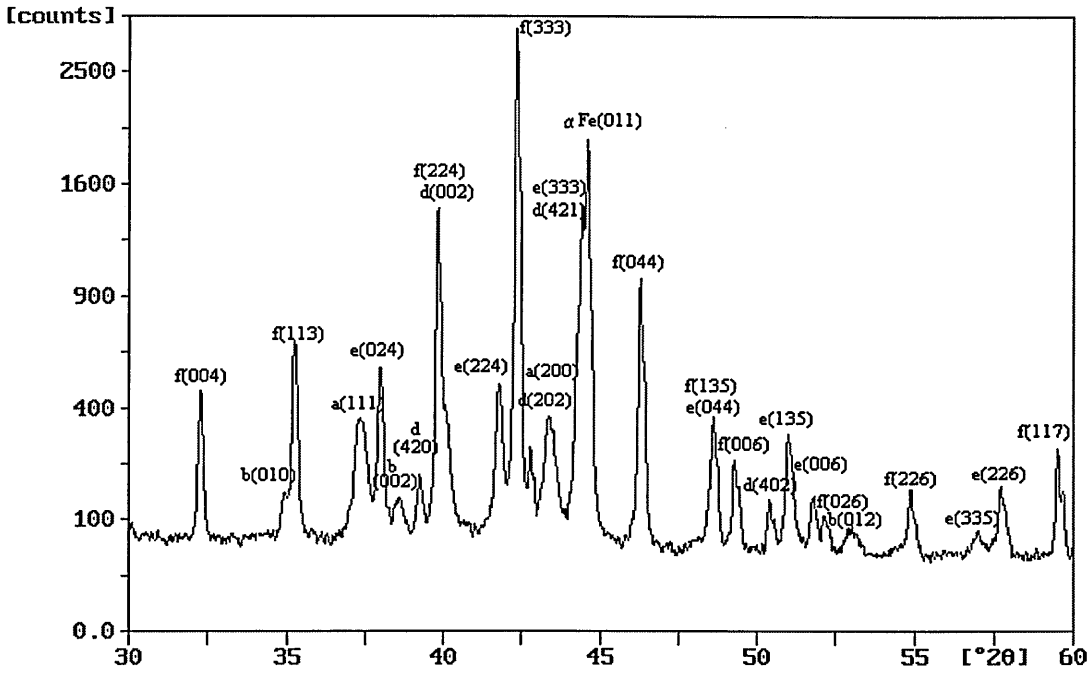

Figure 6.8 X-ray diffraction pattern of specimen tempered at 700°C for 500 hrs: a - MC, b - M_2C, d - M_7C_3, e - $M_{23}C_6$, f - M_6C

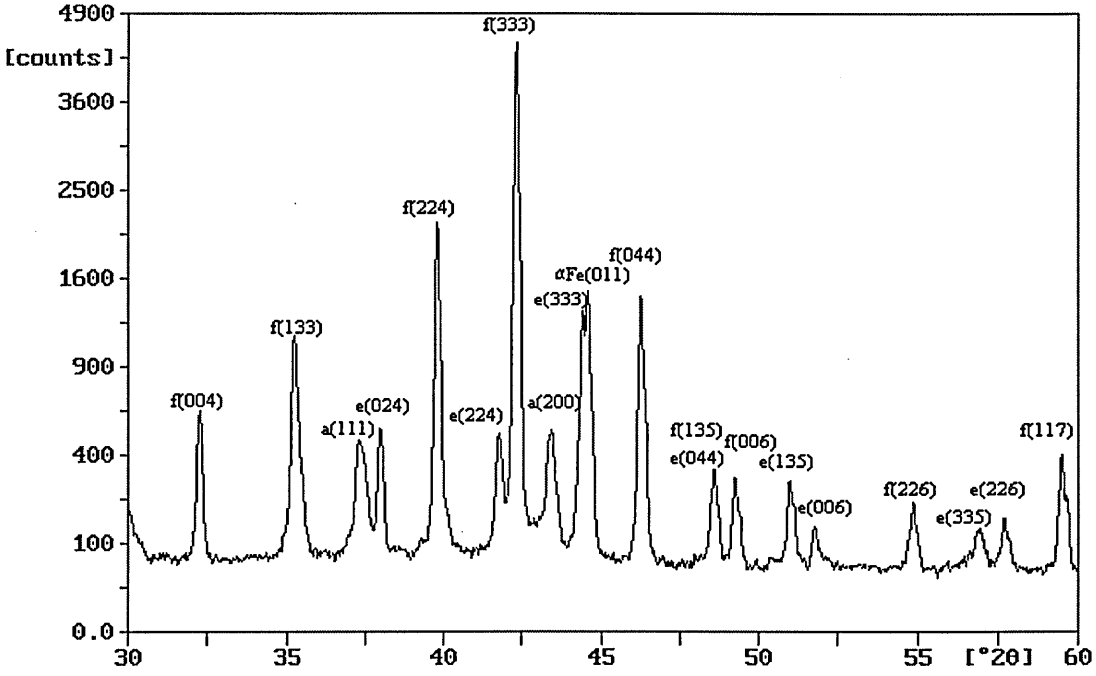

Figure 6.9 X-ray diffraction pattern of specimen tempered at 700°C for 1000 hrs: a - MC, e - $M_{23}C_6$, f - M_6C

The XRD results was in very good agreement with TEM/EDX examination results. The sequence of carbide transformation after the different tempering treatments and systematic investigations both by XRD and TEM/EDX is shown diagrammatically in Figure 6.10.

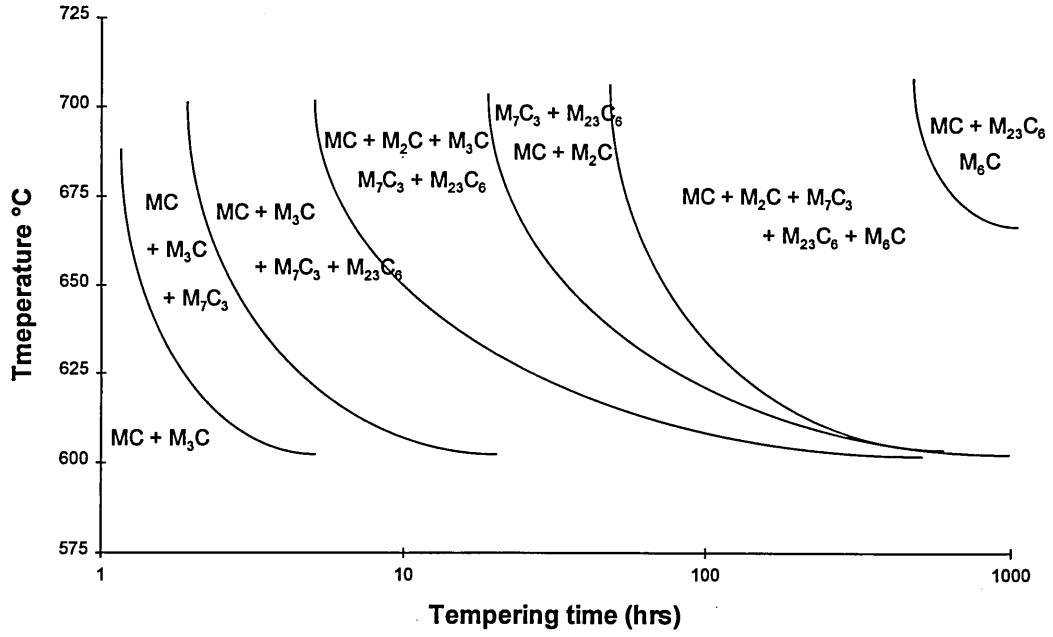

Figure 6.10 Carbide phase transformation diagram for 2CrMoNiWV steel during tempering

The sequence of carbide precipitation was also calculated using MTDATA. It was achieved by finding the equilibrium carbide and then suppressing its formation and repeating the calculation. Thus the previous carbide to form in the sequence was found (Thomson, 1992). Previous calculations in Chapter 4 (Figure 4.9) shows that final equilibrium carbides are M_6C, $M_{23}C_6$ and V_4C_3 [FCC_A1, phase (2)] in this 2CrMoNiWV rotor steel. Presumably without M_6C formation in this system, the calculation was repeated with the same parameters and a plot is given in Figure 6.11 in which $M_{23}C_6$ is the most stable carbide. Then M_6C and $M_{23}C_6$ were suppressed, the repeated calculation result is illustrated in Figure 6.12 in which M_7C_3 automatically came out as stable carbide. Finally M_6C, $M_{23}C_6$ and M_7C_3 were all suppressed to form, the calculation result is exhibited in Figure 6.13 in which cementite stands out as stable carbide. In Figures 6.11-6.13, FCC_A1 [phase (2), corresponding to MC(V_4C_3) in this study] always appears as equilibrium phase. MC_SHP phase is a (W, Mo)-rich carbide phase with simple hexagonal crystal structure, which can be correlated to M_2C type carbide in this study. After this series of calculations, the sequence of carbide precipitation could be drawn as follows:

$$\text{Matrix} \Rightarrow MC + M_3C + M_2C \Rightarrow MC + M_7C_3 + M_2C \Rightarrow MC + M_{23}C_6 + M_2C \Rightarrow MC + M_{23}C_6 + M_6C$$

Generally, the thermodynamic prediction using MTDATA is in quite good agreement with experimental results. The difference could be easily explained due to that theoretical prediction is based upon final equilibrium condition without consideration of kinetics. In the real tempering process, the material could be taken out at any stage before putting into service which might be far away from equilibrium condition and carbide transformation from one to the other will overlap for a long time.

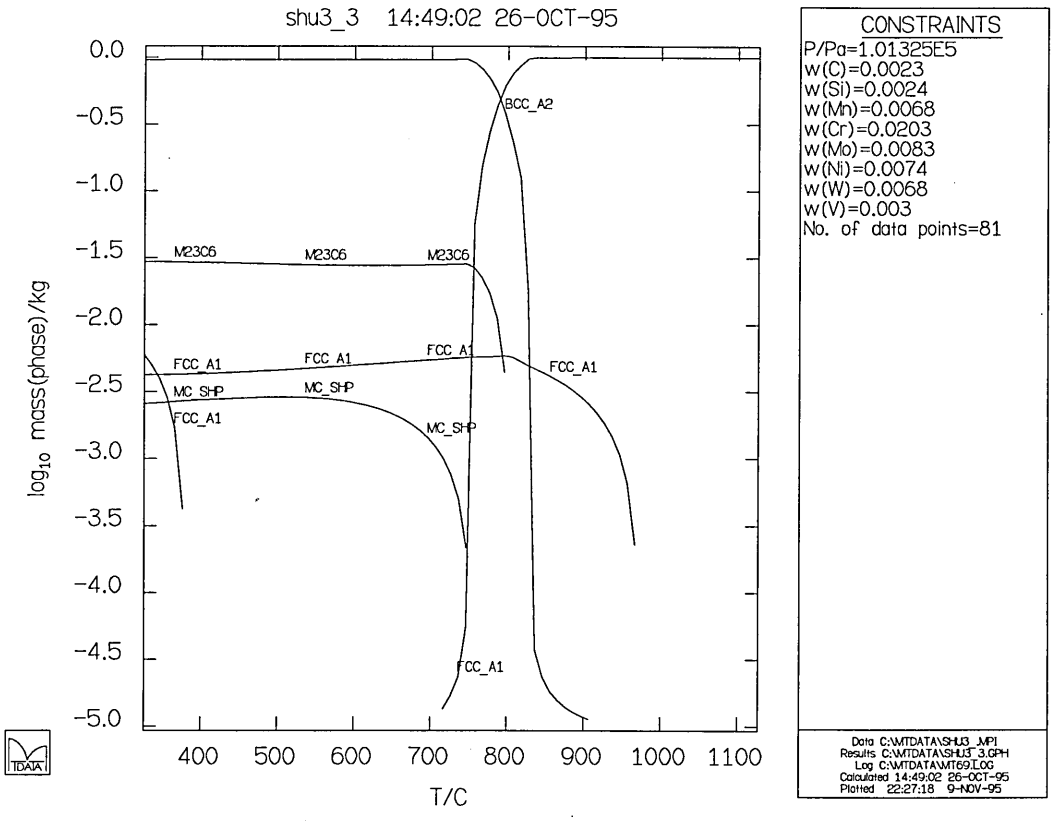

Figure 6.11 Thermodynamic calculation without M_6C

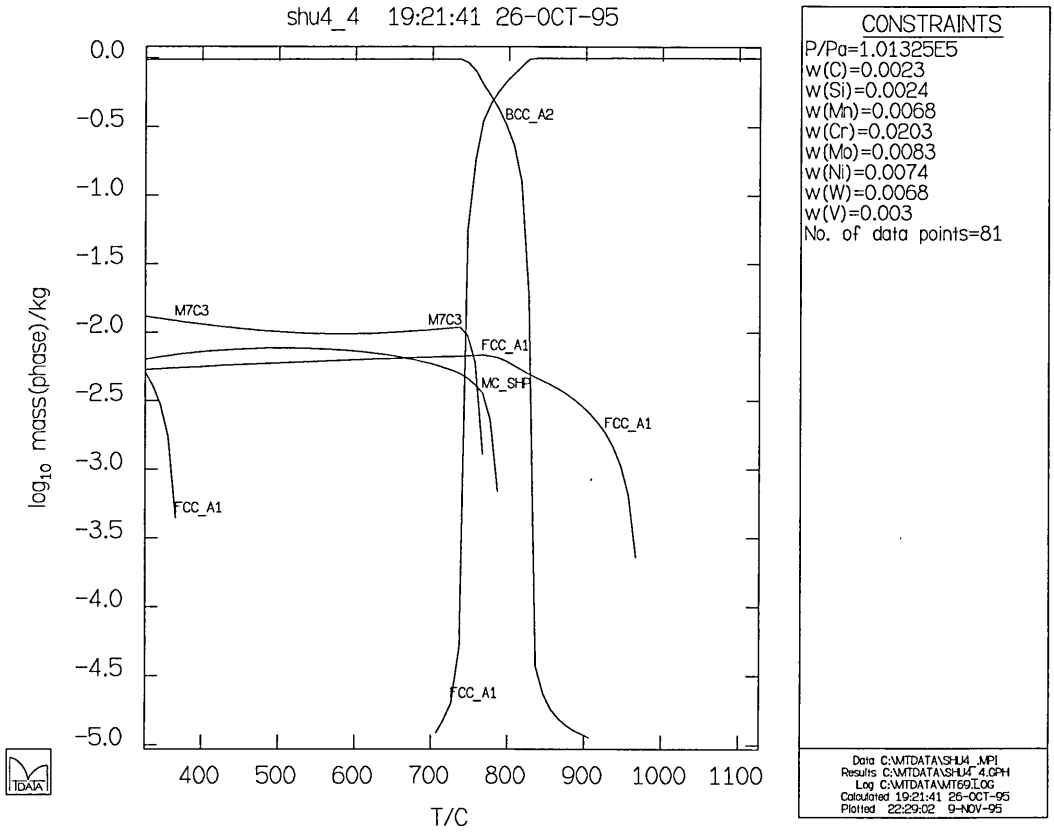

Figure 6.12 Thermodynamic calculation without M_6C and $M_{23}C_6$

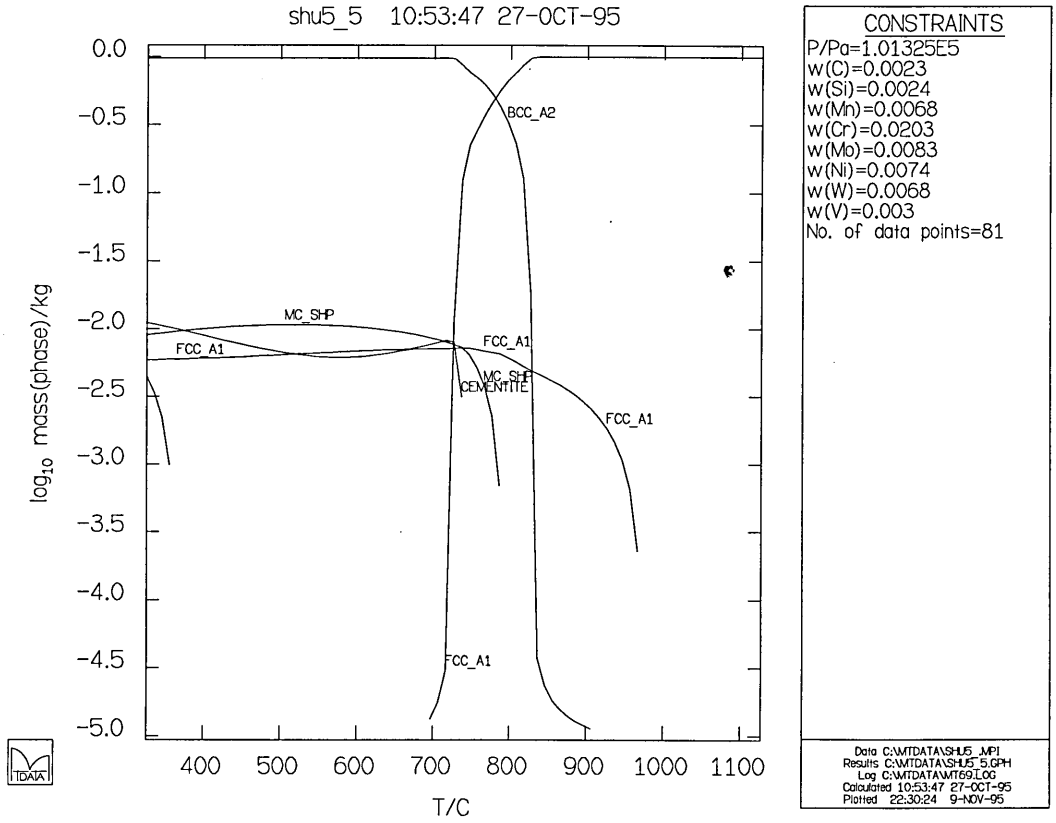

Figure 6.13 Thermodynamic calculation without M_6C, $M_{23}C_6$ and M_7C_3

The lattice parameters for $M_{23}C_6$ extracted from different heat-treated specimens of the 2CrMoNiWV steel were calculated using measured values of d-spacing. Specific data on W and Mo containing $M_{23}C_6$ are scarce and no detailed descriptions of corresponding patterns can be found. Neither does the literature give any indication that a particular difference with respect to (Fe, $Cr)_{23}C_6$ might exist apart from a common feature of the different patterns is the absence of {111}, {200}, {220}, {444}, {642} and {842} reflections. The incorporation of Mo or W into the lattice of $M_{23}C_6$ may not only affect the diffracted intensities, it will also modify the carbide's lattice constant. The magnitude of the changes depend mainly on the difference in atomic radius between Cr, Fe and above metal atoms and on the number of lattice positions these atoms occupy. The lattice parameters of the (Cr, Fe, W, $Mo)_{23}C_6$ carbides subject to the present study can roughly be estimated. Errors may arise in the measured values of the d-spacings due to the positioning of the specimen in the diffractometer, absorption in the specimen, *etc.* An estimate of the amount of correction to be applied was attained by using the d-spacing from αFe (011) as an internal standard reference, which is known to a high degree of accuracy. $M_{23}C_6$ is cubic and therefore the d-spacings and plane indices are related by the equation:

$$d_{hkl}^2 = \frac{a^2}{h^2 + k^2 + l^2} \quad \text{.....(6.1)}$$

The adjusted d-spacing were applied to this equation and the calculated lattice parameters differed by no more than 0.02 Å. The $M_{23}C_6$ peaks in the XRD traces do not have a constant lattice parameter. They might be either greater or smaller than the normally quoted parameter which means at least one of the cubic directions might have slightly changed. This is because the

Mo and W contents (about 8 mass%) introduced some distortion into the lattice structure.

6.4 The advantages of the new carbide extraction method

The innovative carbide extraction method proved to be very successful for the identification of carbide phases. There are some distinct advantages over traditional electrochemical dissolution of the matrix to extract carbide residues.

Firstly the new method is efficient and able to extract existing carbide completely without any dubious losses of carbide species during washing and residue separating processes, even those finest particles would not escape. The ability to detect each individual carbide in low alloy ferritic steels through bulk extractions has proved to be of great benefit in the study of creep strengthening mechanisms, and offers considerable potential in the remnant life assessment of high temperature components. It does not require any special equipment or apparatus for the operation, the method can be easily adopted by other researchers working in the same field.

Secondly the specimen size required is very small (~ ϕ5 x 5 mm) which can be taken from the same sample straight after carbon extraction replica being produced. Detailed TEM and EDX examination can give information such as carbide morphology, size, distribution and composition, *etc.*, but X-ray diffraction pattern would evidently give what carbide phases exist and relative percentage of each carbide using a single scan. That EDX examination combined with XRD analysis exhibited excellent reproducibility in this study, thus giving the most potent data to demonstrate the experimental results.

Finally because of sample matrix as substrate, in the X-ray diffraction pattern there always is a strong αFe (011) peak which can be taken as a calibration line for other carbide reflection peaks if they shift away from normal 2θ position due to high dissolution of alloy elements into the anticipated carbide species and the positioning of the specimen in the diffractometer. Compositional changes in carbides are reflected in corresponding changes in lattice parameter which can readily be determined by XRD analysis of extracted carbides using this method. If the relationship between composition and lattice parameter can be defined, measurement of the latter would eliminate the time consuming analysis of individual carbides.

These advantages as stated above give an indication of the great value of the new carbide extraction technique.

6.5 Discussion

From the carbide precipitation sequences, it is evident that MC carbide always exists during any tempering stages and its composition almost remains the same. It suggests that V should have the strongest affinity to C among the alloy elements and MC be an equilibrium phase once it is formed. V carbide exerts a beneficial influence on the creep resistance of these bainitic steels because it occurs in a very finely divided state and resists coalescence and growth at elevated temperatures. So it will be better to increase V content to this steel from 0.3% up to 0.42% for improving creep strength (Wiemann, 1991). In contrast to Baker and Nutting's study (1959), M_2C is not the first alloy carbide to form and its precipitation closely related to the M_3C, actually M_2C was found after M_3C disappeared. M_3C itself forms quickly and is controlled by the diffusion of carbon. It contains a proportion of alloy elements but the metallic atoms are predominantly Fe. The Cr content of the M_3C increases with

time, due to diffusion, so that beyond a certain time the hexagonal carbide M_7C_3 replaces the Cr enriched M_3C. In the M_7C_3 carbide more than half of the metallic atoms are Cr. The next stage is the formation of the carbide $M_{23}C_6$ with more other alloy elements. Finally when Mo and W are rich enough there can be a final stage to M_6C in which M_2C makes a contribution to M_6C by dissolving itself.

The sequence of precipitation in these alloy carbides thus appears to depend on the principle that, M_3C can form with Fe and alloy atoms in similar proportions to the matrix, alloy elements diffuse into carbides first, having a greater affinity for C, with the object of replacing Fe. The ratio of metal atoms to C increases more or less progressively to the highest possible ratio (6:1).

When Mo and W are present they appear at first to diffuse preferentially to certain sites and form M_2C which later on may convert directly to M_6C. The M_2C was found after 50 hrs at 650°C and the fact M_6C was found after 100 hrs at 700°C in this study, implying that an $M_{23}C_6$ phase might not act as an intermediate stage in this sequence and it might have been expected to remain until very late stage. The fact that M_7C_3 persists beyond 1000 hrs at 650°C confirms the transformation from M_7C_3 to $M_{23}C_6$ has not completed at this point (Figure 6.3). When the temperature is raised to 700°C the tempering time needed to reach equilibrium became less than 1000 hrs and in fact only MC, $M_{23}C_6$ and M_6C phases were found (Figure 6.9).

The improved resolution of the modern focusing diffraction equipment coupled with this powerful new carbide extraction technique made it possible to detect new features in the X-ray diffraction patterns, showing that $M_{23}C_6$ carbides extracted from this W-containing alloy differ from $(Cr, Fe)_{23}C_6$ observed in more conventional stainless steels. The distinctions are related to the lattice parameters, as well as the intensities of specific diffraction maxima.

These difference can be explained in terms of the theoretical considerations of Goldschmidt (1967) who predicted that W and Mo, when incorporated in $Cr_{23}C_6$, will preferentially occupy specific positions in the unit cell.

The equilibria in this 2CrMoNiWV multicomponent, multiphase system was performed with MTDATA using critically assessed data for simpler systems. The amounts of species within each phase for a given temperature and pressure or volume can be calculated by minimising the Gibbs free energy of the system for specified component amounts. The main advantage is that calculations can be performed for the specific composition of individual materials under investigation.

Consideration may be given to the effect of temperature on the time to reach a given condition so that a change in carbide phase occurs, *i.e.*, a step forward in the appropriate sequence. Assuming 'final equilibrium' at application temperature is the same as at 700°C, then the time required to reach that equilibrium is much longer. Since there appears to be considerable evidence for the view that creep deformation in such steel is retarded as long as precipitation processes or carbide reactions are proceeding. That is why many research works are dedicated in designing new compositions of steels so that they produce such sequences for as long as possible.

Chapter 7

THE ROLE OF TUNGSTEN IN 2CrMoNiWV ROTOR STEEL

7.1 Introduction

It has been well established that V confers marked secondary hardening on creep resistant low alloy steels (Irvine and Pickering, 1960). Norton and Strang (1969) recommended that V:C ratio of 1½:1 to 2:1 would give best combination of creep strength and ductility in large 1%Cr-Mo-V steam turbine rotor forgings. The role of V in 2CrMoNiWV has also been studied by GEC ALSTHOM (Wiemann, 1991) and a V:C ratio of approximately 2 was suggested to obtain the highest creep strength for this material. Since the days when steels were first used under creep conditions, Mo has been recognised as a potent strengthening element that confers creep resistance. It is clear that Mo contributes by solid solution strengthening and by stabilising to M_2C phase (Brigg and Parker, 1965). However, W has a similar effect to Mo in that it stabilise the M_2C precipitates and contributes to solid solution strengthening. Fujita et al (1978) investigated the creep rupture properties of a steel containing W additions up to 1.7 mass%. They claimed that a strength maximum was obtained when Mo and W were present together at levels of the Mo equivalent, (mass% Mo + 0.5 mass% W), approximating 1.6 mass%. Thus a systematic investigation of the role of W in the 2CrMoNiWV rotor steel becomes a pertinent feature in this work.

W dissolves in both γFe and αFe but, having a bcc structure, tends to stabilise αFe (ferrite). It therefore raises the A_3 temperature and, like Cr, forms

a closed γ-loop in the phase diagram. Unlike Cr, however, it inhibits grain growth and therefore has a grain refining effect. It also reduces decarburisation during working and heat treatment. Both of these features are useful since high temperatures are involved during the heat treatment of this W bearing steel.

As the solubility of Mo and W in M_3C is small, much of the alloy elements will be in solid solution in the ferrite and it is probable that much of the creep resistance of this steel is associated primarily with solid solution hardening as Mo and W are particularly effective in this respect.

Although the general effects of Mo and W in improving the properties of ferritic steels are clear, there are considerable gaps in the knowledge base. In this study, work has been conducted in an attempt to understand the role of alloying elements, especially W, with respect to its improving creep strength whilst not significantly affecting ductility using advanced electron microanalysis, together with thermodynamic predictions of phase equilibria using MTDATA.

7.2 EDX Microanalysis

Analytical electron microscopy was extensively used in this study and detailed sample preparation and analytical procedures were given in Chapter 3. The modern version of STEM-EDX has the ability to resolve special features normally on the nm scale and also provide elemental information from very small volumes. Up to 200 kv electron beam can be focused onto the specimen with beam diameter <10 nm hence a very small X-ray source region is obtained. Because the sample is thin (either thin foil or small particles on extraction replica), no absorption or fluorescence correction need be applied to the X-ray data in most cases. This allows the application of relatively simple procedures for obtaining quantitative analyses of samples.

As the size and composition change from particle to particle and there is a spread in distribution in a given sample especially at the beginning of tempering, it can be considered in two ways to achieve more accurate data. The first one is to do analysis only on particles of one size -- critical size, mean size or any specially defined size. Another is to do more analysis randomly to enhance the confidence level. The first one, although reasonable theoretically, is subjective due to the difficulty in deciding the critical size of precipitates with complicated shape experimentally. In that case, more analyses by random choice had to be done to establish the shape of the distribution curve. At least 20 analyses were done on each kind of carbide in the sample. At the beginning of the tempering, the composition of M_3C was so divergent that as many as 100 analyses were needed to minimise the standard error to an acceptable amount.

A considerable effort was directed to the analysis of the H-type carbides, but the result was not convincing. Firstly the spot size was bigger than the carbides. It was possible to put the spot on to the wing edge without covering the central MC, on the contrary, it was not easy to analyse the central MC without covering the M_2C wings unless the centre carbide was big enough. Secondly, because of the small size, the count rate was very low. To accumulate enough data, either extending accumulating time or increasing the electron beam spot size, both of which would cause serious contamination. In addition, it was not easy to find separate H-type carbide in the right orientation to carry out the microanalysis.

Although the difficulties mentioned above, the results showed the centre MC with constant composition. The wing analysis seems to show a trend to have higher V and Cr content at longer tempering time. From the analyses, it is also found that MC does not dissolve Mn and Fe but M_2C does in small amounts.

The representative energy dispersive X-ray spectra of various carbides are presented in Figure 5.10, Chapter 5. The experimentally determined average chemical composition ranges of the alloying elements in the carbides in mass percentage covering all experimental tempering temperatures and times are summarised in Table 7.1.

Table 7.1 Average chemical composition ranges of the carbides in mass%

Carbide	Fe	Cr	Mn	Mo	W	V
M_3C	75 - 90	5 - 20	2 - 3	2 - 3	2 - 3	1 - 2
MC	0	3 - 7	0	3 - 6	3 - 6	85 - 95
M_7C_3	30 - 40	50 - 60	3.5 - 4.5	6 - 9	3 - 6	2 - 3
M_2C	0 - 1	7 - 15	0 - 1	45 - 55	30 - 40	10 - 15
$M_{23}C_6$	40 - 50	35 - 45	2 - 4	6 - 10	6 - 10	1 - 2
M_6C	25 - 30	3 - 8	0	35 - 40	25 - 35	1 - 2

The Cr content of the M_3C was found to increase steadily with time at the tempering temperature, the rate of enrichment being higher at the higher temperatures. On the contrary, the Cr content of M_7C_3 was found to decrease with time at the tempering temperature and the rate was faster at the higher tempering temperature. The Cr content in $M_{23}C_6$ exhibited exactly the same trend as in M_7C_3 except the Cr content was lower than in M_7C_3. Cr is chosen as an indicator of composition change because of its large alloy concentration; The Fe content simply mirrors the changes in Cr content. The total Mn and V contents were relatively small and therefore any errors would be relatively large. Mo and W have larger atomic masses when compared with Fe, Cr, Mn or

V. The microanalytical measurements were carried out assuming that all elements absorb the X-rays to a similar degree. The Mo and W data were likely to be flawed, the extent of the error depending on the thickness of the particle along the electron beam direction. The V content of M_2C was much higher than in the other carbides. The compositions of MC and M_6C were relatively constant at all stages of tempering. A strong dependence of compositional change on particle size was observed, the smaller particles compositional change more quickly than the larger ones. M_6C carbides once they were formed were larger than any other types of carbide, any further compositional change in M_6C was too small to be differentiated.

An effort was made to measure the chemical composition in the matrix directly under TEM on thin foil specimens after various heat treatment. Due to the fact that the alloying element concentrations were very low after alloy carbide precipitation, the EDX measurement results were unsatisfactory. In order to know the alloying element contents remaining in ferrite after tempering, particularly W content, tempered specimens were selectively chosen to dissolve electrolytically with 5% HCl aqueous solution. The undissolved carbide residues were isolated from the solutions and then the solutions were analysed by using inductively coupled plasma (ICP) techniques. The results were summarised in Table 7.2.

Table 7.2 shows V nearly depleted in the matrix in the early stage of tempering, indicating V has higher affinity than Cr, Mo and W for carbon forming a fine dispersion of V-rich carbides. W and Mo contents in ferrite matrix decreases with the increasing of tempering parameter (LMP), but still remain approximately half of their contents in the ferrite matrix, which indicates that W and Mo play important roles in promoting creep resistance of the steel not only by forming fine dispersion of M_2C type carbides but also by retaining certain amounts of W and Mo in the ferrite as solid solution strengthening elements.

Table 7.2 ICP analysis results for various tempered specimen dissolved electrolytically in 5% HCl aqueous solution (mass%)

Tempering condition (LMP)	Cr	Mo	Ni	W	V
600°C for 5 hrs (18.07)	1.8	0.55	0.71	0.44	0.12
650°C for 20 hrs (19.66)	1.3	0.46	0.60	0.35	0.07
700°C for 20 hrs (20.73)	1.6	0.44	0.64	0.34	0.09
700°C for 100 hrs (21.41)	1.5	0.40	0.65	0.32	0.06
Bulk comp. of the steel	2.03	0.83	0.74	0.68	0.30

Several investigations have demonstrated that the creep resistance of ferritic steels is affected by the level of Mo in the matrix (Foldyna, *et al,* 1972; Johnson and Glen, 1972). It was suggested that the mechanism of delay was connected to the difference in atomic volumes between Fe and the alloying elements (Fujita and Takahashi, 1978). The atomic volumes of Fe, Mo, W and V are as follows: Fe: 7.1 cm^3/mol, Mo: 9.4 cm^3/mol, W: 9.53 cm^3/mol and V: 8.35 cm^3/mol. Thus, it seems that the degree of resistance to the softening process increases with the difference in atomic volumes. From this point of view, W has the largest atomic volumes among these alloying elements, so it can be concluded that the remaining W in ferrite would contribute solid solution strengthening effect to the creep resistance. Nevertheless V is still the most potent element in terms of obtaining good creep strength because MC (V_4C_3) is more stable than M_2C.

7.3 Comparison of Experimental Results and Theoretical Predictions

A preliminary choice of tempering temperature according to the hardness values in Table 5.3 is 675°C. The temperature of operation is usually 550°C. The equilibria for the two temperatures was calculated using MTDATA and the amounts of alloying elements distribution in individual phase are shown in Tables 7.3 - 7.4.

Table 7.3 Calculated equilibrium at 550°C (mass%) without the stoichiometric carbon concentration to enable direct comparison with EDX measurements

Phase	Fe	Cr	Mo	W	V
Ferrite	Balance	0.79	0.14	0.18	0.025
MC	--	14.1	9.4	7.1	70
$M_{23}C_6$	34.2	44.7	20.5	1.1	--
M_6C	24.5	--	12.7	61.2	--
Bulk comp. of steel	Balance	2.03	0.83	0.68	0.30

The equilibrium calculations were extended to 300 - 1100°C which is shown in Figure 4.13, Chapter 4, showing the mass fractions of each phase in this temperature interval. The chemical composition of the matrix and the different kinds of precipitates were also calculated. Figure 7.1 shows the chemical composition of the matrix as a function of temperature. The amount

of W decreases from the tempering temperature to the temperature of operation. The corresponding diagram for M_6C, Figure 7.2, shows a decrease in W and an increase in Fe from the tempering temperature to the operation temperature. Similar trend in the diagram for $M_{23}C_6$, Figure 7.3, but mass fraction of component W in $M_{23}C_6$ is much lower.

Table 7.4 Calculated equilibrium at 675°C (mass%) without the stoichiometric carbon concentration to enable direct comparison with EDX measurements

Phase	Fe	Cr	Mo	W	V
Ferrite	Balance	1.2	0.24	0.40	0.028
MC	--	14.7	12.9	13.5	59.4
$M_{23}C_6$	45.3	33.7	18.4	2.6	--
M_6C	26.5	--	12.2	59.2	--
Bulk comp. of steel	Balance	2.03	0.83	0.68	0.30

This 2CrMoNiWV rotor steel differs mainly from conventional 1CrMoV rotor steels in that it has double the Cr content and an addition of W. It has been demonstrated that W addition was beneficial to the distinct improvement of toughness and without detrimental effect to the creep strength and ductility through the experimental work (Wiemann, 1991). It would be of great help in understanding the effect of various W addition to this system and MTDATA demonstrated a great advantage in this aspect. In Chapter 4, two cases were considered for thermodynamic calculations: (I) With the actual composition of the 2CrMoNiWV steel, to predict the A_{C1}, A_{C3} and to see whether there were

any phase existing in the austenite range; (II) Without W addition in the system to repeat the calculation to see whether there were any differences in the austenite range. The results of thermodynamic calculations using MTDATA were shown in Figure 4.14 and Figure 4.15. Another three different W additions without altering other alloying elements content were considered to predict the effect of W variations on the equilibria of the system.

Firstly, the thermodynamic calculation was performed using MTDATA with only half of the actual W content and the result of calculation is shown in Figure 7.4. The major differences between Figure 7.4 and Figure 4.14 (with the actual composition of the 2CrMoNiWV steel, replotted on next page for the convenience of comparison) were mass fraction of M_6C phase fewer and without the formation of MC_SHP phase (corresponding to M_2C phase in this study); Secondly, the calculation was carried out with double the actual W content (1.36 mass%) and the result of the calculation was plotted in Figure 7.5. It was obvious that the mass fraction of M_6C phase was greater than that of Figure 4.14. Another difference was that the M_6C phase would form again between A_{C1} and A_{C3} temperature range and finally dissolve at approximately 910°C; Thirdly, the calculation was conducted with 5 mass% W, deliberately much higher than the actual W content, and the result was presented in Figure 7.6. As expected, the mass fraction of M_6C phase was much more than that of Figure 4.14 and the M_6C phase would not dissolve until approximately 1100°C in solution treatment temperature range. The mass fraction of FCC_A1 phase (2) [corresponding to MC (V_4C_3) phase in this study] became less and without the formation of MC_SHP phase.

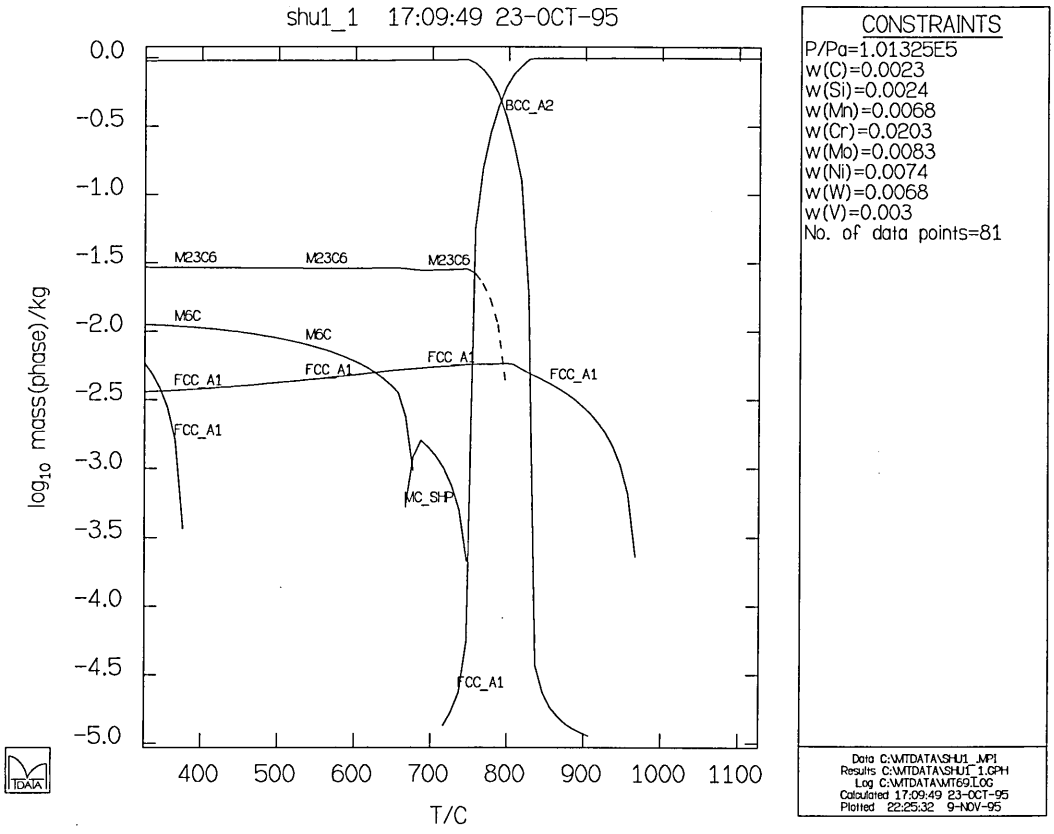

Figure 4.14 Thermodynamic calculation with actual composition (replotted here for the convenience of readers)

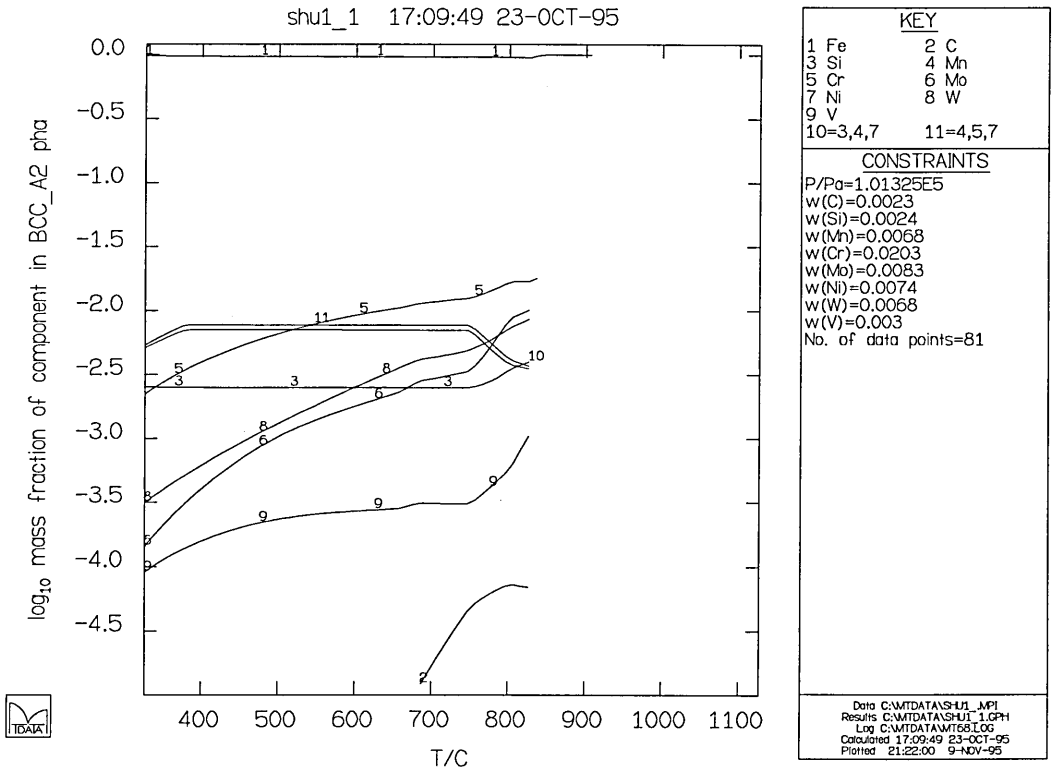

Figure 7.1 Calculated equilibrium composition of matrix as function of temperature

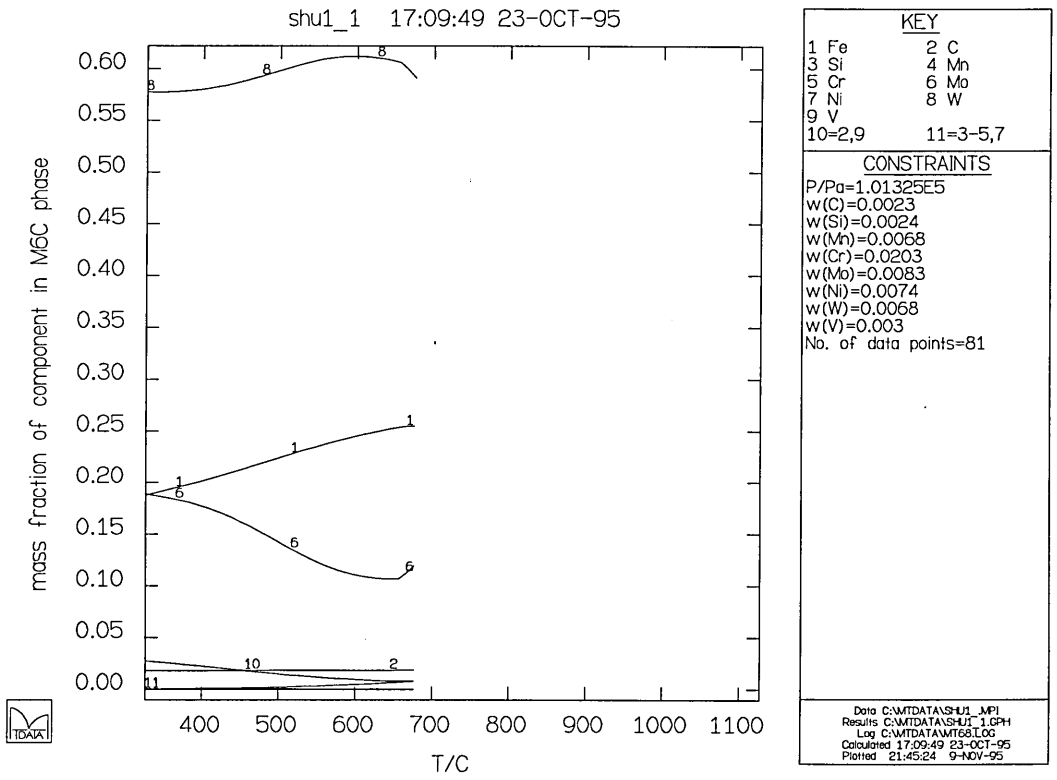

Figure 7.2 Calculated equilibrium composition of M_6C as function of temperature

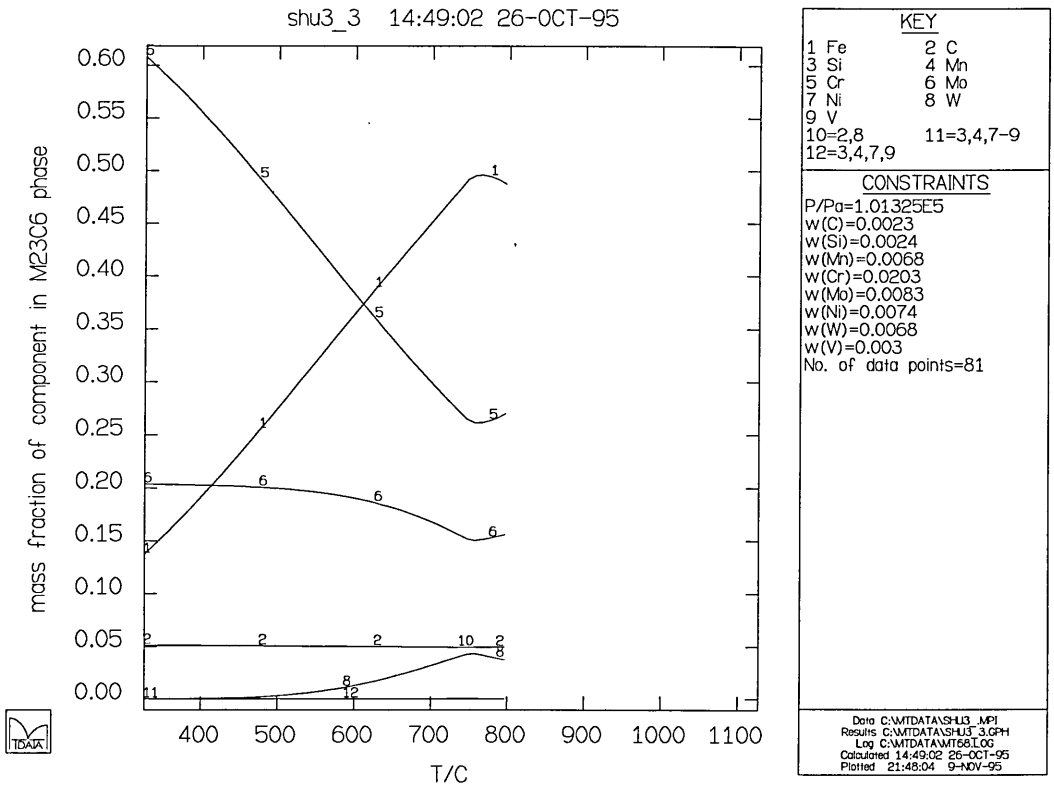

Figure 7.3 Calculated equilibrium composition of $M_{23}C_6$ as function of temperature

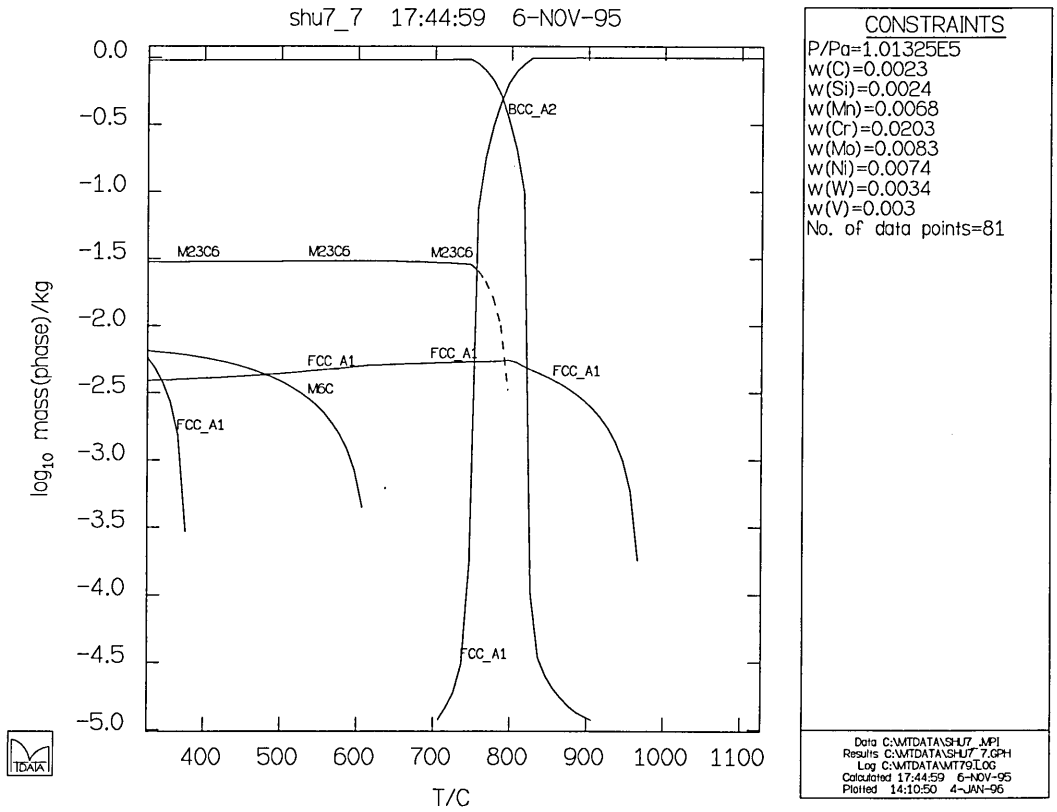

Figure 7.4 Thermodynamic calculation with half of actual W content

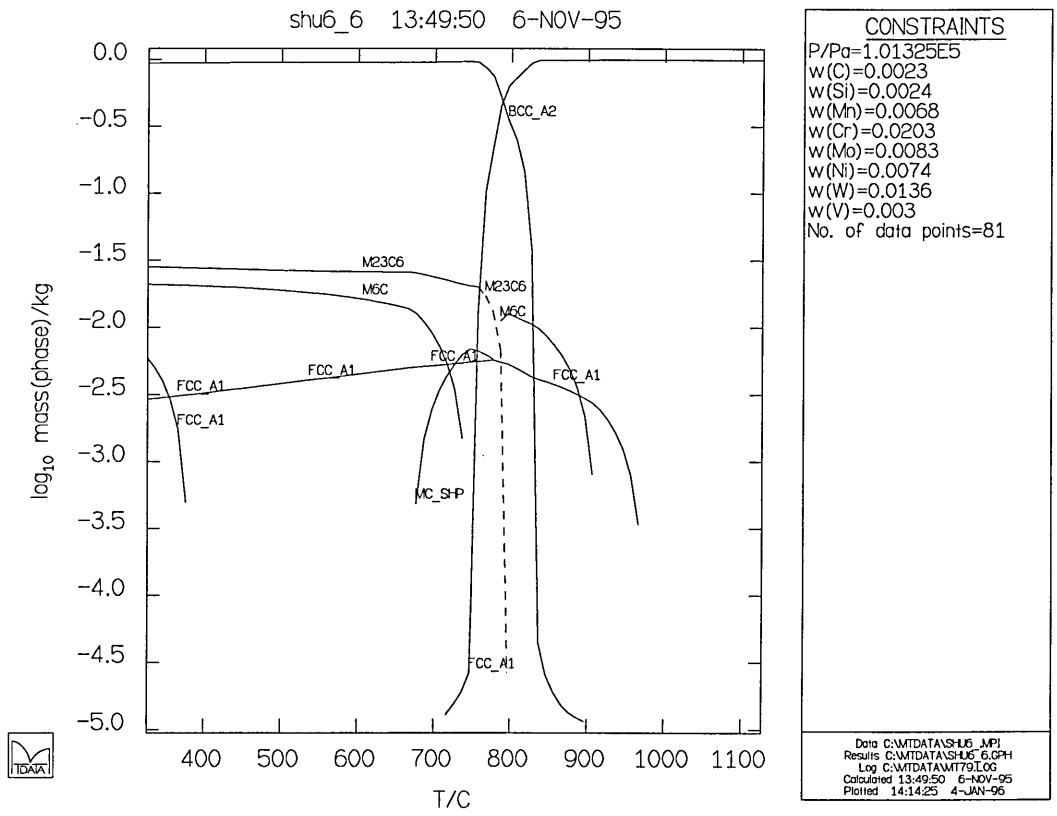

Figure 7.5 Thermodynamic calculation with double of actual W content

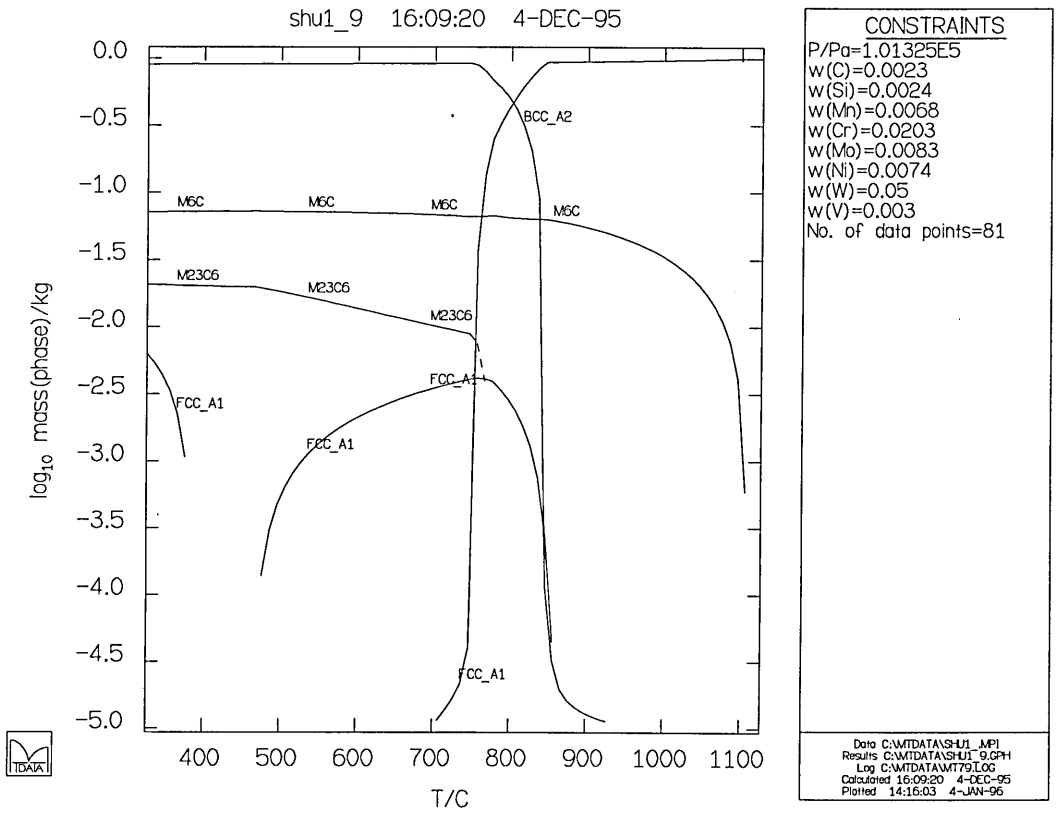

Figure 7.6 Thermodynamic calculation with 5 mass% W content

7.4 Discussion

It has been shown by many workers (Senior, 1988; Woodhead and Quarrell, 1965) that V, Cr and Mo are necessary additions for low alloy creep resistant steels. It is apparent that W plays an important role in the further improvement of toughness related properties with at least equivalent creep properties in this type of steel (Wiemann, 1991). In the present work, during tempering, W together with Mo substituted a little for Fe in cementite and stabilised it, and had a greater solubility in the M_7C_3 and $M_{23}C_6$ carbides and eventually an even much higher solubility in M_6C carbide. W and Mo also formed $(Mo, W)_2C$ within the matrix and on the existing MC carbides forming H-type carbides. It stabilised the MC carbides and $(Mo, W)_2C$ itself was stabilised by the V dissolution. Except for the large carbides inherited from the large cementite, $(Mo, W)_2C$ maintained a small size in the matrix even after tempering for a long time so that a strengthening effect was achieved. Because the W and Mo contents in M_6C are constant this fine distribution of $(Mo, W)_2C$ carbides would be stable for very long periods of time.

The most important factor in long time creep-resistance is the microstructure stability. One of the best ways of obtaining this in low alloy ferritic steels is to form a stable dispersion of alloy carbides which are both resistant to growth and to any further phase change. Practical experience demonstrates clearly that different types, shapes and dispersions of particles vary considerably in their effectiveness. Any attempt to assess the effectiveness of the various carbides is also complicated by the effects of the solutes on the matrix, *e.g.* Mo and W are particularly good solution strengtheners and therefore the creep resistance of a steel containing Mo and W will be influenced not only by the type and composition of the carbides but also by the amounts of Mo and W in solid solution in the ferrite. Especially the

solid solution hardening effect of Mo and W contributes a lot towards the initial creep resistance. This conclusion was deduced from the ICP analysis on various tempered specimen compositions (see Table 7.3) and was supported by theoretical prediction in Figure 7.1. Asakura *et al* (1990) demonstrated in their work, the longer term effects of (2-3)Cr-(2-2.25)W-(0.2-0.4)V-0.01Ti steels to a conventional 2.25Cr-1Mo steel. They concluded that both 0.2% proof strength and creep-rupture strength at 500°C for 100 000 hrs of the developed steels were about twice those of the conventional 2.25Cr-1Mo steel, suggesting that W solid solution strengthening effect would be significant. But of course the effect of solid solution hardening effect is less than precipitation hardening in this type of low alloy creep resistant steels.

In this particular steel, because the Mo concentration is higher than W, W does not form its own carbide but combines with Mo forming M_2C or M_6C. Mo and W are also soluble in a very small amounts into other types of carbides. These carbides dissolve very slowly in steel when the steel is heated, and only dissolve completely at very high austenitising temperatures. Once in solution the dissolved W renders transformations extremely sluggish (Colbeck and Rait, 1950) and that is why the transformation product from austenite is predominantly bainite. When successfully hardened, steels containing W have a great resistance to tempering conditions and can be heated in the range 600-700°C before carbides begin to precipitate and softening sets in.

It was observed in the TEM examination on carbon extraction replicas that the coalescence of precipitated carbide particles were retarded by the addition of W to the steel and the resultant fine precipitates during tempering were considered to be the main reason for the improved resistance to temper softening and the potential increase of creep rupture strength. As experimental results shown above, W was to precipitate as a part of metallic elements in alloy carbides (Table 7.1) and a certain amount was to remain in solution (Table 7.2). One of the roles of W in this case could be interpreted as retarding

coarsening of the precipitates, with the relatively small size of alloy carbides containing W suppressing strength drop at elevated temperatures. Thus, retardation of the coalescence of carbides is an important factor for ensuring high tempering hardness and high creep rupture strengths.

The effect of various W additions was also investigated using MTDATA. It was found that the formation of the M_6C phase was closely connected with the amount of W in the system. Without W addition, there would not be the formation of the M_6C phase during tempering and service temperature range (see Figure 4.10). If with half of actual W addition, there would not be the formation of the M_6C phase in normal tempering temperature range, which meant that W addition would not have its precipitation strengthening effect. Figure 7.5 showed that the increase of W addition up to double the actual content (1.36 mass%) would have the similar precipitation strengthening effect to the improvement of the creep strength, but due to more W content remaining in the matrix which would influence the ductility and toughness of the steel. However, when W content increased up to 5 mass%, the steel would form a large fraction of the M_6C phase and it would not dissolve until very high solution treatment temperatures. On the other hand, it would be certainly detrimental to creep properties if there was only large M_6C precipitates at grain boundaries. This series of theoretical calculations demonstrated that the combination of this steel composition was reasonable. The W addition was beneficial to balance the phase equilibria of alloy carbides, and also contributed to the solid solution strengthening effect by a considerable amount of W remaining in matrix.

Chapter 8

CONCLUSIONS AND SUGGESTIONS FOR FURTHER WORK

The object of this study was to investigate the heat treatment and precipitation characteristics of a new 2CrMoNiWV creep resistant rotor steel. Throughout this study, a clear picture has been developed for the microstructural characterisation of 2CrMoNiWV rotor steel, which involves the high temperature autenitising behaviour that ensures dissolution of the carbides and their precipitation in subsequent tempering treatment, the type, amount, and distribution of these carbide phases would have a profound influence on the high temperature properties of the material.

- Two continuous cooling transformation (CCT) diagrams derived from dilatometric and metallographic work provide useful information on the hardenability of this specific material, defining quite accurately the cooling rates at which various transformation products will form. The cooling rates from the rim to the core of a large diameter rotor after oil quenching from austenitisation can be correlated to the various cooling rate on the CCT diagram. A high bainitic hardenability meant that the 2CrMoNiWV steel transformed to a fully bainitic microstructure over a wide range of cooling rates and this feature proved the steel suitable for the large diameter rotor application.

- A powerful innovative carbide extraction technique for the X-ray diffraction identification of carbide phases has been developed which could be easily applied in the development of new creep resistant alloys, remnant creep life prediction and similar fields of research work.

- The usefulness of equilibrium thermodynamic calculations using MTDATA in predicting the microstructural change and carbide evolution has been demonstrated in this work, particularly the separate effect of composition on the stable carbide dispersion where a thermodynamic approach offers great benefits. Very good agreement was found between the experimental results and theoretical thermodynamic equilibria prediction performed with MTDATA on those critical transformation temperatures and similar carbide evolution sequence was obtained.

- Regarding austenitising temperature and cooling rate it was found that:
- 1). All carbides and other intermediate phase were almost completely dissolved after 5 hours austenitisation at 975°C.
- 2). The austenite grain size increased with increasing austenitising time and temperature.
- 3). The increase of austenitising temperature led to an increase of the bainitic hardenability of the material because of the increase of C in solution.
- 4). This particular 2CrMoNiWV steel exhibited very high hardenability so that in a wide range of cooling rates bainite was the dominant microstructure.
- 5). At cooling rates slower than 0.5°C/min from the austenite, the softer microconstituent, proeutectoid ferrite, will become an increasing portion of the microstructure.
- 6). This 2CrMoNiWV rotor steel should be austenitised in the temperature range 975-985°C. For temperature below this there will be a risk for undissolved carbides, particularly V-rich MC type carbide, and above this temperature range, a risk of austenite grain growth.

- Regarding tempering temperature and time it was found that:
- 1). The tempering temperature at 700°C, coarsening of carbides occurred. To obtain the required room temperature mechanical properties and optimum

creep properties, it would appear that the tempering temperature should be in the range 670 - 680°C.

- 2). The fine precipitation, MC, was found at every trial of tempering condition, but at high tempering temperature the alloy carbide dispersions tended to be more homogeneous.
- 3). The carbide size and interparticle spacing increased with increasing tempering temperature and time. This resulted in a decrease of hardness at ambient temperature.
- 4). The hardness value as a function of tempering parameter (LMP) was the better reflection of the combination effects of tempering time and temperature.
- 5). During tempering the fast cooling rate from austenite led to more M_7C_3 precipitates, while slower cooling rate from austenite resulted in more $M_{23}C_6$ precipitates (Figures 5.40-5.41). In commercial heat treatment practice, for the large diameter rotor forgings, due to different cooling rates across the section it may produce different microstructure from the rim to the core after oil quenching from austenitisation. A higher tempering temperature (above 670°C) would lead to a more homogenous dispersion and the formation of stable alloy carbides.
- 6). This material tempered at 675°C for 20 hours proved to have a microstructure with a uniform dispersion of alloy carbides and appropriate hardness at ambient temperature.

- After systematic investigation utilising advanced instruments and techniques, the sequence of carbide transformations for this 2CrMoNiWV steel has been established (Figure 6.10), which together with the composition range for each type of carbide (Table 7.1) can be used as monitoring parameters for this material during service at elevated temperature.

- The role of W in the enhancement of both creep strength and toughness of this alloy system was investigated and discussed. The experimental results (Table 7.2) and theoretical calculation demonstrated that the combination of the steel composition was reasonable and the W addition was adequate and beneficial to balance the phase equilibria. Meanwhile W addition contributed to the solid solution strengthening effect by remaining certain amount of W in matrix. The improved toughness of 2CrMoNiWV rotor steel with at least equivalent creep strength to conventional CrMoV steel (Wiemann, 1991) was partly attributed to the addition of W, which would give distinct rise to initial solid solution strengthening as well as precipitation hardening in the later stage, but their contributions are quite dependent on thermal history.

- A possibly optimised heat treatment route was suggested for the material which involves austenitising at 975°C for 10 hours following by oil quenching for large diameter rotor forgings and then tempering at 675°C for 20 hours following by air cooling.

It was believed that all of these systematic investigations laid a sound foundation for a more detailed study of creep rupture mechanisms with respect to the relevant microstructure. So the further work is supposed to conduct creep rupture test on laboratory treated specimens cooled from the austenitised temperature at rates similar to those encountered in a large rotor, and examine this material prior to testing in order to determine the effect of microstructure upon the creep properties. The extension of this work to include its long term creep test, would yield significant fundamental data involved in developing new creep resistant alloys.

Appendix

OPERATION COMMAND ON MTDATA

The following macro file shows the sequence of command used in setting up the calculation for the 2CrMoNiWV rotor stee with a brief explanation for each command.

```
; First enter the ACCESS module and define the system. Select 'SHU1_' as the
; root name for the output files
;
acc
def sys 'Fe,C,Si,Mn,Cr,Mo,Ni,W,V' so sgte_sol out 'shu1_' !
;
; Classify absent all but the phases of interest and SAVE the data
;
cl ab p(*) no p(fcc,bcc,cem,m3c2,m7c3,m23c6,m6c,m5c2,v3c2,mc_shp) ! save
;
; Go to MULTIPHASE, read in the 'SHU1_' data and classify all phases
;NORMAL. This is required as a missing interaction will initially cause a phase
to be classified as ABSENT. A miscibility gap must be classified for FCC.
;
ret mult def da 'shu1_' ! cl norm p(*) m(fcc) 1 !
;
; Set the composition of the system in mass terms, 1kg of system in total.
; the mass of Fe is set to UNDEF so that it will make up the difference
; when the total mass is set 1kg.
;
```

```
;C:0.23; Si:0.24; Mn:0.68; Cr:2.03; Mo:0.83; Ni:0.74; W:0.68; V:0.30
set W( ) undef .23/100 .24/100 .68/100 2.03/100
 .83/100 .74/100 .68/100 .30/100 !
;
set w 1 ! li sy set !
;
; Step the temperature between 600 and 1400K with 10K step
; The temperature is defaulted in Kelvins, the default pressure is 101325 Pa
;
ste t 600 1400 10 !
;
; Compute with INIT=LAST and PRINT=GRAPHICS
;
; Initialise the CPU timer
[CPU_TIME=RESET
;
co in las pri gr !
:
: Results for your computer are:
[CPU_TIME
;
; Plot the logarithmic graph with ordinate mass of phases versus temperature
;
or mas p log y ! pl g
;
; Plot the graph with label characters and temperature in Celsius
;
pl key char !
;
quantify t Cels ! pl g
;
```

; The way to get the component distribution of a single phase, in MULTIPHASE,

; is to classify all but that phase absent. For example, for M_6C this would be:

;

pl file 'shu1_1' !

:

class ab p(*) norm p(m6c) !

;

; Because the alloying element usually soluted in small amount in each phase,

; plot the logarithmic graph with ordinate mass of the phase versus temperature

;

or comp_d log y ! pl g

REFERENCES

AARONSON, H. I., (1986)
'Bainite Reaction', Encyclopaedia of Materials Science and Technology, Pergamon Press, Oxford, p263

ANDERSON, L. M., CARTER, C. B. and BENTLEY, J., (1995)
'The Self-supporting Disc: A Specimen Geometry Exhibiting Low Secondary Characteristic Fluorescence', Proc. of the 29th Annual Conf. of the Microbeam Analysis Society, Breckenridge, Colorado, USA, August 6-11, 1995, *Microbeam Analysis* (ed. S. Edgar), p285

ANDREWS, K.W. and HUGHES, H., (1958)
'Micro-constituents in Steels; Their Electrolytic isolation and X-ray Study', *Iron and Steel,* **30**, p43

ANDREWS, K. W., (1965)
'Empirical Formulae for the Calculation of Some Transformation Temperatures', *Journal of the Iron and Steel Institute*, **203**, p721

ANDREWS, K. W., DYSON, D. J. and KEOWN, S. R., (1967)
'Interpretation of electron diffraction patterns', Publ., Hilger and Watts, London

ASAKURA, K., KOHYAMA, A. and YAMADA, T., (1990)
'Mechanical Properties and Microstructure Changes of Low-activation 3Cr-2W-V-Ti Ferritic Steels Developed for Nuclear Applications', *ISIJ International*, **30**, p947

ASHBY, M. F., (1971)
'Strengthening Methods in Crystals', (ed. A. Kelly and R. B. Nicholson), Elsevier, London, p137

ASHBY, M. F. and JONES, D. R., (1980)
'Engineering Materials --An Introduction to their Properties and Applications', Publ. Pergamon Press, Oxford

BAKER, R. G. and NUTTING, J., (1959)
'The tempering of 2.25Cr-1Mo steel after quenching and normalising', *Journal of the Iron and Steel Institute*, **191**, p257

BAKER, T. N., (1983)
'Yield, Flow and fracture of Polycrystals', Applied Science Publ., London, p235

BARRY, T. I. and RAND, M. H., (1992)
'Standards for Representation of Thermodynamic Data for Inorganic Methods', *computerization and Networking of Materials databases*, ASTM STP 1140, (eds. T. I. Barry and K. W. Reynard), American Society for Testing and Materials, Philadephia, USA

BARFORD, J. and WILLOUGHBY, G., (1971)
'Effect of Structure on Creep Strength of a Low-Alloy Cr-Mo-V Steel', *Metal Science*, **5**, pp32-37

BATES, H.G.A. and RIDAL, K.A., (1963)
'Factors Governing the Creep Properties in Large Diameter 1Percent Chromium-Molybdenum-Vanadium Rotor Forgings', *Proc. Conf. Inst. Mech. Engs.*, New York, Paper 72, p99

BERGER, C. H., SCARLIN, R.B., MAYER, K.H. THORNTON,.D.V. and BEECH, S. M., (1994)
'Steam Turbine Materials: High Temperature Forgings', *Materials for Advanced Power Engineering 1994,* Proc. Conf. held in Liege, Belgium, 3-6 Oct., Part I, p47

BHADESHIA, H. K. D. H., (1987)
'Worked Examples in the Geometry of Crystal', The Institute of Metals, London

BHADESHIA, H. K. D. H., (1988)
'Bainite in Steels', *Phase Transformation '87* (ed. G. W. Lorimer), Institute of Metals, London, p309

BHADESHIA, H. K. D. H., (1992)
'Bainite in Steels', The Institute of Materials, London

BHADESHIA, H. K. D. H. and CHRISTIAN, J. W., (1990)
'Bainite in Steels', *Metallurgical Transactions*, **21A**, p767

BHADESHIA, H. K. D. H. and EDMONDS, D. V., (1979)
'The Bainite Transformation in a Silicon Steel', *Metallurgical Transactions*, **10A**, p895

BHADESHIA, H. K. D. H. and WAUGH, A. R., (1982)
'Bainite: An atom probe study of the incomplete-reaction phenomenon', *Acta metallurgica,* **30**, p775

BILBY, B. A. and PICKERING, F. B., (1959)
'Precipitation Processes in Steels', Iron & Steel Institute, London, p373

BJÄRBO, A., (1994)
'Austenitizing, hardening and tempering of a modified 12% chromium steel', *Scandinavia Journal of Metallurgy*, **23**, p103

BRIGG, J. Z. and PARKER, T. D., (1965)
'The Super 12%Cr Steels', Climax Molybdenum Co, New York

BUCHI, G. J. P., PAGE, J. H. R. and SIDEY, M. P., (1965)
'Creep properties and precipitation characteristics of 1% Cr Mo V steel', *Journal of The Iron and Steel Institute,* **203**, p291

CARRUTHERS, R. B. and COLLINGS, M. J., (1981)
Proc. Conf. on *High Spatial Resolution*, Manchester, March 25-27, Metals Society, London, p108

CHANCE, J. and RIDLEY, N., (1981)
'Chromium Partitioning During Isothermal Transformation of a Eutectoid Steel', *Metallurgical Transactions*, **12A**, p1205

CHRISTIAN, J. W., (1971)
'Strengthening Methods in Crystals', (ed. A. Kelly and R. B. Nicholson), Elsevier, London, p261

CHRISTIAN, J. W. and EDMONDS, D. V., (1984)
'The Bainite Transformation', Phase Transformation in Ferrous Alloys, ASM, Metals Park, Ohio, p293

CLIFF, G. and LORIMER, G.W., (1975)
'The quantitative analysis of thin specimen' *Journal of Microscopy,* **103**, p203

COLBECK, E. W. and RAIT, J. R., (1950)
'Creep-Resisting Ferritic Steels', *High-Temperature Steels and alloys for Gas Turbines*, p107

COTTRELL, A. H., (1953)
'Dislocations and Plastic Flow in Crystals', Oxford University Press, London

COX, A. R., (1967)
'Metallograpy and Strengthening Mechanisms of 0.3%C and 0.3%C - 1.5%Cu Steels', *Journal of The Iron and Steel Institute*, **205**, pp51-57

DAVIES, R. H., (1995)
'New features of MTDATA', *Seventh MTDATA Users' Group Meeting*, organised by MTDATA Users Gorup and National Phsical Laboratory, Teddington, UK

DAVIES, R. H., DINSDALE, A. T., *et al.*, (1990)
'Application of MTDATA to the modelling of multicomponent phase equilibria', *High temperature Science*, **26**, p251

DAVIES, R. H., DINSDALE, A. T., *et al.*, (1991)
'MTDATA - The NPL Databank for Metallurgical Thermochemistry', "Users Aspects of Phase Diagrams" (ed. F. H. Hayes), Institute of Metals, London

DINSDALE, A. T., HODSON, S. M., BARRY, T. I. and TAYLOR, J. R., (1989)
'Computations using MTDATA of Metal - Matte - Slag - Gas equilibria', *Computer Software in Chemical and Extractive Metallurgy*, Pergamon Press, Oxford, UK, p59

DYSON, D. J. and ANDREWS, K. W., (1969)
'Carbide M_7C_3 and its formation in alloy steels', *Journal of The Iron and Steel Institute*, **207**, p208

DU, X., (1986)
'Carbide Composition Change in A Power Plant Steel During Long Term Tempering', PhD thesis, Sheffield University, Sheffield, UK

EVANS, R. C., (1966)
'An Introduction to Crystal Chemistry', Cambridge Univ. Press, Cambridge

FLEISCHER, R. L., (1967)
'The Strengthening of Metals' (ed. D. Peckner), Reinhold, p93

FOLDYNA, V., JAKOBOVA, A., PRNKA, T. and SOBOTKA, J., (1972)
Proc. Conf. on Creep Strength in Steel and High Temperature Alloys, Sheffield, Metals Society, London, p230

FRANCK, F. J., TAMBUYSER, P. and ZUBANI, I., (1982)
'X-ray powder diffraction evidence for the incorporation of W and Mo into $M_{23}C_6$ extracted from high temperature alloys', *Material Science*, **17**, p3057

FUJITA, T., SATO, T. and TAKAHASHI, N., (1978)
'Effect of Mo and W on Long Term Creep Rupture Strength of 12%Cr Heat-resisting Steel Containing V, Nb and B', *Trans. ISIJ*, **18**, P115

GISBY, J. A., BARRY, T. I, DINSDALE, A. T. and DAVIES, R. H., (1993)
'MTDATA: Applications in Extraction Metallurgy', *Computer Software in Chemical and Extractive Metallurgy*, Conf. Vol. of Quebec 93 Metallurgists (of the Canadian Institute for Mining, Metallurgy and Petroleum), Quebec, Canada

GLADMAN,T. and PICKERING, F. B., (1983)
'Yield, Flow and Fracture of Polycrystals' (ed. Baker, T. N.), Applied Science Publ., London, p141

GOLDSCHMIDT, H. J., (1967)
'Interstitial Alloys', Buttewords, London

GOLDSTEIN, J. I., LORIMER, G. W. and CLIFF, G., (1976)
Conf. Proc. of 6th European Congress on Electron Microscopy, Jerusalem, p56

GRANGE, R. A., (1966)
'Strengthening Steel by Austenite Grain Refinement', *Trans. American Society for Metals*, **59**, p26

GULLBERG, R., (1971)
'Comparison of chromium content in (Fe, $Cr)_{23}C_6$ carbides as determined by electron microprobe and by X-ray diffraction', *Journal of The Iron and Steel Institute*, **209**, p71

HALL, E. O., (1951)
Proc. Phys. Soc., Vol. 64B, p747

HILLERT, M., (1995)
'The Nature of bainite', *ISIJ International*, **35**, No.9, p1134

HODSON, S. M., (1988)
'A mathematical description of MULTIPHASE: A computer program for the calculation of complex phase equilibria in chemical and metallurgical systems', NPL Report DITC(A) series

HONEYCOMBE, R.W.K., (1981)
'Steels-Microstructure and Properties', Publ. Edward Arnold Ltd, London

HONEYCOMBE, R.W.K., (1985)
'The Plastic Deformation of Metals', Publ. Edward Arnold Ltd, London, p180

HORNBOGEN, E. and STANIEK, G., (1974)
'Grain-size dependence of the mechanical properties of an age-hardening Fe-1%Cu alloy', *Journal of Material Science*, **9**, p879

IRVINE, K. J. and BAKER, T. N., (1984)
'The Influence of Rolling Variables on the Strengthening Mechanisms Operating in Niobium Steels', *Materials Science and Engineering*, **64**, p123

IRVINE, K. J., GLADMAN, T. and PICKERING, F. B., (1969)
'The Strength of Austenitic Stainless Steels', *Journal of The Iron and Steel Institute*, **207**, p1017

IRVINE, K. J., LLEWELLYN, D. T. and PICKERING, F. B., (1961)
'High-strength austenitic stainless steel', *Journal of The Iron and Steel Institute*, **199**, p153

IRVINE, K. J., MURRAY, J. D. and PICKERING, F. B., (1961)
'Structural Processes in Creep', ISI Special Report No.70, p246

IRVINE, K. J. and PICKERING, F. B., (1960)
'The tempering characteristics of low-carbon low-alloy steels', *Journal of The Iron and Steel Institute*, **194**, p137

JOHNSON, R. F., and GLEN, J., (1972)
Proc. Conf. on Creep Strength in Steel and High Temperature Alloys, Sheffield, 1972, Metals Society, London, p37

KASSNER, M. E., MILLER, A. K. and SHERBY, O. D., (1982)
'The Separate roles of Subgrains and Dislocations in the Isotropic Hardening of Type 304 Stainless Steel', *Metallurgical Transactions*, **13A**, p1977

KELLY, A. and NICHOLSON, R. B., (1971)
'Strengthening Methods in Crystals', Elsevier, London

KELLY, A., (1973)
'The Quantitative Relationship between Microstructure and Properties in Two-Phase Alloys', *International Metallurgical Review*, **18**, p31

KOCKS, U. F., (1979)
Proc. 5th Int. Conf. on 'Strength of Metals and Alloys' (ed. P. Haaasen, V. Gerold and Gkosttorz), Pergamon Press, Oxford, Vol. III, p1661

KRAUSS, G., (1980)
'Principles of Heat Treatment of Steels', American Society for Metals, Metals Park, Ohio, USA

KUO, K., (1953)
'Carbides in Chromium, Molybdenum and Tungsten Steels', *Journal of The Iron and Steel Institute*, **173**, p363

KUO, K. H. and JIA, C. L., (1985)
'Crystallography of $M_{23}C_6$ and M_6C Precipitated in a Low Alloy Steel', *Acta Metall.*, **33**, p991

LAPOINTE, A. J. and BAKER, T. N., (1982)
'Analysis of strengthening contribution at peak hardening from precipitation in vanadium steels continuously cooled from austenite', *Metal Science*, **16**, p207

LEITNAKER, J. M., KLUEH, R. L. and LAING, W. R., (1975)
'The composition of eta carbide phase in 2.25Cr 1Mo steel', *Metallurgical Transactions,* **6A**, p1949

LIVINGSTON, J. D., (1963)
'Dislocation Studies in Copper Using Etch Pits', *The Journal of the Australian Institute of Metals,* **8**, p15

LORIMER, G. W., AL-SALMAN, S. A. and CLIFF, G., (1977)
Conf. Proc. of EMAG'77, Inst. of Phys. Conf. Series, p369

MALIK, L. and LUND, J. A., (1972)
'A Study of Strengthening Mechanisms in Tempered Martensite from a Medium Carbon Steel', *Metallurgical Transactions*, **3**, p1403

MARDER, A. R. and KRAUSS, G., (1970)
Proc. 2nd Int. Conf. on Strength of Metals and Alloys, ASM, Metals Park, Ohio, p822

MARTIN, J. W., (1980)
'Micromechanisms in Particle Hardened Alloys', Cambridge Univ. Press, Cambridge

McLEAN, D., (1962)
'Mechanical Properties of Metals', John Wiley and Sons, New York, p153

McLEAN, D., (1967)
'Deformation at High Temperatures', *Metallurgical Review*, **7**, p481

MORRIS, P. L., DAVIES, N. C. and TREVERTON, J. A., (1977)
Conf. Proc. of EMAG'77, Inst. of Phys. Conf. Series, p377

MOTT, N. F., (1960)
'The Work Hardening of Metals', *TMS-AIME,* **218**, P962

MURPHY, M. C., and BRANCH, G. D., (1969)
'The microstructure, creep, and creep-rupture properties of Cr-Mo-V steam turbine casing casting', *Journal of The Iron and Steel Institute*, **207**, p1347

MURPHY, M. C., and BRANCH, G. D.,(1971)
'Metallurgical changes in 2.25CrMo steels during creep-rupture test', *Journal of The Iron and Steel Institute*, **209**, p546

NABARRO, F. R. N., (1977)
'The theory of solution hardening', *Philosophical Magazine*, **35**, p163

NABARRO, F. R. N., BASINSKI, Z. S. and HOLT, D. B., (1964)
Advances in Physics, **13**, p193

NORTON, J.F. and STRANG, A., (1968)
'Metallurgical developments in the manufacture of large 1%CrMoV steam turbine rotor forgings', *English Electric. Journal*, **23**, p20

NORTON, J.F. and STRANG, A.,(1969)
'Improvement of Creep and Rupture Properties of Large 1%Cr-Mo-V Steam Turbine Rotor Forgings', *Journal of The Iron and Steel Institute*, **207**, p193

OHMORI, Y. and HONEYCOMBE, R. W. K., (1971)
'The isothermal transformation of plain carbon steels', Proceedings ICSTIS, *Supplementary transactions of the Iron and Steel Institute of Japan*, **11**, p1160

OKA, M. and OKAMOTO, H., (1986)
'Isothermal transformations in hypereutectoid steels', *Proc. of International Conf. on martensitic transformations*, ICOMAT '86, Japan Institute of Metals, p271

ONEL, K. and NUTTING, J., (1979)
'Structure-property relationships in quenched and tempered carbon steels', *Metals Science*, **13**, p573

OROWAN, E., (1948)
'Symposium on Internal Stresses in Metals and Alloys', Inst. Metals, London, p451

PATCH, N. J., (1953)
Journal of The Iron and Steel Institute, **174**, p25

PICKERING, F. B., (1958)
Proc. 4th. Int. Conf. On Electron Microscopy, Springer-Verlag OHG Berlin. p628

PICKERING, F. B., (1976)
'The Basis of Quantitative Metallography', Monograph No.1, Publ. Metals and Metallurgy Trust for the Institute of Metallurgical Technicians, London

PICKERING, F. B., (1978)
'Physical Metallurgy and the Design of Steels', Applied Science Publ., Essex

PICKERING, F. B., (1990)
'Microalloyed Vanadium Steels', (ed. M. Korchynsky *et al*), Assoc. of Polish Met. Eng. and Strategic Minerals Corporation (USA), Krakow, Poland, p79

PICKERING, F. B., (1990)
'Some Aspects of Creep Deformation and Fracture in Steels', *Proc. Conf. of Rupture Ductility of Creep Resistant Steels* (ed. A. Strang), York, UK, p17

PICKERING, F. B. and GLADMAN, T., (1963)
'Metallurgical Development in Carbon Steel', Iron and Steel Inst., Special Report No. 81, p10

PILLING J. and RIDLEY, N., (1982)
'Tempering of 2.25 Pct Cr-1 Pct Mo Low Carbon Steels', *Metallurgical Transactions,* **13A**, p557

POTER, L. F. and DABKOWSKI, D. S., (1970)
'Ultrafine Grain Metals', (ed. J. J. Burke and V. Weiss), Syracause Univ. Press, Syracuse, p133

RITCHIE, R. O., PARKER, E. R., SPENCER, P. N. and TODD, J. A., (1984)
'A New Series of Advanced 3Cr-Mo-Ni Steels for Thick Section Pressure Vessels in High Temperature and Pressure Hydrogen Service', *J. Materials for Energy Systems*, **6**, No.3, p151

ROBERTS, B. W. and STRANG, A., (1987)
'Metallurgical aspects of turbine component life extension', *Inst. Mech. Eng.* **C292/87**, p205

ROBERTS, M. J., (1970)
'Effect of Transformation Substructure on the Strength and Toughness of Fe-Mn Alloys', *Metallurgical Transactions*, **1**, p3287

SEAL, A. K. and HONEYCOME, R. W. K., (1958)
'The Effect of Tantalum and Niobium on the Tempering of Certain Vanadium and Molybdenum Steels', *Journal of The Iron and Steel Institute*, **188**, P343

SEEGER, A., (1957)
'Dislocations and Mechanical Properties of Crystals', (ed. J. C. Fisher *et al*), John Wiley, New York, p243

SELLARS, L. M., (1974)
'Creep Strength in Steel and High Temperature Alloys', The Metals Society, London, p20

SENIOR, B.A., (1988)
'A Critical Review of Precipitation Behaviour in 1Cr-Mo-V Rotor Steels', *Materials Science and Engineering,* **A103**, p263

SHI, J. and ENDO, T.,(1995)
'A New Approach for Creep Life Assessment Based on the Imaginary Initial Strain Rate', *Scripta Metallurgica et Materialia,* **32**, p1159

SPENCER, P. N., DAUSKARDT, R. H., PARKER, E. R. and RITCHIE, R. O., (1989)
'Fracture toughness, fatigue crack propagation and creep rupture behaviour in thick section weldments of 3Cr-Mo pressure-vessel steels developed for high-temperature/high-pressure hydrogen service', *High Temperature Technology,* **7**, No.1 p17

SMITH, R. and NUTTING, J., (1957)
'The Tempering of Low-Alloy Creep-Resistant Steels Containing Chromium, Molybdenum, and Vanadium', *Journal of the Iron and Steel Institute,* **187**, p314

STARK, I., SMITH, G. D. W. and BHADESHIA, H. K. D. B., (1987)
'The element redistribution associated with the incomplete-reaction phenomenon in bainitic steels: An atom prob investigation', *Proc. Int. Conf. 'Phase Transformation 1987'*, Institute of Metals, London, (ed. G. W. Lorimer), p211

STEVENS, R. A. and LONSDALE, D., (1987)
'Electrolytic Extraction of Carbide Precipitates from Low Alloy Ferritic Steel Power Plant Components', Central Electricity Generating Board Report OED/STB(S)/87/0028/R

STRANG, A., (1972)
'Some Aspects of Rupture Ductililty in 1CrMoV Steels', Proc. Int. Conf. on *Properties of Creep Resistant Steels*, Düsseldorf, Germany

STRANG, A., (1995)
Private communication, Large Steam Turbine Laboratory, GEC ALSTHOM, Rugby, UK

STUART, H. and RIDLEY, N., (1966)
'Thermal Expansion of Cementite and other Phases', *Journal of The Iron and Steel Institute,* **204**, p711.

THOMSON, R. C., (1992)
'Carbide composition changes in power plant steels as a method of remanent creep life prediction', PhD thesis, Cambridge, UK

THOMSON, R. C. and BHADESHIA, H. K. D. H., (1992)
'Carbide Precipitation in 12Cr1MoV Power Plant Steel', *Metallurgical Transaction*, **23A**, p1171

TITCHMARSH, J. M., (1978)
'Electron Microscopy' *Proc. 9th Inst. Congress* (ed. J. M. Sturgess), Microscopical Society of Canada, Toronto, ON., Vol. 1, p618

TITCHMARSH, J.M., (1979)
'The identification of second-phase particles in steels using an analytical transmission electron microscope', ARE (Harwell) Report No. R9661

TOFT, L. H. and MARSDEN, R. A., (1961)
'Structural Progresses in Creep", Iron & Steel Institute, Special Report No.70, p276

TOWNSEND, R. D., (1993)
'Mechanisms of High Temperature Structural Degradation and Techniques of Life Prediction', *Proc. 1st. Int. Conf. on Microstructures and Mechanical Properties of Aging Material* (ed. P. K. Liaw *et al*), The Minerals, Metals & Materials Society, Chicago, USA

WADA, T. and BISS, V. A., (1983)
'Restoration of Elevated Temperature Tensile Strength in 2.25Cr-1Mo Steel', *Metallurgical Transactions,* **14A**, p845

WHITEMAN, J. A., (1977)
'Low Carbon Steels for the Eighties', The Inst. of Metall., London, Series 3, No.6, p1

WIEMANN, W., (1991)
'The Development of an Improved 2%CrMoNiWV HP/IP Rotor Material' (ed. J. B. Marriott), Commission of the European Communities, Luxembourg

WILLIAMS, K. R. and WILSHIRE, B., (1981)
'Microstructural Instability of 0.5Cr-0.5Mo-0.25V Creep-resistant Steel During Service at Elevated Temperature', *Materials Science and Engineering*, **47**, p151

WILSON, P., (1990)
'Remanent Creep Life Prediction in Low Alloy Ferritic Steel Power Plant Components', PhD thesis, Cambridge, UK

WOODHEAD, J.H. and QUARRELL. A. G., (1965)
'Role of Carbides in Low-alloy Creep Resisting Steels', *Journal of The Iron and Steel Institute*, **203** p605

WONG, R. and DUNLOP, G. L., (1984)
' The Crystallography of Secondary Carbide Precipitation in High Speed Steel', *Acta Metall.* **32**, p1591

YU, J., (1989)
'Carbide Stability Diagrams in 2.25Cr-1Mo Steels', *metallurgical Transactions*, **20A**, p1561